SCINTILLATION COUNTER STUDIES OF PHOTOPROTON REACTIONS

by

T. R. Ophel,

Research School of Physical Sciences.

A dissertation submitted to the Australian National University for the degree of Doctor of Philosophy.

April, 1958.

PREFACE.

The work described in this thesis comprises a part of a photo-disintegration programme being carried out at the Research School of Physical Sciences.

Following a suggestion by Professor E. W. Titterton of a method whereby scintillation counters could be used to detect externally produced photoprotons, the method of using a scintillation crystal as both target and detector in the examination of (γ,p) reactions was developed by Professor A. K. Mann, Mr. I. F. Wright and myself. The initial measurements of the $Na^{23}(\gamma,p)$ reaction were made by all three of us and the energy calibration, cross-section measurements and non-resonance radiation work were completed by Mr. I. F. Wright and myself subsequent to Professor Mann's departure.

At the completion of the study of the $Na^{23}(\gamma,p)$ and $I^{127}(\gamma,p)$ reactions, the work was divided such that Mr. I. F. Wright investigated the $Cs^{133}(\gamma,p)$ reaction in CsI, while I independently performed the experiments with KI, LiI and $Li^{6}I$. I would like to thank the above-named for much helpful assistance and guidance and, where necessary, criticism.

Acknowledgements are due to Dr. F. C. Barker for the analysis given in Appendix II of Chapter II and Mr. I. F. Wright for the data shown in Fig.2.3.

Thanks are also due to the workshop staff, in particular to Messrs. H. Owen and G. Kalmar, for the construction of apparatus; to the

electronics group for their willing attention to the ever-persistent needs of the kicksorters and, most of all, to Mr. N. F. Bowkett for maintenance and operation of the high-tension accelerator.

Some of the work described in this dissertation has been reported in the following publications:-

(i). The Photodisintegration of Sodium with $Li^7(p,\gamma)$ Gamma Rays, Bull. Am. Phys. Soc., 2, 181A, 1957 (with A. K. Mann and I. F. Wright).

(ii). The Photodisintegration of Sodium with $Li^7(p,\gamma)$ Gamma Rays, Proc. Phys. Soc., February, 1958 (with I. F. Wright).

(iii). The Response Curves of the Alkali Halides with special reference to the $Li^6(n,\alpha)$ Reaction in Lithium Iodide, J. Nucl. Inst. (in press).

(iv). The Photodisintegration of Potassium with $Li^7(p,\gamma)$ Gamma Rays (submitted to Proc. Phys. Soc.) - ANU/P-184.

No part of this dissertation has been submitted for a degree at any other University.

T.R.Opfel

TABLE OF CONTENTS.

CHAPTER I.

1. Introduction.

Photodisintegration studies have been hampered by both experimental and theoretical difficulties.

On the experimental side, the small cross-sections of photonuclear processes and the restrictive nature of the available gamma-ray sources have limited the extent to which measurements have been made. Particle reactions, chiefly proton capture reactions, are a convenient source of monochromatic radiation though the intensity that such reactions provide is low and the number of gamma-ray energies available is few. However, it is singularly fortunate that the gamma-ray energies of the radiation from some (p,γ) reactions are in the region where the most interesting phenomena of photodisintegration, viz. the giant resonances, occur. On the other hand, the bremsstrahlung radiation produced by electron accelerators overcomes the problem of intensity but any advantage is partially offset by the continuous distribution of gamma-ray energies which comprise bremsstrahlung. Although it is possible to gain information on the variation of absorption cross-section with gamma-ray energy, bremsstrahlung cannot easily be applied to study the emission process at any one gamma-ray energy.

On the theoretical side, an exact analysis of the processes will require the wave functions of the states involved in any particular transition. These wave functions depend on the nucleon motion within the nucleus. In view of the present ignorance of the inter-nucleon forces and the mathematical difficulties which a many-body system present,

calculations cannot be made. Thus neither the process of absorption, which demands a knowledge of the charge and current distributions within the nucleus and therefore can only be obtained from the wave functions, nor the process of emission of photo-particles can be treated in detail. As a partial solution to these difficulties, various models based on simplifying assumptions have been proposed. Examples of these are the Goldhaber-Teller model (Go 48) which considers the incident gamma ray to excite a dipole vibration within the nucleus whereby the protons and neutrons move in opposite directions with a weak inter-coupling, and a model proposed by Wilkinson (Wi 56) which is based on the shell model, i.e. each nucleon is considered to move in the average field produced by the motion of the other nucleons. While these (and other) models show some agreement with experimental data, the validity of any one of them with regard to general application is uncertain since each, though based on different assumptions, fits experiment to some extent.*

Consequently, an essential approach toward an understanding of the processes is a phenomenological one, in the hope that sufficient experimental evidence can be obtained to indicate some solution of current theoretical difficulties.

The present work has been concerned with the development and application of a new technique which enables energy spectra of charged photo-nucleons, produced by monochromatic gamma rays, to be obtained. In so far as this method has permitted the observation of a number of (γ,p) reactions which have not been observed before, a contribution has been

*It has been shown that the two models referred to above are equivalent in some instances (Br 57).

made to the systematic accumulation of experimental data. Of much greater importance, though, is the fact that the (γ,p) spectra which have been obtained are the first good resolution (5%) of the energy spectra of particles emitted from photonuclear reactions induced by monochromatic radiation. Such measurements could provide a means by which the relative importance of such concepts as compound nucleus formation and decay and the direct photoeffect, whereby a quantum is absorbed by individual nucleons without subsequent compound nucleus formation, may be examined. In addition, (γ,p) reactions have not been much examined and any extension of the existing data will contribute to such comparisons as the (γ,p) and (γ,n) cross-sections for nuclei where previously only (γ,n) measurements, being the easier to make, were available. In other words, the emphasis has been placed on more refined measurements and the extension of existing data rather than the verification or examination of aspects of any particular model.

In the following sections, various techniques which have been used previously to study photonuclear reactions involving the emission of charged particles are discussed briefly, and the new method is compared with them. Measurements of photo-neutron spectra are not discussed since few have been attempted and these only with bremsstrahlung (see next section). The fact that neutron spectroscopy is so intrinsically difficult is further reason for the importance of well-resolved proton spectra.

2. Review of previous techniques.

Rather than classify the various techniques according to

whether they are applicable to use with bremsstrahlung or low-intensity monochromatic radiation from particle reactions, each is considered separately since there is some overlap in their application.

On the other hand, the relative merit of a particular method depends very much on the feasibility of its use with each type of radiation. With regard to energy spectra of photo-particles, only the methods which can be employed with monochromatic radiation serve as a means of measurement since, only then, can individual transitions be observed.

2.1. Residual activation. The irradiation of targets, usually with bremsstrahlung, and the subsequent detection of the residual activation which follows the emission of particles as a result of the irradiation, has contributed most to the present knowledge of the absorption process (reviewed by Strauch - St 53). The technique has been employed with bremsstrahlung to obtain the general features of the excitation functions of a large number of reactions (predominantly (γ,n)), and has shown the existence of the giant resonances in them. In addition, the systematics of the location of the giant resonances as functions of mass number have been determined (Mo 53).

The particular value of the technique, apart from the above considerations, is its ability to determine, for some reactions, the relative cross-sections of the various processes which can occur, e.g. (γ,n), (γ,p), $(\gamma,2n)$ and (γ,pn). In such measurements, the various target activities are analysed in detail with a gamma-ray spectrometer

(Ca 57; Ca 58). Other than this, no information on the emission of nucleons can be obtained.

2.2. Irradiation of foil targets and the external detection of photo-particles. Energy spectra of the protons, deuterons and alpha particles emitted from a number of reactions have been obtained by irradiating foils and detecting the particles produced with scintillation crystals (Lo 58) and photographic plates (reviewed by Titterton - Ti 55). A few such experiments have been carried out with monochromatic radiation but the majority have used bremsstrahlung and, for this reason, are able to indicate only the general features of the break-up of the excited nucleus.

It is possible to obtain the angular distributions of the emitted particles by placing an array of plates around the target or, in the case where scintillation counters are used, by rotating the counter about the target. Such measurements constitute the most important contribution of the method although, again, the use of bremsstrahlung limits their value.

Zinc sulphide detectors, which can be used to measure proton yields, are not capable of energy resolution. The systematics of the proton yield variation as a function of atomic number have been measured using this type of detector (Ha 51).

2.3. Observations of reactions within detecting media. The general method of observing photonuclear reactions within detecting media has been employed with gas proportional counters, cloud chambers and nuclear

emulsions. Each of these detectors is capable of energy resolution of the reaction products produced within them.

2.3a. Gas proportional counters. The use of gas counters is restricted to those gases which have "good" counter properties, i.e. the rare gases, deuterium, nitrogen and methane, and the reactions $H^2(\gamma,p)$ - Ba 52; $C^{12}(\gamma,3\alpha)$ - Ca 55; $N^{14}(\gamma,p)$ and $N^{14}(\gamma,\alpha)$ - Ha 56; $Ne^{20}(\gamma,p)$ and $Ne^{20}(\gamma,\alpha)$ - Ha 56a; and $A^{40}(\gamma,p)$ - Wi 53; have been examined in this way. The method has essentially 4π detection of the emitted particles and can therefore be used with low-intensity radiation. The above reactions were observed at 17.6 Mev using gamma rays from the $Li^7(p,\gamma)$ reaction while the $H^2(\gamma,p)$, having a low threshold, has also been investigated at 6.1, 12.1 and 16.7 Mev with gamma rays from the $F^{19}(p,\alpha)$ and $B^{11}(p,\gamma)$ reactions.

With the exception of the $H^2(\gamma,p)$ and $C^{12}(\gamma,3\alpha)$ reactions (where the question of levels in the final nucleus does not arise), the resolution obtained limited the degree to which transitions through levels in the residual nuclei could be identified.

2.3b. Cloud chambers. Cloud chambers are similar to gas counters in that reactions in some gases can be studied, though the visual observation of particle tracks is sometimes an advantage, e.g. with reactions where two or more charged photo-particles are emitted.

The chief deterrent to the use of cloud chambers is the long running times required, even with bremsstrahlung, to accumulate the number of events needed for energy spectra of statistical precision.

Thus the only reactions examined have been $He^4(\gamma,p)$ - Ga 51; $N^{14}(\gamma,p)$ and $N^{14}(\gamma,n)$ - Wr 56; $(\gamma,p\alpha)$ reactions in Ne^{20} - Mo 56 and $H^2(\gamma,p)$ - Pl 50. Of these, only the $H^2(\gamma,p)$ reaction was observed with monochromatic radiation (6.1 Mev).

2.3c. Photographic emulsions. The general method and the experiments which have been carried out are reviewed by Titterton (Ti 55). Reactions involving either the constituent nuclei of the emulsion, e.g. $C^{12}(\gamma,3\alpha)$, $O^{16}(\gamma,4\alpha)$ and $Br^{81}(\gamma,\alpha)$, or nuclei incorporated or "loaded" into the emulsion, e.g. $Li^7(\gamma,t)$ and $B^{10}(\gamma,\alpha)$, can be investigated. The reactions best suited to study within emulsions are those reactions which are readily identifiable from the background of tracks in the emulsion by means of unique features of the tracks produced by the break-up particles, e.g. the three-pronged star from the $C^{12}(\gamma,3\alpha)$ reaction and the "hammer track" from the $Be^9(\gamma,p)$ reaction. Where this is not possible, the energy balance of the particles serves as identification, providing the gamma-ray energy producing the event is known. If the plates are exposed to bremsstrahlung, identification of the tracks without energy balance is necessary.

It is tedious to analyse a large number of events and the resolution which can be obtained is inferior in most instances to that which can be obtained with gas counters, but the use of emulsions has two important advantages over the other methods which have been discussed:

(i) the photodisintegration of most light nuclei can be observed and, if monochromatic radiation is used, energy spectra (of fair resolution) can be obtained. Thus it is the only

method which allows a systematic study of these nuclei, which are of interest because they are more amenable to theory than heavier nuclei, and a number of models have been proposed for the disintegration of such nuclei as Li^6, Li^7 and Be^9.

(ii) it has already been pointed out that if an event can be identified by means of characteristic features of the break-up particle tracks, then the gamma-ray energy responsible for the event can be assigned. If then a plate is irradiated with bremsstrahlung, the number of events as a function of gamma-ray energy can be obtained and, with corrections for the shape of the bremsstrahlung spectrum, the excitation function also. Because of the energy resolution that can be obtained and the fact that an excitation function is derived without recourse to a yield curve, such excitation functions can demonstrate the presence of structure in the excitation function, and thus resonance absorption into levels of light nuclei, in a manner akin to the formation of compound nuclei in particle reactions, has been found.

2.4. Summary.

In summary, it is apparent that none of the methods discussed can conveniently provide comprehensive data concerning the relative intensities of transitions to levels of the residual nucleus and the angular distributions of these transitions, which are the important

parameters of the break-up mechanism. In fact, with the exception of studies of reactions within nuclear emulsions, whereby detailed excitation functions have been obtained, and measurements within gas counters of the $H^2(\gamma,p)$ reaction (for which the cross-section at particular gamma-ray energies is of prime importance in determining the parameters of the interactions assumed for the p-n nuclear model), none of them, to the present time, has contributed more than the general features of the reactions which have been studied with them.

3. The present method.

The present work has extended the general method of Section 2.3 by examining reactions in small thin scintillating crystals. Experiments of this nature have not been carried out previously but several advantages are immediately obvious:

(i) Scintillating materials of good counting properties which incorporate lithium, sodium, potassium, rubidium and cesium (along with iodine) are available, and there are a large number of other scintillators whose properties have not yet been fully evaluated. The alkali halides provide the opportunity of investigating a series of nuclei of increasing atomic number. Gas counters offer a similar range but the difficulty and cost of obtaining such gases as krypton and xenon of sufficient purity and in sufficient quantity to fill a reasonably large high-pressure counter have been prohibitive.

(ii) The target, i.e. the crystal, is dense and the difficulties

of high-pressure counters and the low loading concentrations which can be incorporated into emulsions are avoided.

(iii) The fast decay times of the alkali halides allow fast counting rates without the pile-up of small electron pulses due to the gamma-ray flux being a serious problem. With gas counters, it is often necessary to use relatively long pulse clipping times to obviate resolution spread due to the origin of pulses in various portions of the counter. This limits the allowable counting rates.

(iv) The resolution attainable with scintillating crystals used in this way is approximately a factor of two better than that obtained with either gas counters or emulsions.

(v) The concentration of target nuclei in the crystal and the compactness of the ancillary fittings which go to make up a scintillation spectrometer allow investigations to be made with monochromatic radiation from particle reactions since the counter can be placed very close to the target which acts as the source of the radiation, and so full use of the available intensity is made.

(vi) Since the number of protons or other particles detected depends on the loss corrections applicable to the particular crystal dimensions used, and these corrections depend in turn on the angular distribution of the particles, it is possible, in principle, to measure these angular distributions. Similar

measurements could be made with emulsions, but the use of crystals provides a more satisfactory method from the point of view of convenience and statistics.

All the measurements which are presented have been made with radiation from the $Li^7(p,\gamma)$ reaction. It would be possible to use bremsstrahlung but measurements of particle spectra made with monochromatic radiation are the most important, as has already been indicated in preceding sections.

4. Presentation of material.

Chapter II contains a complete summary of the apparatus and experimental techniques which have been developed to obtain, calibrate and interpret charged particle spectra arising from the irradiation of some of the alkali halide scintillators.

In Chapters III, IV and V, the results obtained for the $Na^{23}(\gamma,p)$, $I^{127}(\gamma,p)$ and $K^{39}(\gamma,p)$ reactions are given. Since the energy level schemes for none of the residual nuclei of these reactions is well known, a considerable portion of the work was devoted to the identification of transitions and the assignment of level schemes to the nuclei concerned. Subsequently, the discussion in each of these latter chapters considers only this aspect of the measurements.

The relation of the work to the general problems of the photodisintegration process is summarised in Chapter VI.

Chapter VII contains the results of what amount to little

more than preliminary measurements with LiI and Li^6I, and some information on the various reactions which can occur in these scintillators has been obtained.

The final chapter discusses the future of measurements using method and shows that a great deal of useful experimental work remains to be done.

CHAPTER II.

EXPERIMENTAL TECHNIQUES.

Introduction.

In this chapter, various techniques pertinent to the use of a scintillation spectrometer to obtain photoproton spectra are described.

Sections 2.1 and 2.2 are concerned with the actual spectrometer itself, dealing with the counter assembly, electronics and the preparation and properties of the phosphors employed.

Sections 2.3 and 2.4 relate to the gamma-ray source, reviewing the $Li^7(p,\gamma)$ reaction and describing the methods of target preparation and the means of flux measurement.

The final sections consider the problems of energy calibration and cross-section measurement which arise as special features peculiar to this type of experiment.

Section 1. The spectrometer - circuitry and assembly.

1.1. Circuitry. Throughout our experiments, E.M.I. Type 6097B phototubes, incorporated in the circuit of Fig.2.1, were used.

The power supply - an E.K. Cole 1033A - was chosen for its ease of fine control adjustment and long-term stability. Pulses from the cathode follower were amplified by a low gain linear amplifier and analysed with a Hutchinson-Scarrott type multi-channel pulse height analyser. Experiment showed that this analyser was not linear for very short pulses, and consequently a double integrating circuit was inserted between the detector output and the amplifier to increase the pulse rise time to approximately 2 microseconds.

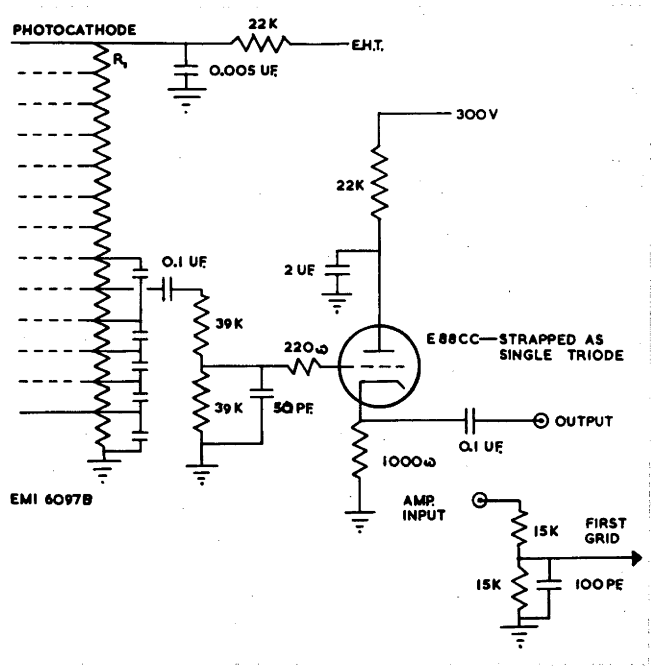

Fig. 2.1. Circuit diagram of phototube resistor chain and cathode follower. All resistors in the chain were 470 K except R_1 which was 680 K. Capacitors in the lower part of the chain were 0.001 microfarads.

1.2. Counter assembly. The counter assembly was designed so that it could be adapted to use in vacuum as a part of the calibration chamber (Section 5) and in air for crystal irradiations (Chapters III-VI). The essential features of the counter assemblies for both applications are illustrated in Fig.2.2.

The normal E.M.I. tube base, by nature of the semi-transparency of the polythene insulation and a central hole, needed considerable modification before it could be employed in such an assembly. A tight-fitting ebonite plug was inserted into the central hole and the base painted with several coats of a solution of black picein wax in trichlor-ethylene (or ether). So treated, the base was light-tight and could be mounted in a way that required only the phototube volume to be sealed, leaving the components of the dynode system and the cathode follower exposed and accessible.

Thin (0.015") brass telescopic tubing was used for the counter casing to minimise the number of electrons produced in the vicinity of the crystal by the incident radiation.

1.3. Gain variations. In the course of the development of the present technique, it was found that gain variations of as much as 25% occurred when crystals were irradiated with gamma rays, and the technique became feasible only when some understanding of the nature of variation was achieved and (more important) when an easily applied method of gain measurement and correction was developed.

Variations of phototube gain with counting rate and temperature

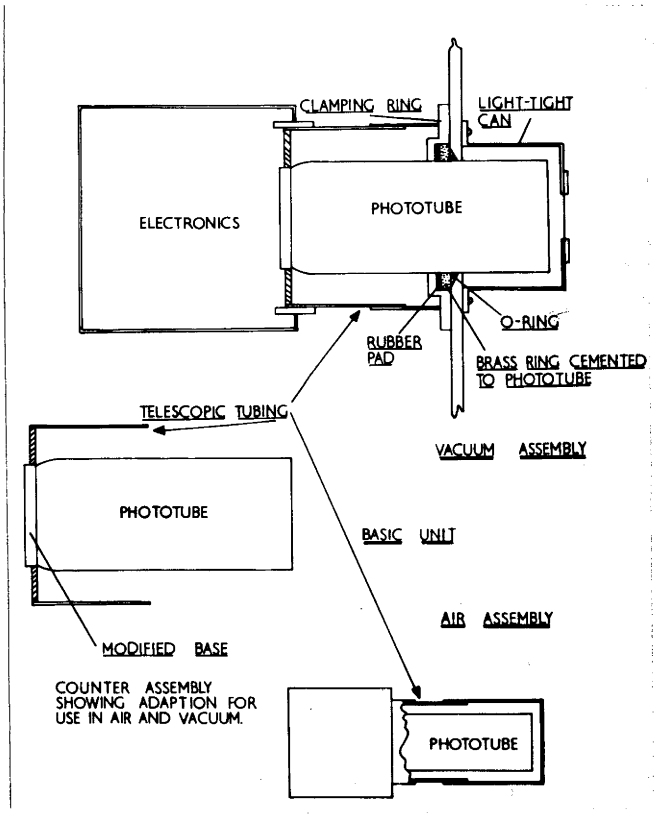

Fig. 2.2. Basic unit to house the phototube and its incorporation into both air and vacuum assemblies.

have been reported (Be 55; Ev 54 and We 55) and these factors were investigated. A considerable portion of the data discussed in this section was obtained over a period of eighteen months with the phosphors and experimental assemblies which are described in succeeding sections, but a general consideration can be made at this juncture without loss of continuity.

(a). Gain monitoring. A constant check on the stability of the total gain of the system was maintained in both counter assemblies with a (ThC + ThC') alpha particle source mounted behind a polythene shutter. To keep the position (pulse height) of the higher energy alpha group constant, the phototube voltage was set so that the counting rates were equal in the two adjacent channels (of the kicksorter display) defining the peak position. A drift in gain produced asymmetry in the two channels and a gain variation of less than 0.25% could be observed and corrected by adjustment of the phototube voltage.

Gain changes over a period of time (Figs.2.3 and 2.4) were obtained from the voltage adjustments required to maintain a constant pulse height in conjunction with the measured gain dependence of the phototube with voltage.

(b). Investigation of gain dependence on temperature. The gain variation of a phototube with temperature was measured by observing the pulse height of the higher energy alpha group from a (ThC + ThC') source as water of variable temperature was circulated around the outside of the counter, and a variation of approximately -1%/C° was recorded.

Sodium iodide, the phosphor used for the investigation, exhibits a pulse height temperature/dependence of $(-0.14 \pm 0.02)\%/C^{\circ}$ (We 55), so that the variation of the phototube itself must be reduced accordingly.

Thus the observed shifts could have resulted, at least in part, by reason of the proximity of the detector (phosphor and phototube) and the bombarded lithium target, which can attain a comparatively high temperature as a result of the high beam currents (50 - 200μa) used. However, the gain shifts persisted when water of temperature constant to within $\pm$ 0.2°C. was circulated through copper tubing soldered to the counter casing. Nevertheless, water cooling was maintained on the counters throughout the experiments.

(c). Variations with counting rate.

(i) Summary of previous investigations. Bell et al. (Be 55), using R.C.A. phototubes, reported increases of pulse height by as much as 20% with changes of counting rate from a few tens to a few thousand counts per second. This change was almost instantaneous, both with regard to its appearance after increasing the counting rate and recovery to the original pulse height when the counting rate was reduced again. A small, long-term effect which persisted for several days, similar to that reported by Caldwell and Turner (Ca 54), was also observed.

Bell et al. also reported a gain increase of 10-30% following the exposure of phototubes (R.C.A. Type 6292) to a weak

light source, providing voltages were applied to the dynodes. We observed this effect with a 6097B tube, which was exposed to weak light with normal voltages on all dynodes. The gain increased by 7%, returning to normal in 40 minutes, whereas Bell et al. found the effect to persist for periods of 24 hours or more. However, such an effect is not applicable in the present instance.

Evans and Parkinson (Ev 54) mentioned gain instability of EMI Type 5311 tubes at high count rates but gave no details of either the magnitude or the nature of the shifts.

(ii) Present observations. It was soon apparent that the gain variations observed were dependent on counting rate or the counting history of the tube, but the effects differed from those reported by Bell et al. Plots of gain versus time for two different counting conditions are given in Figs.2.3 and 2.4. Fig.2.3 shows the gain variation of an EMI Type 6097B tube over a period of 20 hours' continuous counting with two different counting rates. A tendency to a gain increase with the faster counting rate may be seen, but the change is neither instantaneous nor does the increase remain so long as the faster counting rate is maintained. The general features of this curve, viz. the early rise, a relatively long period of nearly stable gain and finally a sharp decrease falling below the original gain setting, were characteristic of almost all the EMI tubes examined, particularly when they were new. Fig.2.4 was also obtained with an EMI tube; after a period of very fast counting when the gain increased,

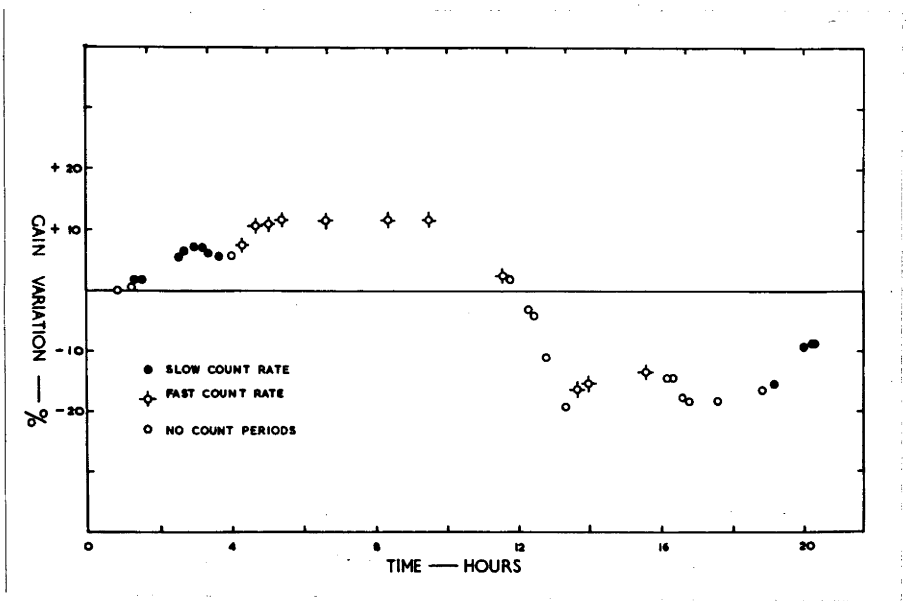

Fig. 2.3. Gain change of an EMI Type 6097B phototube over a period of ten hours with counting at two different rates.

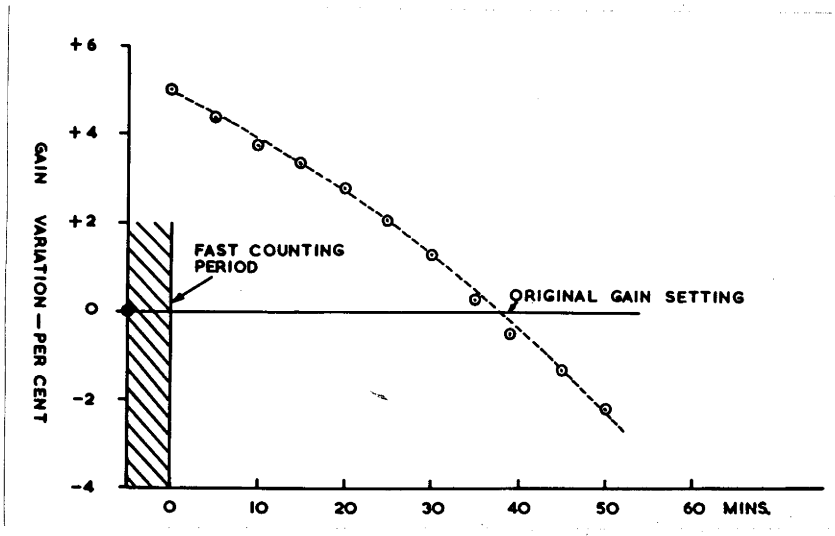

Fig. 2.4. Gain decrease of an EMI Type 6097B phototube after 5 minutes' fast counting.

the gradual decrease of the gain was followed to below the original setting. The same tube, tested a week later under identical conditions, was stable.

An RCA Type 6551 tube showed similar long-term variations at fast counting rates while an instantaneous gain increase was observed with a Dumont Type 6292 tube when the count rate was increased but, as before, the new gain level was not stable.

Figs.2.3 and 2.4 must be regarded only as indications of the observed gain changes. Neither is typical because other tubes behaved only in roughly the same way and, furthermore, the gain variations of a particular tube were not reproducible from day to day. However, as has been mentioned above, the kind of variation shown in Fig.2.3 was most typical of new tubes. Usually the gain of tubes which had been used continuously, i.e. for 10-12 hours per day for a week or more, at high counting rates stabilised, and it was possible to make runs of at least 8-10 hours' duration with an overall gain variation of less than 2%.

(d) Origin of the gain shifts. A systematic investigation into the origin of the gain variations was not attempted since the object was merely to understand the phenomenon sufficiently to enable experiments of the type discussed in Chapter I to be done. In this regard, the knowledge that there were reasonably long periods of time during which the gain was virtually stable or otherwise changed slowly and regularly (and so would allow correction) was of prime importance. However, it

would seem that a surface effect of the dynodes is responsible for the variations. Bell et al. found that, with phototubes exposed to light, the gain shifts occurred only if voltages were applied to the dynodes, i.e. the shifts were the result of electron bombardment of the dynodes, and also, the resolution of the tube was improved so long as the gain shift persisted. These measurements, and the present observations, which showed that the variations were not reproducible from day to day and seemed to depend on the counting history of the tube, provide a strong case for believing that a dynode surface effect is the cause of the shifts rather than the charging of the dynode insulators as Evans and Parkinson suggest.

Section 2. Phosphor preparation and properties.

The scintillation crystals used for the present work fulfilled a dual purpose in that they were both target and detector. As such their dimensions - in particular, thickness - required more careful attention than is normally the case. Although preliminary investigations and the spectrometer calibrations were made with the detector unit within an evacuated chamber, it was desirable to use crystals in air so that protection of hygroscopic phosphors from moisture was necessary. These two factors were the major features of phosphor preparation which had to be considered.

This section describes the preparation of each phosphor and discusses the properties (resolution, particle responses, decay time, etc.) of some of them in so far as a knowledge of the properties was

necessary to interpret spectra arising from gamma-ray irradiation of a particular phosphor.

2.1. Sodium iodide.

(a). Preparation. Sodium iodide blocks were cleaved into pieces approximately 1/8" thick and, in a moisture-free atmosphere, one face was polished and cemented to perspex or directly onto the face of a phototube with Ciba cold-setting Araldite 101. The polishing was done in two stages; the exposed face was cleaned with a fifty-fifty mixture of acetone and chloroform and then polished with soft tissue moistened with carbon tetrachloride.

Since the use of crystals mounted directly onto a phototube is somewhat restrictive, crystals were usually mounted into perspex discs about 1/8" thick. Optically bonded to the phototube face with Dow-Corning silicone fluid, the discs were centrally located with a perspex holder or clamped between brass retaining blocks which were cemented to the phototube with araldite.

It is not usual practice to cement sodium iodide directly to perspex because the crystal-perspex interface deteriorates (due, presumably, to absorbed moisture in the perspex or chemical reaction between the two materials) to an extent ultimately destroying energy resolution by the crystal. A glass disc interposed between the perspex and the crystal will prevent this effect, but the direct mounting was preferred in order to remove any background effects arising from reactions in the glass. If the discs were thoroughly dried in a dry box before sodium

iodide was cemented to them, the crystals could be used for about 21 days on average, although deterioration did occur within a day or two in some cases.

To obtain a uniform crystal thickness, the apparatus shown in Fig.2.5 was used. The sliding fit of the disc holder within the cylinder enabled the crystal to be "cut down" with a damp cloth while ensuring that the exposed face was parallel to the cemented face. Crystals prepared in this fashion were uniform to within at least 0.001", but allowance had to be made for the thickness of araldite which was approximately 0.002". When the precise crystal thickness was required, e.g. for cross-section measurements, the araldite layer was measured at the completion of the run by dissolving away the crystal with a suitable solvent.

Several techniques for protecting sodium iodide from water vapour have been reported in the literature; the general method being to seal a freshly cleaved crystal within a small volume of dry air. Such a procedure was not suitable in the present instance because:-

(a) a sealed detector cannot be used in vacuum.

(b) a form of protection was desired whereby changes of crystal dimension could be made easily, i.e. protection which could be readily removed and re-applied.

These requirements were finally met in the following way. When the required thickness was attained with the apparatus of Fig.2.5, the exposed face of the crystal was quickly dried with tissue, polished with tissue moistened with acetone, and smeared with vaseline. In this

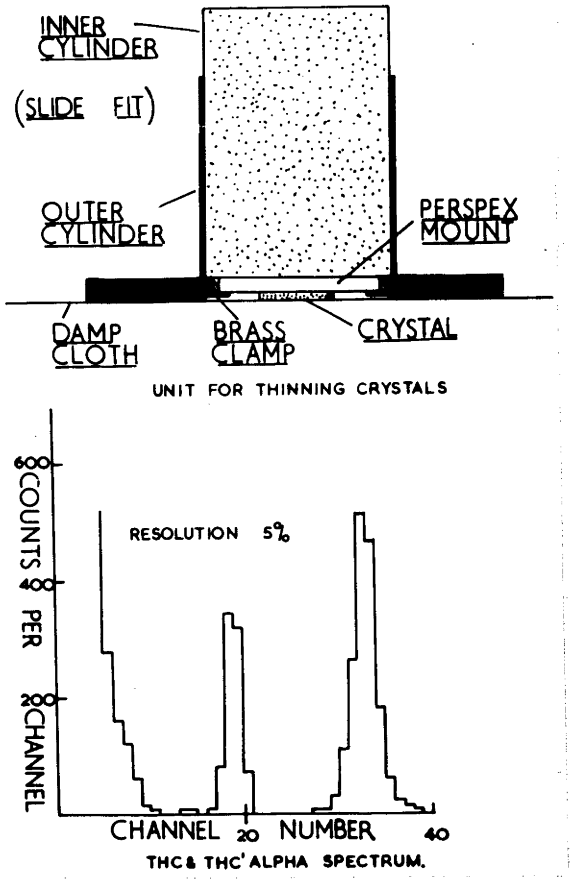

Fig. 2.5. (a) Unit used to prepare thin uniform crystals.

(b) (ThC + ThC') alpha particle spectrum with a resolution of 5% obtained with sodium iodide.

way, a cleaned and polished surface was possible without the inconvenience of having to carry out the operation in a dry box. An aluminium foil (1.5 mgm/cm^2) was then placed over the crystal. By carefully smoothing the foil, any excess vaseline was squeezed out of the foil-crystal interface to form a moisture-proof seal around the sides of the crystal. Tests with alpha particles of various energies demonstrated that absorption by the residual thin grease film over the crystal was well within the error of the assigned thickness of the aluminium foil. Crystals so protected maintained good energy resolution almost indefinitely and the covering foil remained in position when the detector unit was placed under vacuum.

(b). Particle spectra and resolution. Fig.2.5 shows a typical alpha particle spectrum of (ThC + ThC') obtained with a sodium iodide detector of dimensions 1/4" x 1/4" x 0.040"; the energies of the groups being reduced from 8.8 and 6.1 Mev to 7.2 and 4.3 Mev by a 1.5 mgm/cm^2 aluminium foil over the crystal. With a high degree of collimation of the alpha particles, the optimum resolution attained with 7 Mev alpha particles was 4% (full-width at half height); crystals used to obtain $Na^{23}(\gamma,p)$ spectra gave 5-6% resolution with only the fair collimation afforded by the mounting of the alpha source which was used for gain checks.

Proton spectra of the $B^{10}(d,p)$ reaction are given in Fig.2.23 (Section 5). Transitions to the ground state and first two excited states are in evidence with a resolution of 6%, but further collimation would have improved this value since an energy spread of the incident protons accounts for portion of this width.

(c). Heavy particle responses in sodium iodide.* During the calibration of the spectrometer (Section 5) both the proton and alpha particle responses were obtained. The proton response, in agreement with the work of Franzen et al. (Fr 50 and 52) and Taylor et al. (Ta 51), was linear above 3 Mev, but extrapolation to the origin was not sufficiently accurate to provide any evidence for the reported non-zero intercept at -25 Kev (Be 56).

The (ThC + ThC') alpha source, which had been used to check gain stability, enabled a simultaneous determination of the alpha response. The alpha response shape+ was identical to that of the response curves reported by Taylor et al. and Lovenberg (Lo 51), but if the present result and that of Taylor et al. are normalised against their corresponding proton responses, the S_p/S_α ratios for a given energy differ considerably (Fig.2.6). The response of 5.3 Mev alpha particles measured relative to the response of 661 Kev gamma rays by Franzen et al. (Fr 50) is also shown in this diagram. It was observed, too, that the S_p/S_α ratios (for a given energy) varied for different batches of sodium iodide. Both these observations are consistent with the notion of the dependence of the relative responses on the thallium concentration of the crystal (Eb 54; Ha 52).

---

*The response of sodium iodide to Ne^{22} ions is discussed in Chapter IV.

+The calibration alpha response was only established with two alpha energies. The result was later checked with a larger number of energies by interposing a series of aluminium absorbers between an alpha source and the crystal.

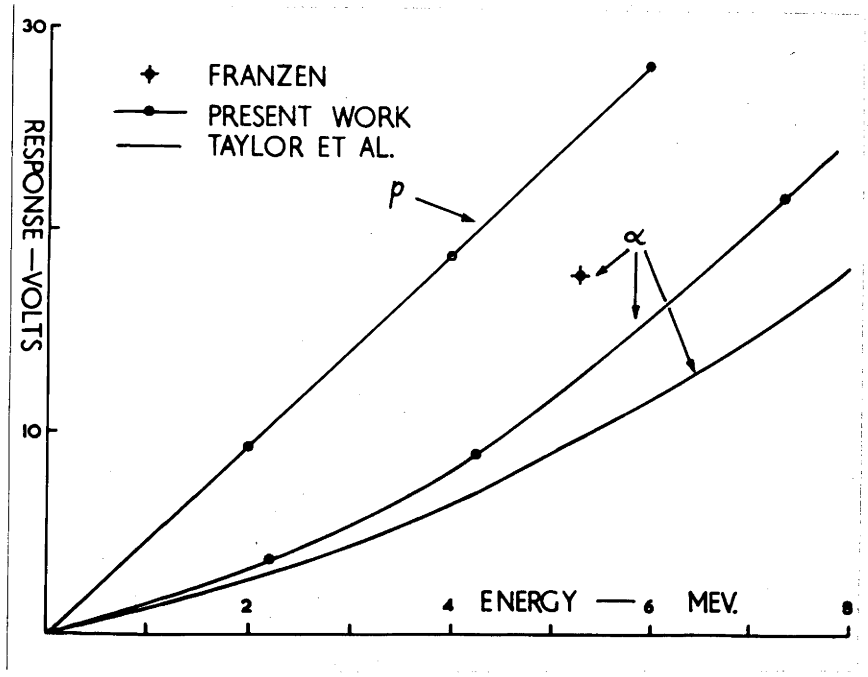

Fig. 2.6. Proton and alpha-particle response curves for sodium iodide.

In view of this evidence, it is important to realise that the relative responses of a particular spectrometer to heavy particles must be measured before meaningful energy calibrations of one particle in terms of the response of another can be assigned. This fact has not always been appreciated in the literature.

(d). Proton range-energy curve. The range-energy relation for protons in sodium iodide (Fig.2.7) was calculated on the basis of the method discussed in Section 6.

2.2. Potassium iodide.

(a). Preparation. This phosphor is not hygroscopic, so that polishing and mounting present no special problems. Water and acetone were used to clean and polish crystals of potassium iodide and it was not necessary to work in a dry box, but otherwise the procedure of Section 2.1(a) was adopted. Although it was not required as a form of protection, an aluminium foil was usually placed over the crystals to improve light collection at the photo-cathode.

(b). Particle spectra and resolution. No measurement of the light output of potassium iodide relative to sodium iodide was attempted but Franzen et al. (Fr 50a) reported a value of 1/4. Resolution comparable to that obtained with sodium iodide was obtained for both alpha particles and protons.

(c). Background due to K^{40}. Long-lived K^{40}, of an isotopic concentration of 1.19×10^{-4} in natural potassium (En 54), is the source of an electron and gamma-ray background in KI detectors. Endt and Kluyver

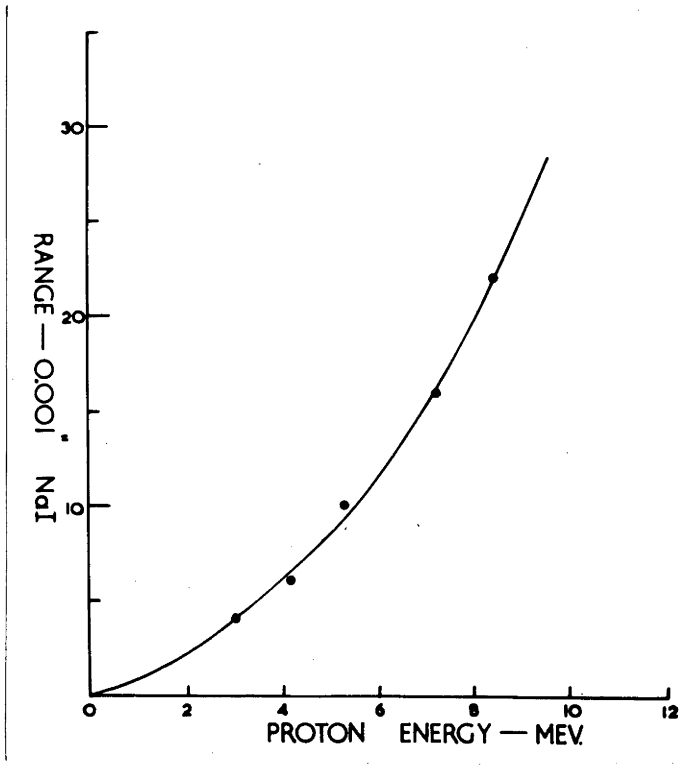

Fig. 2.7. Calculated range-energy relation of protons in sodium iodide.

(En 54), from a summary of experimental data, report that 11% of the transitions proceed by electron capture through A^{40} giving rise to a 1.46 Mev gamma ray; the remaining 89% of the transitions decay by beta emission to Ca^{40}, the electron end-point energy being 1.33 Mev. Using a 3/4" x 1/2" x 1/2" crystal, the decay spectrum of K^{40} was examined, principally as a means of observing the reported 2 milli-second phosphorescence of KI(Tl) (Be 50). The electron spectrum is shown in Fig.28. The inset of Fig.2.8 is a spectrum recorded with better resolution and the 1.46 Mev "photopeak", though not properly resolved, is evident. The energy calibration was obtained with Na^{22} and Co^{60} gamma rays. The existence of a relatively long-lived phosphorescence is demonstrated by the low-energy "tail" of the spectrum which obscures the low-energy portion of the electron spectrum. Neither the one-electron pulses from the phosphorescence nor the K^{40} decay products contribute pulses beyond the lowest energy at which photoprotons were observed, viz. 2 Mev (Chapter VI) so that further consideration was unwarranted.

(d). Proton range-energy curves. The range-energy curve for protons in potassium iodide (Fig.2.9) was calculated on the basis of the method discussed in Section 6.

2.3. Lithium iodide.

(a). Preparation. Lithium iodide is extremely deliquescent - far more so than sodium iodide - and consequently the mounting of lithium iodide crystals required more careful attention than had been necessary for the other scintillators.

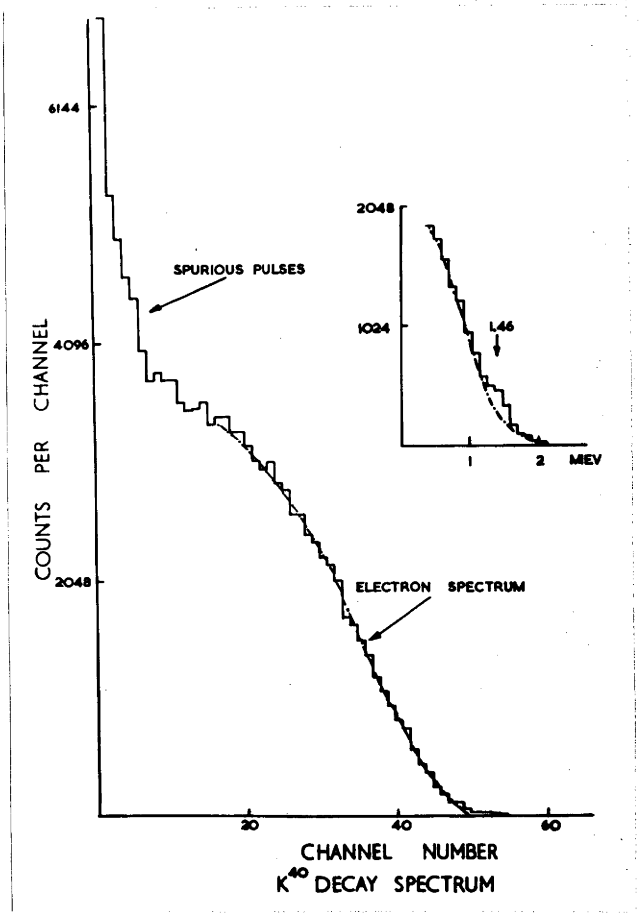

Fig. 2.8. K^{40} decay spectrum showing spurious low-energy pulses which arise from phosphorescences in potassium iodide. The inset shows a spectrum in which the 1.46 Mev gamma-ray is partially resolved.

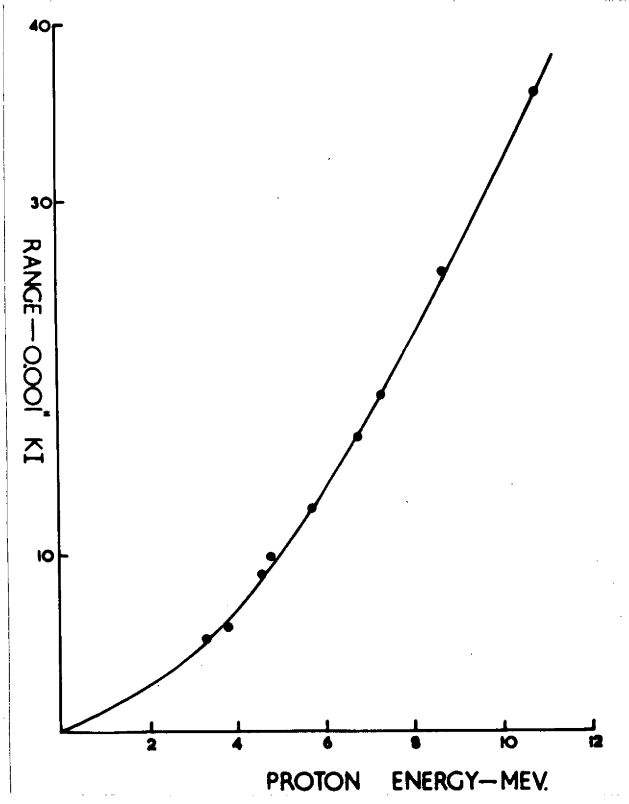

Fig. 2.9. Calculated range-energy curve of protons in potassium iodide.

As before, crystals were mounted on perspex discs, but it was found necessary to interpose a glass disc between the crystal and the perspex, otherwise the crystals deteriorated very rapidly (within a few days - see Section 2.1(a)). In a dry atmosphere, pieces of lithium iodide which had been cut from larger blocks with a fine saw* were polished with acetone and cemented to the mounts with Ciba araldite. To achieve conditions of sufficient dryness, both phosphorus pentoxide and a liquid air trap were used as drying agents in a dry box of standard design.

"Cutting down" to the required thickness and the final polishing of crystals were completed outside of the dry box in the same manner as for sodium iodide except that acetone was used exclusively for both operations. An aluminium foil cover with vaseline surrounding the crystal was again used as a means of protection from water vapour. It was necessary, however, to ensure that all air pockets were squeezed out of the vaseline since even the small amount of mosture contained in these bubbles was sufficient to spoil the crystal. Needless to say, the foils were carefully examined for small pin-holes before being used.

Except for instances where accidental damage of the covering foil occurred, crystals remained clear and retained optimum resolution for periods exceeding one month.

(b). Particle spectra and resolution. The light output of europium-

*Lithium iodide is a plastic-like material (c.f. cesium iodide) and cannot be easily cleaved.

activated lithium iodide* has been reported as 35% of that for sodium iodide for a corresponding energy loss (Ni 55). Resolution comparable to that obtained with sodium iodide was obtained for both alpha particles and protons.

None of the crystals examined showed any evidence of non-uniform activation which is manifested by double peaks in spectra of uncollimated monoenergetic particles or gamma rays.

(c). Response curves of the various particles in lithium iodide. During the calibration of the spectrometer used to examine photonuclear reactions in lithium iodide (Chapter VI), the proton and alpha-particle responses were determined (see also Section 2.3(d)). The resulting curves for both natural LiI and Li^6I are given in Figs.2.10 and 2.11. It will be seen that whereas the proton response is linear, the alpha response, as is characteristic of the alkali halides, is not.

(d). Neutron detection with lithium iodide.

(i) Introduction. Scintillation detection of neutrons with lithium iodide by means of the $Li^6(n,t)He^4$ reaction has been reported by several workers (Ho 51; Sc 52; Be 52; Sc 54 and Ni 55). The cross-section of the reaction is large (930 barns) at thermal energies and a monoenergetic group which is due to the energy loss of the triton plus alpha (Q = 4.785 Mev) within the crystal allows discrimination in the presence of a gamma-ray background.

*All crystals used were activated with europium. The crystals were obtained from the Harshaw Chemical Company, Cleveland, Ohio, U.S.A.

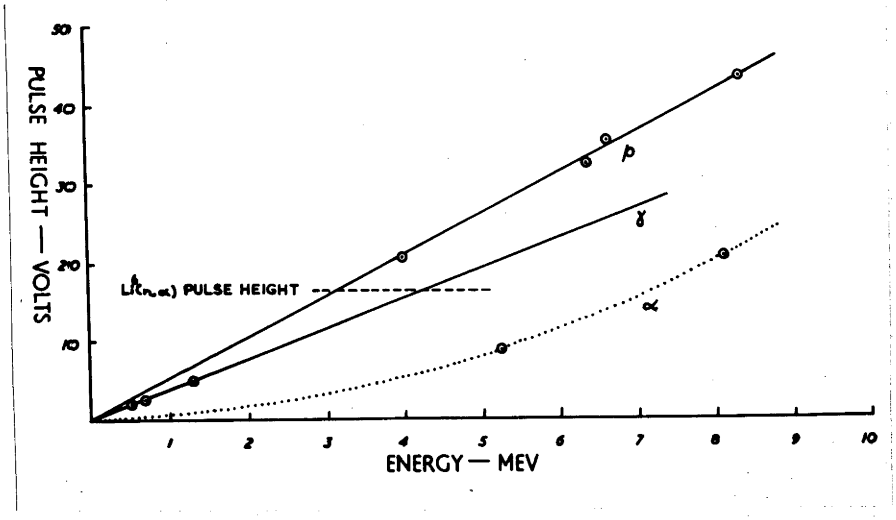

Fig. 2.10. Proton, gamma-ray and alpha-particle responses of natural LiI.

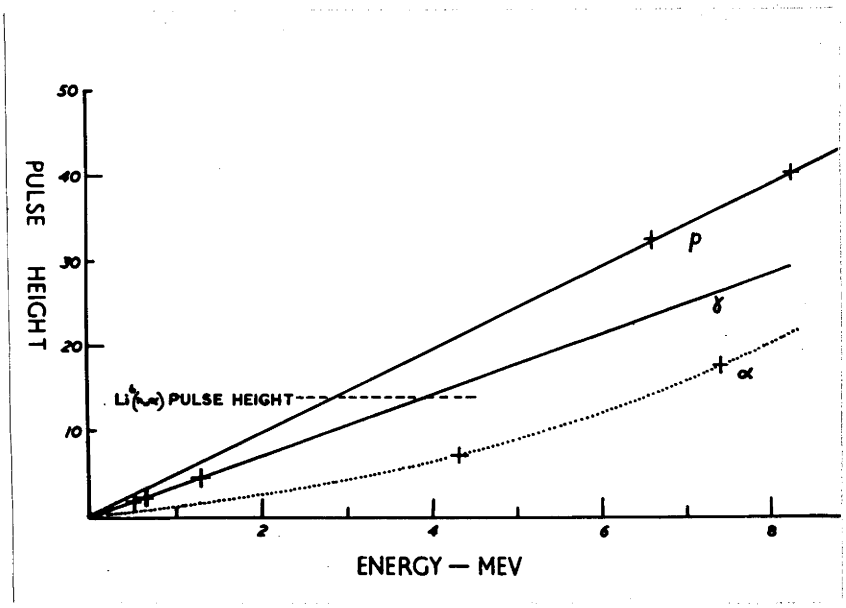

Fig. 2.11. Proton, gamma-ray and alpha-particle responses of Li^6I.

The energy of the triton plus alpha group produced by thermal neutrons has been given as 4.0 Mev (Ni 55), 4.1 (Ho 51), 4.5 (Sc 52) and to within 6% of 4.8 Mev (Be 52); these measurements having been made with lithium iodide activated with either tin, thallium or europium in varying amounts. Each energy measurement was made by comparing the pulse heights of the triton plus alpha group and the 661 Kev gamma-ray line of Cs^{137} or, in the case of Hofstadter et al. (Ho 51), the 1.17 and 1.33 Mev gamma rays of Co^{60}. Schenk and Neiler (Sc 54) extended the measurements to higher neutron energies and found that the energy of the group was not a linear function of $(E_n + Q)$ in the energy region $E_n = 0 - 16$ Mev; the neutron points lay below the gamma-ray response for values of $(E_n + Q)$ less than 8 Mev, and above for values of $(E_n + Q)$ greater than 8 Mev.

While it was realised that the triton plus alpha group produced by thermal neutrons would serve as a useful calibration point for spectra obtained by irradiating LiI crystals with gamma rays, the above data needed further consideration before this could be done.

There is no a priori reason to suppose that the properties of lithium iodide will differ greatly from those of sodium iodide, but in relation to the known responses of the latter phosphor, the above data are difficult to explain. Taylor et al. (Ta 51) showed that, for sodium iodide, the proton and deuteron responses were linear and almost coincident, while the alpha response was non-linear and, at a given energy, considerably less than the proton response (Section 2.1(c)). It has been commonly supposed that both the electron (gamma ray) and triton responses would be linear and identical, or very nearly so, to the proton curve. No

measurements to confirm the latter assumption have been reported in the literature.

Two inconsistencies in the data become apparent. Firstly, it is surprising that the energy release of the triton plus alpha within the crystal is as large as 4-4.8 Mev. The particles would give rise to a group at approximately 3.3 Mev in lithium iodide (the exact energy being determined by the activator concentration (Section 2.1(c)) if the response curves of Fig.2.10 are used and it is assumed that the triton and proton responses are equal. Secondly, the release of energy exceeding $(E_n + Q)$ for some values of E_n is inadmissible. In an attempt to clarify this anomaly, Schenk and Neiler investigated the effect of europium concentration on the energy of the triton plus alpha group produced by thermal neutrons. The energy of the group increased with the amount of activation until a concentration was attained for which the group energy exceeded the anticipated maximum of 4.8 Mev. The energy release would be expected to increase with activator concentration since the proton-alpha ratio (for a given energy) decreases with activator concentration (Eb 54), but it should not exceed the actual total energy of the particles.

Both difficulties are removed if the assumption is made that the triton and gamma-ray responses do not coincide.* Measurements of the proton, gamma-ray and alpha-particle responses of natural LiI and Li^6I (96% Li^6), in conjunction with the $Li^6(n,t)$ group, were made to test the validity of this assumption.

---

*Or, alternatively, the gamma-ray and proton responses coincide but differ from the triton response.

(ii) Experimental procedure. The counter assembly (Fig.2.12) employed was essentially similar to the calibration chamber which is described in Section 5. Protons from the $B^{10}(d,p)$ reaction produced at a deuteron bombarding energy of 300 Kev were used to determine the proton response curve and aluminium absorbers of various thicknesses were interposed between the detecting crystal and the boron target to increase the number of proton energies available. The protons were observed at 90° rather than at 0°, as is the case in the calibration chamber. The 8.78 and 6.1 Mev alpha groups from a (ThC + ThC') source and gamma rays from Cs^{137} (661 Kev) and Na^{22} (0.51 and 1.28 Mev) were employed to establish the alpha and gamma-ray responses. Crystal mounting was as described above. The $Li^{6}(n,t)$ group was obtained with an uncollimated Ra-Be source. A paraffin block, placed between the source and the detector, moderated the neutrons.

(iii) Results. Two sets of measurements were recorded with natural lithium iodide using different crystals and foil thicknesses and were in excellent agreement. The crystal dimensions were 1" x ½" x 0.15" and 1/4" x 1/4" x 0.050". The larger crystal resolved the highest energy gamma ray used, viz. the 1.28 Mev line of Na^{22}, with resolution better than 12% and the $Li^{6}(n,t)$ group with 7% resolution. The Na^{22} and $Li^{6}(n,t)$ spectra for this crystal are given in Fig.2.13. The smaller crystal, though of inferior resolution, was sufficiently large to allow identification of the group at 1.28 Mev.

One measurement was made with a $Li^{6}I$ crystal of dimensions

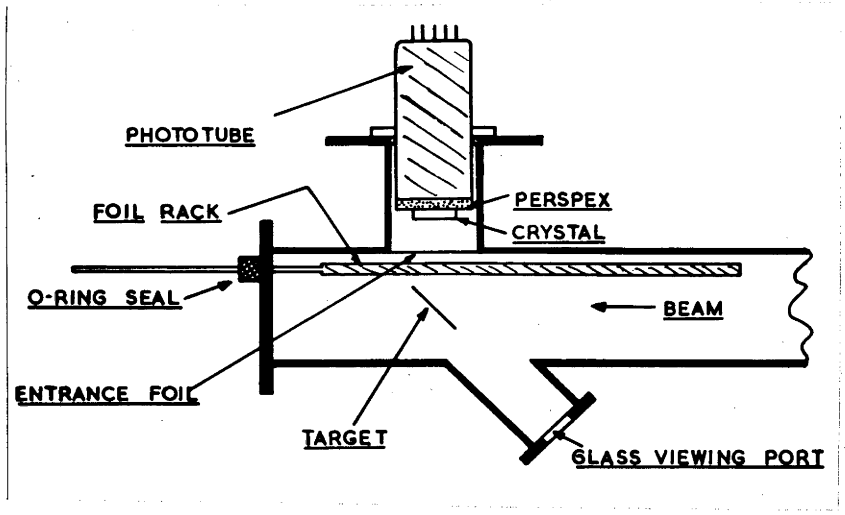

Fig. 2.12. Sketch of target chamber used to obtain the various crystal responses. The alpha source was mounted on the foil rack. Details of the phototube mounting, etc. are given in Fig. 2.2 and Fig. 2.21.

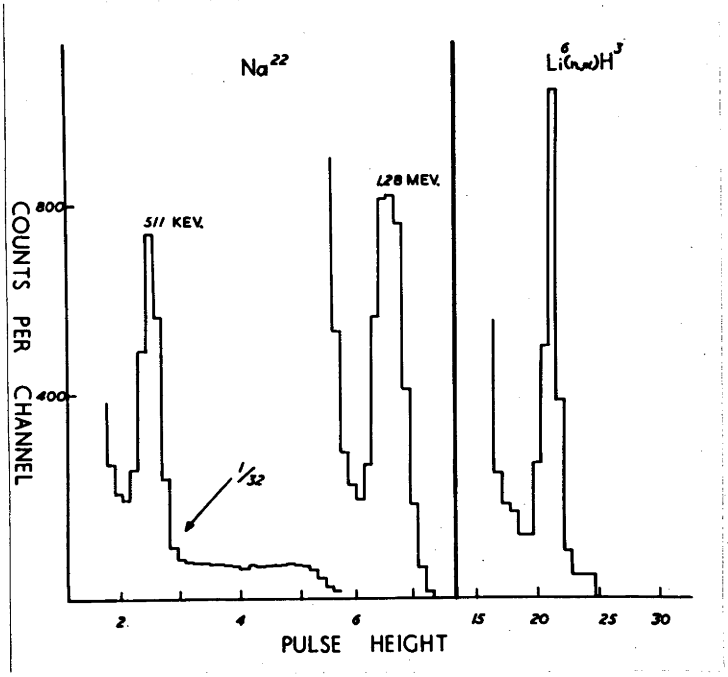

Fig. 2.13. Spectra of Na^{22} gamma rays and the $Li^{6}(n,t)$ group obtained with a lithium iodide crystal of dimensions 1" x $\frac{1}{2}$" x 0.15".

$\frac{1}{2}$" x $\frac{1}{2}$" x 0.15".

Figs.2.10 and 2.11 represent a summary of the above measurements and those made during the calibration (Section 2.3(c)).

It will be seen that there is a difference between the gamma-ray and proton responses, and a linearity check of the electronics (Fig.2.14) ruled out the possibility that the proton and gamma-ray points might be fitted to a common line of non-zero intercept.

The energy of the alpha particle produced (with thermal neutrons) in the $Li^6(n,t)$ reaction is 2.16 Mev and the energy of the triton is 2.6 Mev. In natural lithium iodide, the contribution of the alpha particle is equivalent to that of a 0.5 Mev proton so that the difference between the measured triton plus alpha group energy (relative to the proton response) of 3.25 Mev and the contribution of the alpha particle, viz. 2.75 Mev, is the equivalent proton response of a triton of 2.6 Mev energy. Similarly, it follows for Li^6I that the proton energy giving an equivalent response to a 2.6 Mev triton is 2.4 Mev.

Thus the proton and triton responses can be regarded as approximately equal from this measurement (since the accuracy is limited by the alpha response curve which was only determined with two points). A further discussion of the response of tritons in lithium iodide is given in Chapter VI.

A summary of the results for both scintillators is tabulated in Table 2.1.

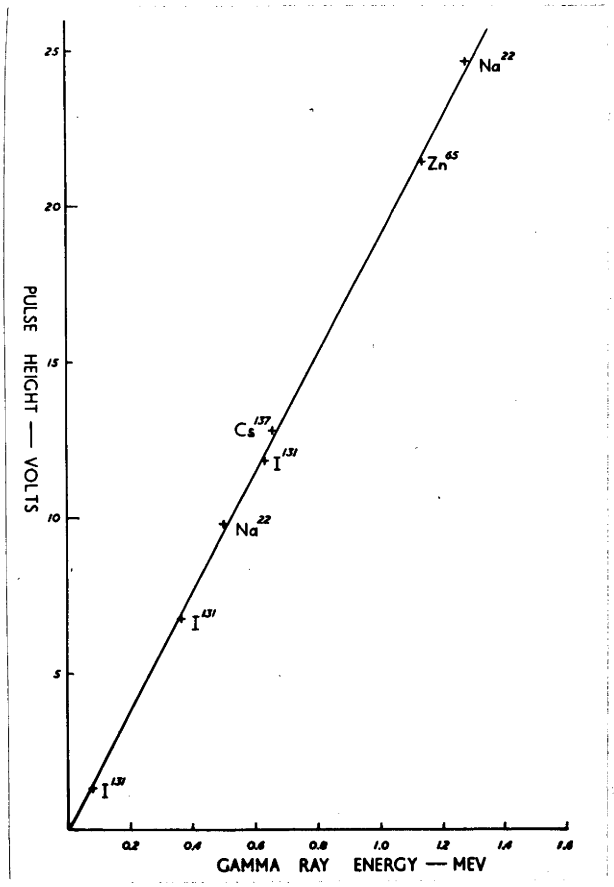

Fig. 2.14. Linearity check of the electronics. Gamma-ray sources used to obtain each point are indicated.

TABLE 2.1.

Dimensions of crystal	Energy of $Li^6(n,t)$ group		Contribution of 2.6 Mev triton
	(1)*	(2)*	
(a) Natural lithium iodide			
1" x ½" x 0.15"	3.2 Mev	4.1 Mev	2.8 Mev
1/4" x 1/4" x 0.04"	3.3 Mev	4.2 Mev	2.7 Mev
(b) Separated Li^6I			
½" x ½" x 0.15"	2.9 Mev	3.8 Mev	2.4 Mev

*(1) Relative to proton response.
(2) Relative to gamma-ray response.

TABLE 2.2.

Scintillator	Electron energy equivalent to a 5 Mev proton
NaI	7.2 Mev
KI	approx. 7.5 Mev
CsI	7.3 Mev
LiI	6.7 Mev
Li^6I	6.9_5 Mev

(iv). Discussion. Having established that the triton and gamma-ray responses of lithium iodide are considerably different, the apparent anomalies discussed above are easily resolved. Clearly, neutron energy measurements are only possible if protons are used for calibrations of the crystal (unless the relative proton (triton)-gamma ray responses are known) or the actual neutron response determined. In relation to the present work, the results indicate that the triton plus alpha group can be used for check calibrations of photoproton spectra providing the energy of the group is taken as 3.25 Mev for natural lithium iodide and 2.9 Mev for Li^6I (for the particular batch of crystals used).

(v). Measurements with other scintillators. Measurements of the proton-gamma ray responses were also made with NaI, KI and CsI, and the results for these scintillators are listed in Table 2.2 where the electron energy giving a pulse height equal to a 5 Mev proton in each of the scintillators is given.

(e). Particle range-energy curves in lithium iodide. The range-energy relation for protons in lithium iodide (Fig.2.15) was calculated on the basis of the method discussed in Section 6. The deuteron and triton curves were estimated from the proton curve by assuming that the rate of energy loss of all three particles depends only on the particle velocity.

Section 3. The gamma-ray source.

3.1. Summary of experimental data of the $Li^7(p,\gamma)$ reaction. The

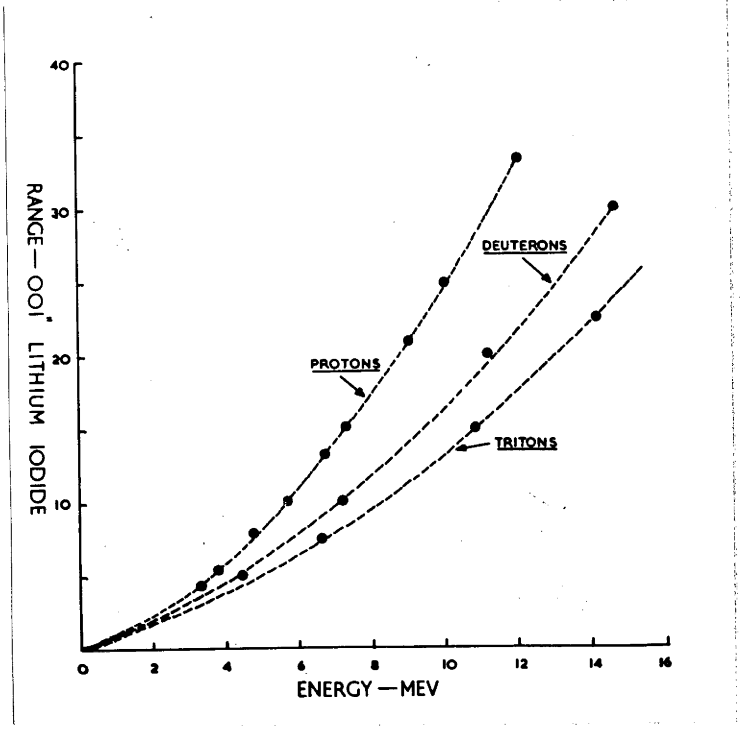

Fig. 2.15. Range-energy curves for protons, deuterons and tritons in lithium iodide.

$Li^7(p,\gamma)$ reaction was used as the gamma-ray source for all of the present experiments. This reaction is well suited to photodisintegration studies since it has a high gamma-ray yield ($10^{-8}\gamma/p$) and gives rise to a relatively simple gamma-ray spectrum apart from the obvious advantage of the high energies of the two gamma rays.

The energies of the main gamma-ray components (any other gamma rays in the spectrum have a total intensity not exceeding 4% - In 53) have been measured at a proton bombarding energy of 441 Kev as (17.6 ± 0.2) Mev and 14.8 ± 0.3 Mev (Aj 55); the width of the higher energy component being only 12 Kev, while measurements indicate that the 14.8 Mev component, which corresponds to a transition through the broad 2.9 Mev level of Be^8, is approximately 2 Mev wide (St 51).

The reaction exhibits two resonance, one at 441.4 Kev and another, but much smaller, resonance at 1030 Kev (Aj 55). Stearns and McDaniel (St 51), using a pair spectrometer, measured the ratio of the gamma-ray intensities at 441 Kev as 1.7 ± 0.2 (17.6 : 14.8) and as 0.62 ± 0.7 at the higher resonance (both measurements at 0°). Devons and Hine (De 49) - geiger counter and absorbers, and Campbell (Ca 56) - scintillation counter, have investigated the region between the two resonances. Both found the ratio of the intensities at 90° to be approximately unity in the region of 650 Kev.

Spectra* of the gamma rays produced at 490 Kev and 805 Kev with a target about 80 Kev thick (Fig.2.16) demonstrate quite clearly the

*See Section 4.2 for details of the gamma-ray spectrometer which was used to obtain the spectra of Fig.2.16.

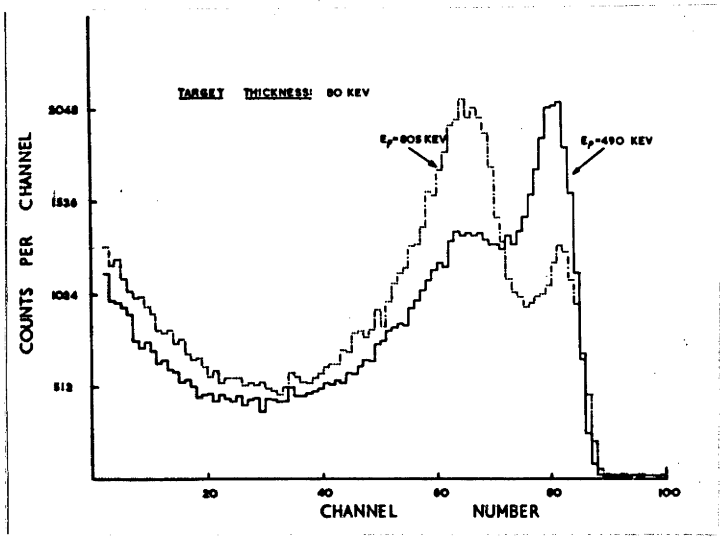

Fig. 2.16. Spectra of the gamma rays from the $Li^7(p,\gamma)$ reaction at resonance and non-resonance proton bombarding energies.

difference of the gamma-ray content at these two proton bombarding energies.

The major portion of the work described in the succeeding chapters was carried out using radiation obtained at the lower resonance since the intensity obtainable is larger and the 17.6 Mev component is predominant, but where difficulties of interpretation occurred, spectra were also recorded using radiation produced at a higher proton bombarding energy. The increased proportion of the 14.8 Mev component at higher proton energies accentuated those portions of the spectra due to 14.8 Mev gamma rays relative to spectra obtained with gamma rays from the low energy resonance and definite identification of transitions could be made.

3.2. Preparation of lithium targets. All targets used to produce $Li^7(p,\gamma)$ radiation were of lithium metal deposited on copper backings either by evaporation or electro-deposition. Thick targets for resonance radiation were made exclusively by the evaporation of lithium metal, but thin targets for the non-resonance runs were prepared by either method although evaporation, being much simpler, was favoured. Some aspects of the two methods are discussed briefly here.

(a). Evaporation. It is customary to silver-plate copper before depositing lithium on it in order to obtain greater adhesion. However, it was found that lithium metal, evaporated directly onto copper without the usual intermediate layer of oxide and nitride which results from the evaporation of lithium, was extremely tenacious. The layer of oxide and nitride was avoided by covering the target backing with a shutter which

was operated externally with a magnet. The backing was exposed only when the contaminants had been boiled off from the lithium metal in the tungsten "boat".

Immediately after evaporation the target, while still hot, could be transferred in air to the target assembly and pumped without deterioration due to water vapour.

(b). Electro-deposition. Lithium metal targets of accurately controlled thickness were prepared by the electro-deposition of lithium from a solution of lithium chloride in pyridine (Aj 52). Since Ajzenberg stresses the necessity of using pure pyridine, suitable precautions were observed. Analar pyridine was initially dried over potassium hydroxide and twice distilled with further drying over potassium hydroxide between distillations. Hydrated lithium chloride was maintained at 110°C for some hours to remove surface water and finally dried by heating in vacuo. In this form the salt could be stored in a vacuum desiccator indefinitely without deterioration. The glass electrolysis cell was airtight to prevent the absorption of water vapour during target deposition. With such checks of purity and dryness, target preparation was straightforward.

Targets were laid down satisfactorily on platinum and aluminium backings, the residual surface of the target backing being protected with a coating of paraffin - a wax insoluble in pyridine but easily removed with other solvents. A solution of paraffin in ether was recommended by Ajzenberg for this purpose, but molten paraffin was found to be more effective in that it was easier and quicker to apply and remove.

Considerable trouble was experienced in depositing directly on to copper, and it became necessary to plate the backings with platinum.

During electrolysis, a brown colouration of the pyridine was produced in the vicinity of the graphite anode, but admixture of this possible contaminant with the cathode compartment was prevented by a glass sinter between the two compartments. Occasionally, an orange-brown jelly-like deposit formed over the target area and interfered with lithium deposition. This was found to be due to the interaction of pyridine with chromic acid which was retained by the sinter after the cell had been cleaned. Prolonged washing of the cell and the use of other cleaning solutions overcame the difficulty.

Targets, both tenacious and uniform, of thicknesses up to 2.5 mgm/cm^2 were prepared in this way.

Section 4. Gamma flux measurement.

4.1. Introduction. The method of gamma-ray flux monitoring or measurement employed in a particular experiment is generally determined by both the type of radiation to be measured (i.e. whether bremsstrahlung or monochromatic gamma rays) and the nature of the experiment. Thus for bremsstrahlung investigations, where high-intensity beams are available, the activities induced in copper or tantalum foils during an irradiation are measured and the gamma flux is deduced from the known data of the (γ,n) reactions in these elements.* Such a measurement is not usually suitable for experiments using monochromatic radiation from particle

*Ion chambers are also employed with bremsstrahlung.

reactions although Hirzel and Waffler (Hi 47), in an activation experiment using 17.6 Mev gamma rays, used copper foils in this way to obtain the relative yields of various (γ,p) and (γ,n) reactions which gave rise to activities with half-lives in the vicinity of the half-life of Cu^{62} (10 minutes).

Photonuclear events in nuclear emulsions are assigned cross-sections by a comparison with the number of $C^{12}(\gamma,3\alpha)$ stars occurring in the emulsion - the cross-section for this reaction having been obtained in terms of the available methods of flux measurement by a number of workers (Go 53; Na 54; Ca 55).

However, for most experiments with monochromatic radiation, the means best suited for monitoring is the use of calibrated geiger counters of the type described by Barnes et al. (Ba 52). Barnes et al. calibrated a thick-walled brass geiger counter at a gamma-ray energy of 6.1 Mev by means of the almost complete one-one correspondence of the low-energy alpha particles and the 6.1 Mev gamma rays emitted at the 340 Kev resonance of the $F^{19}(p,\alpha)$ reaction, and at a gamma-ray energy of 17.6 Mev with an ionisation chamber.

Similar geiger counters were used for the present experiments.

4.2. Construction of the counters. Fig.2.17 shows the details of the counter used by Barnes et al. (Ca 56a), and the sensitivity curve which they obtained from a calibration of it is given in Fig.2.18.

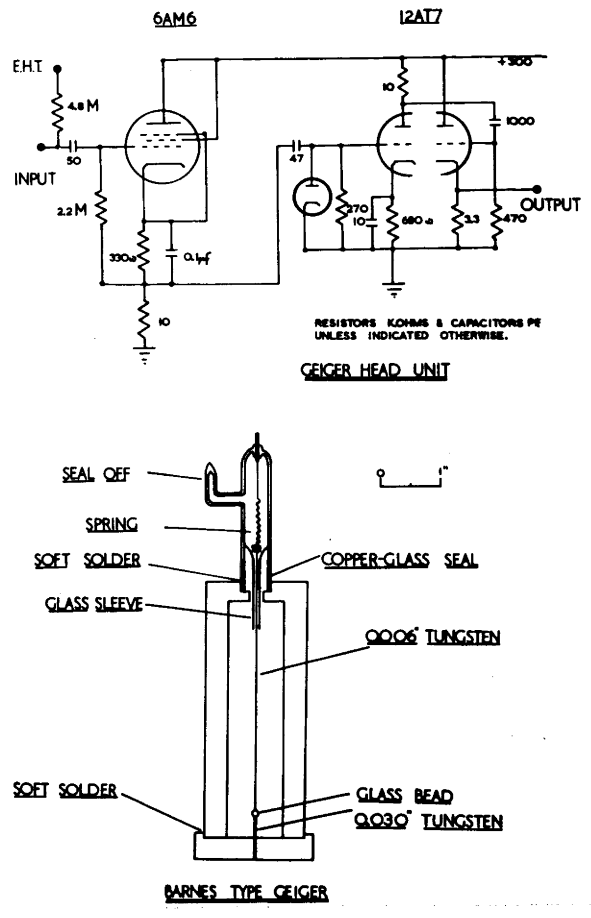

Fig. 2.17. Details of the Barnes type geiger counter and the circuit diagram of the head unit used with the counter.

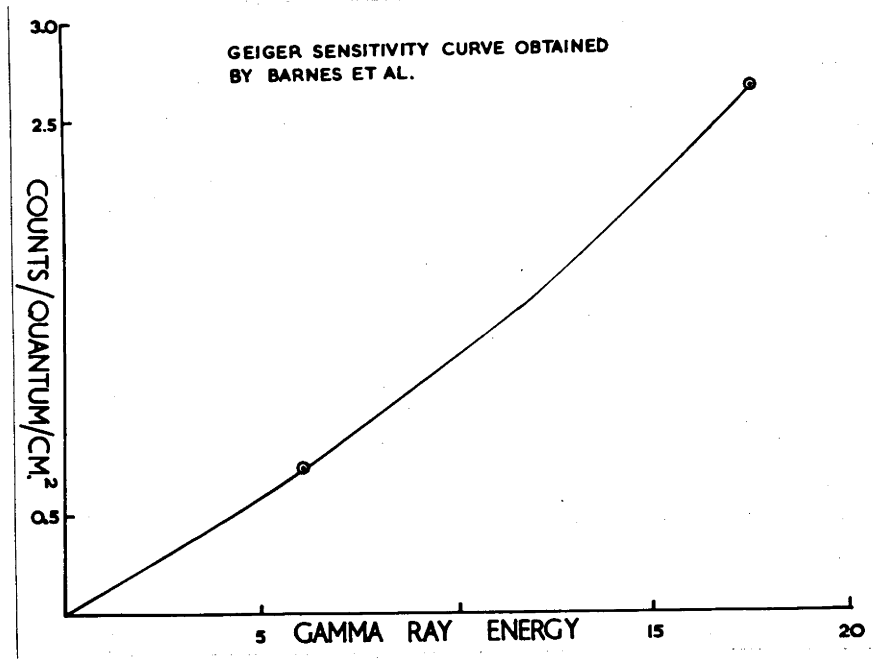

Fig. 2.18. Sensitivity curve reported by Barnes et al. for the Barnes type counter.

Two replicas of this counter were made and compared at 6.1 and 17.6 Mev. The sensitivities were identical to within 5% at both gamma-ray energies. However, the counters had a life of only 4 weeks, presumably due to outgassing of the brass despite efforts made during filling to outgas the counters as completely as possible. Consequently, three commercial glass-walled geiger tubes* (20th Century Electronics Type B.12) were mounted within thick brass cylinders and their sensitivities relative to the Barnes-type counters determined at both 6.1 and 17.6 Mev.

The latter three counters were subsequently used for flux measurements associated with the determination of the cross-sections of the reactions under study. The counter sensitivities were checked from day to day with a Standard Co^{60} source.

4.3. Calibration of the counters. Although the original counters were exact replicas of the Barnes counters and some reliance could be placed in them because their sensitivities were identical, re-calibration would be desirable. Calibration at 6.1 Mev is, in principle, simple, but as the gamma-ray sensitivity was really required for the higher energy $Li^7(p,\gamma)$ radiation and an extrapolation from the lower energy is not necessarily reliable, it was felt that attention should be given to a calibration of the counters at 17.6 Mev.

The use of an ionisation chamber for an accurate measurement

*Type B.12 tubes have a normal argon-alcohol filling. Halogen quenched counters, with the inherent advantage of a much longer life, were examined but the existence of spurious pulses of an oscillatory nature made this tube type unsuitable for quantitative use.

is questionable since the calculation of the absolute sensitivity of such a counter is fraught with difficulty. A more attractive approach to the problem lies in the use of a large sodium iodide crystal as a detector. The absorption coefficients of gamma rays for the various processes in sodium iodide are known and the spectrum of the gamma rays which could be obtained would serve as a valuable guide to the validity of the calculations using them.

Preliminary measurements have been made with a right cylinder of sodium iodide 5" in diameter and 4" high.* It was found that essentially total absorption occurred if the gamma rays were directed into the centre of the crystal through a $\frac{1}{2}$" collimator and spectra similar to the resonance spectrum given in Fig.2.16 were obtained. It therefore appears that the method is feasible, but until such time as accurate measurements are made with the crystal, the sensitivities given by Barnes, viz. 2.66 counts/quantum/cm^2 at 17.6 Mev and 2.1 counts/quantum/cm^2 at 14.8 Mev, have been assumed.

Section 5. Energy calibration.

Some features of the difficulty of assigning energy calibrations to proton spectra produced within a crystal have been mentioned in Section 2, where it was indicated that alpha particles of known energy can only be used if the proton and alpha responses of the particular crystal to be calibrated are known. Even with such information, accurate calibration

*The author would like to thank Mr. D. S. Gemmell of this laboratory who kindly loaned the complete crystal spectrometer for both the measurements of the $Li^7(p,\gamma)$ spectrum (Section 3) and the above geiger calibration.

is unlikely.

Calibrations for the present experiments were obtained by comparing the photoproton spectra arising from the irradiation of each crystal with spectra of protons from the $B^{10}(d,p)$ reaction. This reaction was chosen for calibration purposes since the high Q-value (9.23 Mev) of the reaction and the large level spacing of the lower levels of B^{11} provide well-separated proton groups of energies ranging between 4.5 and 9 Mev (for low deuteron bombarding energies).

5.1. The calibration chamber. The calibration chamber (Fig.2.19) was designed to measure both $B^{10}(d,p)$ spectra and (γ,p) spectra in a way that enabled changeover from one measurement to the other in 15-20 minutes while all of the electronic equipment, including the phototube, was kept operating.

5.2. The calibration procedure. To obtain the $B^{10}(d,p)$ spectra, the target holder is moved to position A and the target (1 mgm/cm^2 natural B_2O_3 on 1.5 mgm/cm^2 aluminium foil) bombarded with a 5μa beam of 300 Kev deuterons. The foil rack immediately behind the target carries aluminium absorber foils which serve to increase the number of calibration points. Generally four foil thicknesses were used, the amounts of absorber depending on the particular calibration. Proton energies were obtained from the data of Ajzenberg and Lauritsen (Aj 55) and the range-energy tables of Aron et al. (Ar 51). A typical set of $B^{10}(d,p)$ spectra, obtained with the absorber thicknesses indicated on each spectrum and at

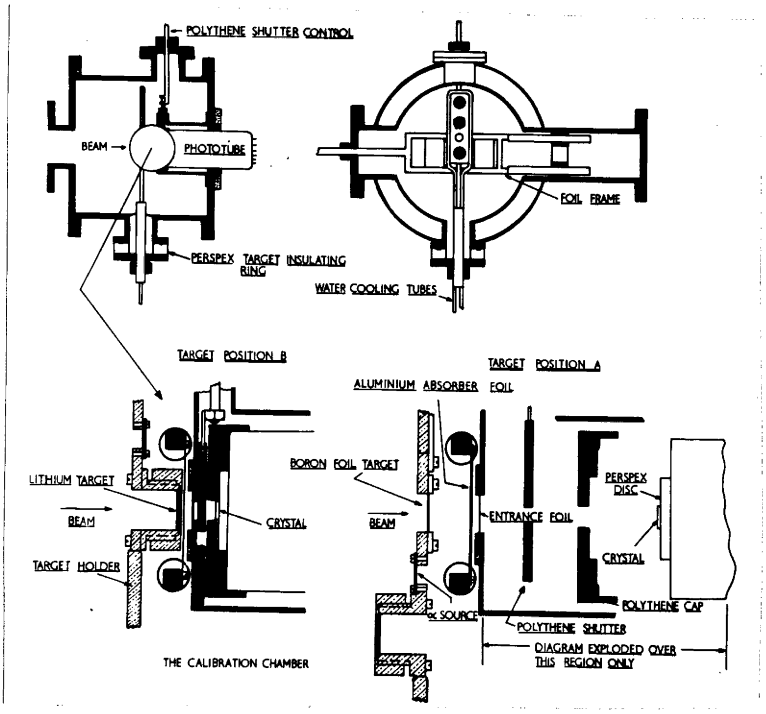

Fig. 2.19. The calibration chamber.

a deuteron energy of 300 Kev, is given in Fig.2.20.

In measuring the (γ,p) spectra, the polythene shutter was closed and the target shifted to position B, in which position the thick lithium target was bombarded with 100μa of protons at 600 Kev. At this proton energy, the field of the beam analysing magnet is the same for both the deuteron and proton beams and any corrections for the slight change in phototube gain caused by the leakage field of the magnet are avoided. The gain of the system was checked with the (ThC + ThC') alpha source before and after each individual run for both the $B^{10}(d,p)$ and (γ,p) spectrum measurements. The (γ,p) measurement was followed by a repeat measurement of the $B^{10}(d,p)$ spectra.

Individual calibrations are described in Chapters III-VI and further discussion pertinent to each particular calibration is given in those chapters.

Section 6. Cross-section measurements.

Introduction. Normally, irradiations were carried out with the crystals as near to the target as possible to make full use of the available intensity, but under such conditions the geometry was poorly defined and special good geometry runs were recorded in order to establish cross-sections. Moreover, a knowledge of the range-energy relations of protons in the various scintillators is necessary for an estimation of the fraction of protons which escape from the crystal. No comprehensive data of this nature exist in the literature.

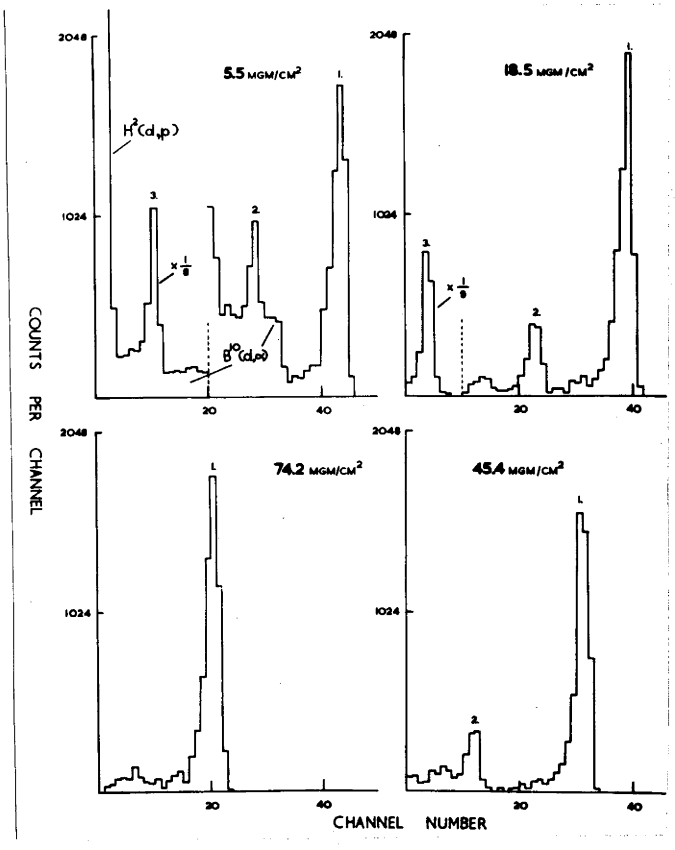

Fig. 2.20. $B^{10}(d,p)$ spectra obtained with the indicated foil thicknesses. Deuteron bombarding energy was 300 Kev.

Each of the above factors is discussed in this section and the method of range calculation is compared with incidental experimental evidence.

6.1. Solid angle considerations of the target-crystal system. The solid angle subtended by a rectangle of dimensions 2a x 2b at a point on the axis of the rectangle at a distance d from the rectangle is:-

$$4 \arcsin \frac{ab}{(a^2 + d^2)^{1/2} (b^2 + d^2)^{1/2}} \quad \text{..... Appendix I.}$$

The finite size of the target makes it desirable to choose a geometry for which the variation of solid angle over the target diameter can be disregarded. In Appendix II, choosing a circular crystal for simplicity of analysis, an expression is derived for the difference between the solid angle at the centre and periphery of a target. The results are summarised in Table 2.3 where the various values of target and crystal size and target-crystal spacings are evaluated in terms of the solid angle variation. From this table, a target diameter of 1/8", crystal dimensions of $\frac{1}{2}$" x $\frac{1}{2}$" and a target-crystal spacing of approximately 0.8" were selected to be used for cross-section measurements.

6.2. Loss corrections. For monoenergetic particles of range R produced isotropically in a layer of infinite extent and thickness 2d, the fraction of particles wholly stopped within the layer is given by:-

$$f = (1 - R/4d) \quad \text{for} \quad R < 2d$$
$$= d/R \qquad\qquad R > 2d \quad \text{(Gr 48).}$$

TABLE 2.3.

Distance from target	Diameter of crystal	$\Delta\omega_o/2\pi$	Distance off axis	$\frac{\Delta\omega_o - \Delta\omega_a}{\Delta\omega_o}$
0.5"	0.5"	0.106	0.25"	0.247
			0.187_5"	0.139
			0.125"	0.062
	0.75"	0.2	0.25"	0.173
				0.097
			0.125"	0.043
0.75"	0.5"	0.0513	0.25"	0.139
			0.187_5"	0.078
			0.125"	0.035
	0.75"	0.106	0.25"	0.110
			0.187_5"	0.062
			0.125"	0.028
1.00"	0.5"	0.030	0.25"	0.084
			0.1875"	0.047
			0.125"	0.021

Using the ranges calculated by the method described in the succeeding section, appropriate corrections for the escape losses were derived.

6.3. Range-energy calculations.

The calculation of the range-energy relations for protons in the various scintillating materials was based on two assumptions, viz. the rate of energy loss of a proton in a compound is determined by the rate of energy loss in each of the constituent elements such that the atoms comprising the compound individually contribute to the slowing down of protons as though the other element was not present, and secondly, that the shape of the range-energy curve is the same for both constituent elements and for the compound. Making these assumptions, it follows that:-

$$A/R = A_1/R_1 + A_2/R_2$$

where

$A = A_1 + A_2$

R_1 = range of proton of energy E in A_1 (mgm/cm^2)

R_2 = range of proton of energy E in A_2

R = range of proton of energy E in A.

Thus for each proton energy for which the range was required, R_1 and R_2 were obtained from the plot of range (mgm/cm^2) versus atomic number using the data of Aron et al. (Ar 51) for aluminium, copper, silver and lead. At high proton energies (above 4 Mev) the four points so obtained lay on a smooth curve, but below this energy there was considerable scatter (Fig.2.21). The corrections for protons in this energy

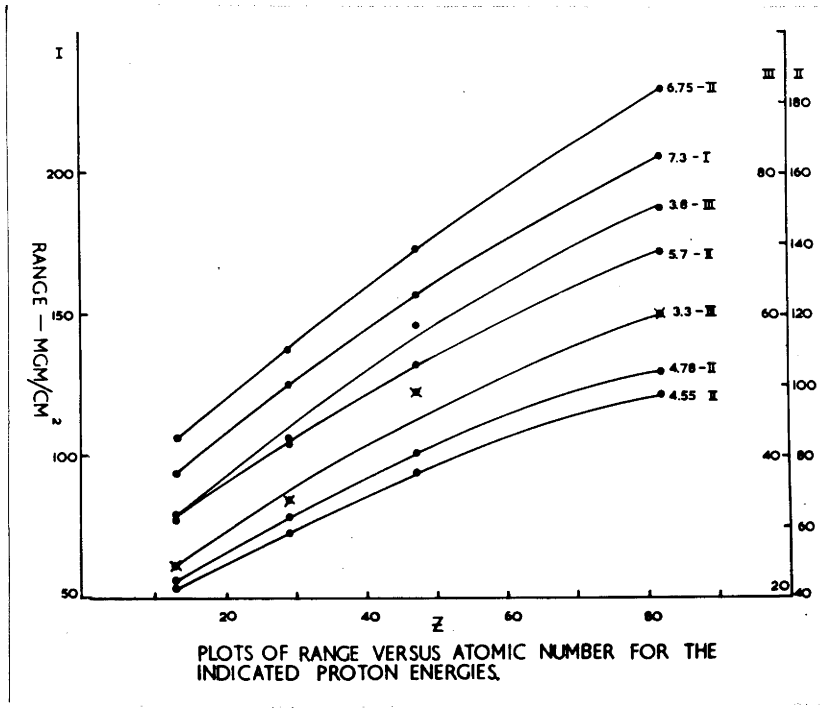

Fig 2.21. Plots of stopping range versus atomic number for various proton energies.

region are small and it was rarely possible to determine the numbers of photoprotons at these energies accurately so that the range estimations below 4 Mev were not important.

Range-energy curves calculated for sodium iodide, potassium iodide and lithium iodide by this method have already been given in Section 2.

6.4. Comparison of calculated ranges with experimental data. No attempt was made to check any one of the range-energy curves experimentally, but some indirect evidence, which at least broadly confirms the results, was obtained.

A 0.016" thick sodium iodide crystal, calibrated with $B^{10}(d,p)$ protons, had a linear response up to an energy of approximately 7 Mev, and the pulse height of a proton group observed beyond this energy was considerably less than would have been expected from an extrapolation of the lower calibration points. When a thicker absorber foil was used to reduce the energy of the group to below 7 Mev, a good fit of the pulse height relative to the other points was obtained. The calculated range of 0.016" for a 7.2 Mev proton would appear to be in good agreement with this observation.

The cross-section measurement described in Chapter III was made with four independent geometries and crystal thicknesses to gain some indication of the consistency with which the loss corrections and solid angle calculations could be made. The good internal agreement of the

results, viz. 2.49, 2.46, 2.68 and 2.57 mb. is further support to the reliability of the range data.

The range of 14 Mev protons in sodium iodide has been reported as approximately 0.040" by Evans and Parkinson which is in fair agreement (considering the accuracy of the measurement) with the calculated range of 0.045".

Appendix I.

Calculation of the solid angle subtended by a rectangle at a point on the axis of the rectangle.

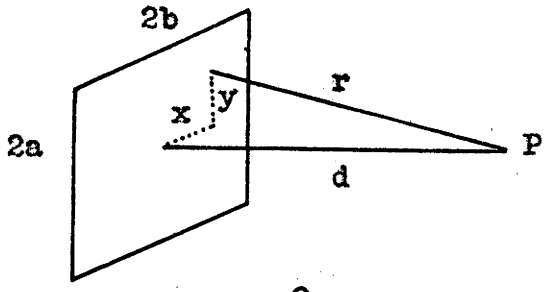

Consider area element dx.dy at (x,y,0). Then the solid angle it subtends at P is given by

$$d\Omega = dx.dy.\cos\theta/r^2 = d.dx.dy/r^3$$

$$= \frac{d.dx.dy}{(x^2 + y^2 + d^2)^{3/2}}$$

Then $$\Omega = d\int_{-a}^{a}\int_{-b}^{b} \frac{dx.dy}{(x^2 + y^2 + d^2)^{3/2}}$$

By successive substitution, the value of this integral is given by

$$I = 2\int_{u_1}^{u_2} \frac{du}{(c^2 - u^2)}^{1/2}$$

where $a^2 + d^2/a^2 = c^2$; $y = d.\tan\theta$ and $u = \sin\theta$

Thus $2I = \text{arc sin}\,(y/(c^2d^2 + c^2y^2)^{1/2})\Big|_{-b}^{b}$

and $$\Omega = \text{arc sin}\left\{\frac{ab}{(a^2 + d^2)^{1/2}(b^2 + d^2)^{1/2}}\right\}$$

Appendix II.

Calculation of the difference of solid angle subtended by a circular crystal at the centre and periphery of a target of finite diameter.

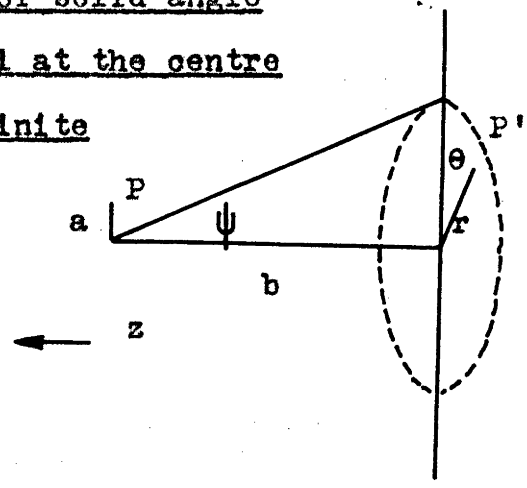

Coordinates of P are (a,0,b) and of P' (r.cos θ, r.sin θ, 0).

$$(\text{Distance } PP')^2 = (a - r.\cos\theta)^2 + (r.\sin\theta)^2 + b^2$$

$$= a^2 + b^2 - 2ar.\cos\theta$$

The projection angle is given by arc cos b/PP'.

If (a) is the solid angle subtended at P, then

$$(a) = \int_0^c r.dr \int_0^{2\pi} b/(a^2 + b^2 - 2arc\ cos\ \theta + r^2)^{3/2}\ d\theta$$

Expanding in powers of a and simplifying,

$$\frac{\Omega(0) - \Omega(a)}{\Omega(0)} = \frac{3a^2.\cos^3\psi.\sin^2\psi}{4b^2(1 - \cos\psi)} + O(a^4/b^4)$$

where $\Omega(0) = 2(1 - \cos\psi)$

CHAPTER III

PHOTODISINTEGRATION OF SODIUM.

1. Electron background.

Introduction. Photoprotons produced within a phosphor material will be observed only if the magnitude of the electron pulses, which result from the gamma-ray flux, is sufficiently reduced. Since sodium iodide was the first scintillator investigated, the nature of the electron background was examined with this scintillator, but the results hold equally well for the other materials in which photoproton reactions were observed. A counter assembly of the type described in Section 2 was employed.

1.1. Source of the electron pulses. High-energy electrons will be produced by the gamma-ray flux in both the materials around the crystal and in the crystal itself. Small changes (approximately 10%) in the magnitude of the background were observed when the thickness of the target backing was reduced, and to minimise the number of electrons produced externally to the crystal, the target backings were 0.040" thick (the minimum thickness which would allow adequate cooling of the target) and the counter casing constructed of thin (0.015") brass telescopic tubing.

High-energy electron pairs, which will travel almost normally to the crystal, lose approximately 500 Kev in traversing a crystal thickness of 0.020", so that large pulses can only be produced by electrons scattered along the crystal or by "pile-up" of a number of these small pulses.

Using a crystal of dimensions 3/4" x 3/4" x 0.020", electron pulses as large as 6.5 Mev* were observed (Fig.3.1). It was estimated

*This energy and those energies given subsequently in relation to the electron background are relative to the proton response of the crystal. The true electron energy is somewhat higher (Chapter II, Section 2.3(d)).

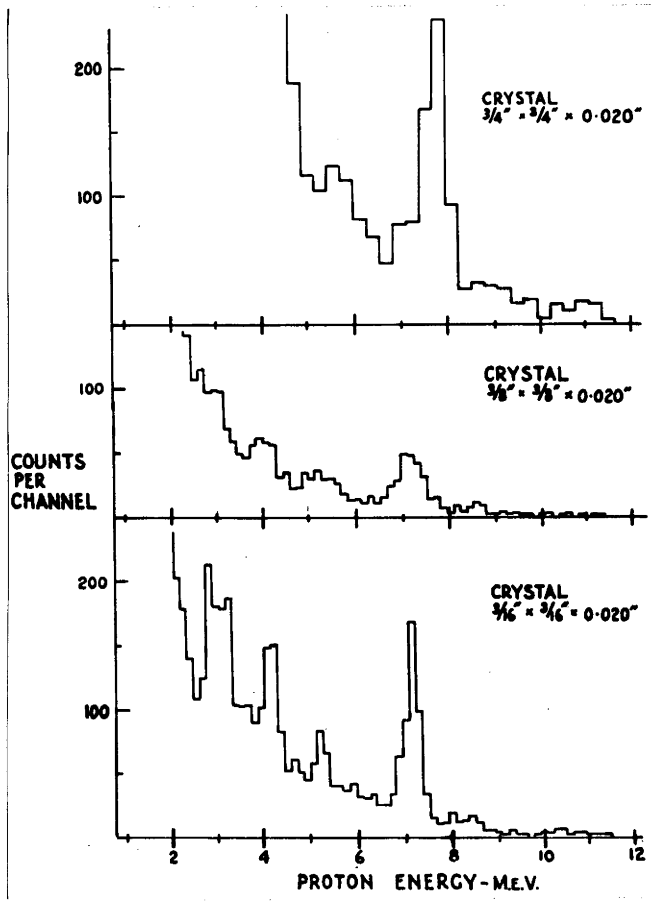

Fig. 3.1. Spectra illustrating the effect of crystal size on electron background.

that too few electrons (approximately 10^5/sec.) would be detected to make pile-up important and, in fact, the electron background was unaltered when the gamma-ray intensity was varied by a large factor; thus few of the higher energy electron pulses were due to pile-up.

The dependence of the background on scattered electrons implies that the factors controlling its magnitude will include the crystal area and thickness in so far as the area will define the maximum path length of a scattered electron (i.e. the energy of the leading edge) and the thickness the extent to which an electron, initially scattered along the crystal, will be retained within the crystal - i.e. the number of electrons which will expend the maximum possible energy in the crystal.

Fig.3.1, in which the spectra of crystals of dimensions 3/4" x 3/4" x 0.020", 3/8" x 3/8" x 0.020" and 3/16" x 3/16" x 0.020" are shown, indicates a reduction of the energy of the leading edge from approximately 6.5 Mev to 2.5 Mev as the area is reduced by a factor of 16 (the energy of the leading edge has been considered as the energy obtained by extrapolating the sharply decreasing portion of the background). Similarly, for a given area, the energy of the leading edge decreased as the crystal thickness was reduced.

The above measurements are in general accord with the simple explanation given above and they serve as a means of choosing crystal size for a particular spectrum measurement. However, the precise nature of the background is by no means clear. It was found that the energy of the leading edge was not merely the energy loss of an electron traversing the

maximum dimension. For instance, the electron background of a crystal of dimensions 1/8" x 1/8" x 0.050" was essentially identical to that of a crystal of area 1/4" x 1/4" and of the same thickness and, also, the energy of the leading edge for crystals of dimensions 1/4" x 1/4" x 0.020" and 1/8" x 1/8" x 0.24" was the same although the magnitude of the "tail" of the background was much less for the smaller crystal (Figs. 3.1(c) and 3.5).

1.2. Selection of crystal size. For a given run, the crystal dimensions were chosen to achieve a compromise between the magnitude of the background in the region to be examined, the photoproton counting rate and the fraction of protons escaping from the crystal.

2. Experimental method.

The counter assembly is shown in Fig.3.2. Details of crystal mounting and protection, the electronics and gain monitoring, have been given in Chapter II. Polythene, of a thickness sufficient to stop protons of energy less than 10 Mev, surrounded the crystal so that protons produced externally would not be detected. No high-energy protons are produced in the polythene since the threshold of the $C^{12}(\gamma,p)$ reaction is 15.95 Mev. Reactions occurring in the perspex and in the aluminium foil over the crystal, mainly $O^{16}(\gamma,p)$ and $Al^{27}(\gamma,p)$, are unavoidable sources of photprotons but their contribution to the total will be approximately 5% for each reaction assuming cross-sections for the $O^{16}(\gamma,p)$ and $Al^{27}(\gamma,p)$ reactions as half and twice the cross-section of the $Na^{23}(\gamma,p)$ reaction.

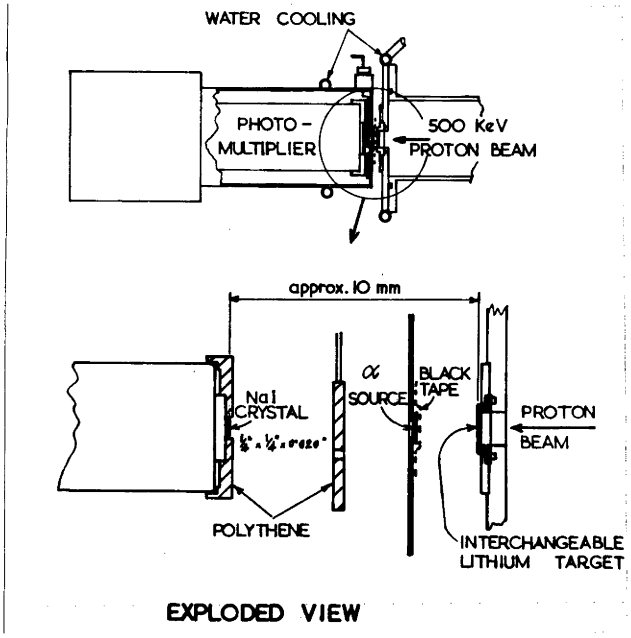

Fig. 3.2. Scintillation counter for studying the $Na^{23}(\gamma,p)$ reaction.

Energy calibration of the crystal has been described in Chapter II, Section 5. Details of the calibration of sodium iodide are given in Section 6.

3. Results.

3.1. Identification of transitions. The following spectra (each representing a summation of a number of individual runs of approximately 45 minutes' duration) were recorded using resonance radiation from a thick target.

(a). Sodium iodide crystal 3/16" x 3/16" x 0.018"* mounted on glass (Fig. 3.1(c)).

(b). Sodium iodide crystal 1/4" x 1/4" x 0.016" mounted on perspex (Fig.3.3).

(c). Sodium iodide crystal 1/4" x 1/4" x 0.038" mounted on perspex (Fig.3.4).

(d). Sodium iodide crystal 1/8" x 1/8" x 0.024" mounted on perspex (Fig.3.5).

Spectrum (c) was intended to cover the region above 7 Mev. The range of a 7.2 Mev proton in sodium iodide is approximately 0.016" (Chapter II, Section 6) and a large proportion of photoprotons with energies in excess of 7 Mev will escape from a crystal 0.020" thick. The other spectra were mainly concerned with the region below 7 Mev.

---

*The actual crystal thickness was 0.018". The dimensions given with Fig.3.1 include araldite thickness.

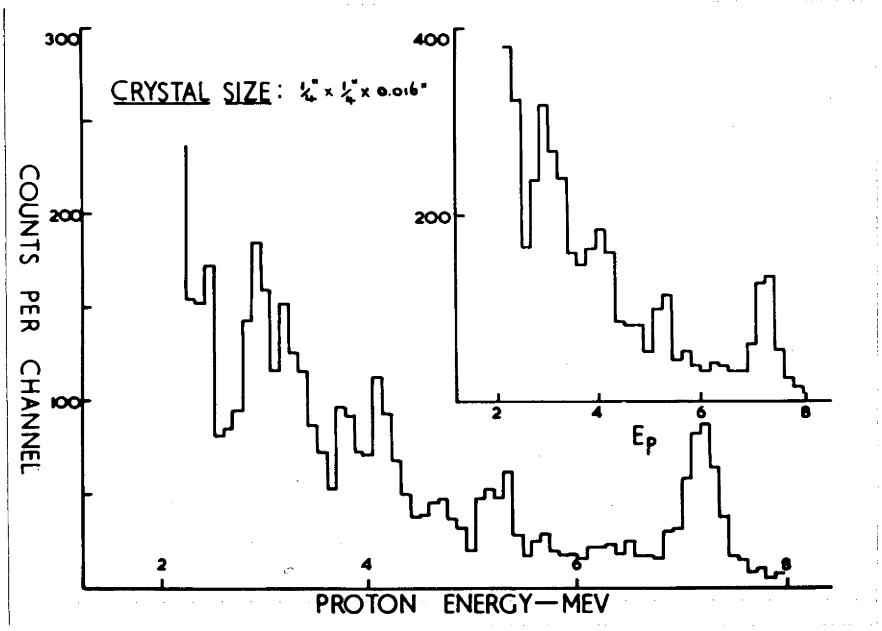

Fig. 3.3. Spectrum for crystal 1/4" x 1/4" x 0.016".

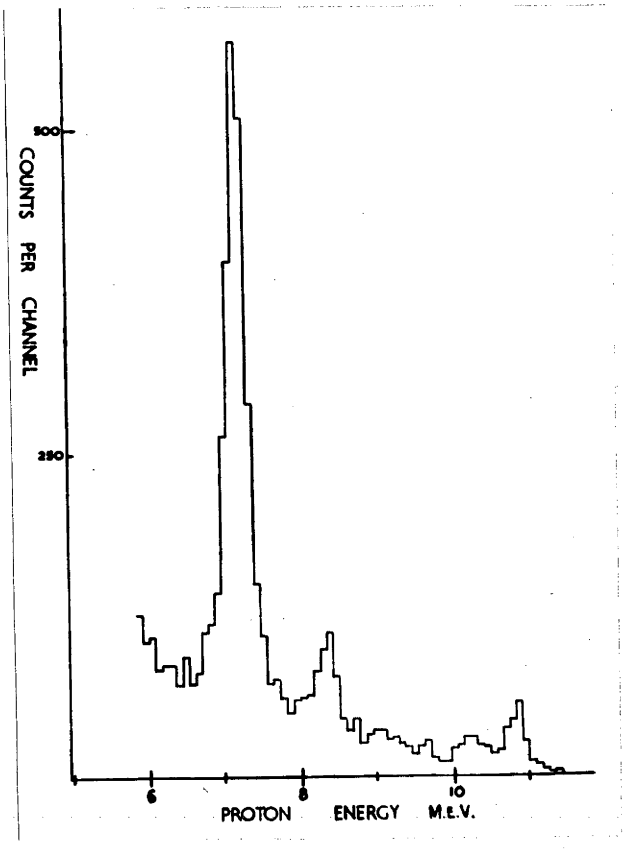

Fig. 3.4. Spectrum showing detail above 6 Mev. Crystal size 1/4" x 1/4" x 0.038", and running time was 2 hours. Most of the protons beyond the 8.4 Mev group are attributed to the $I^{127}(\gamma,p)$ reaction.

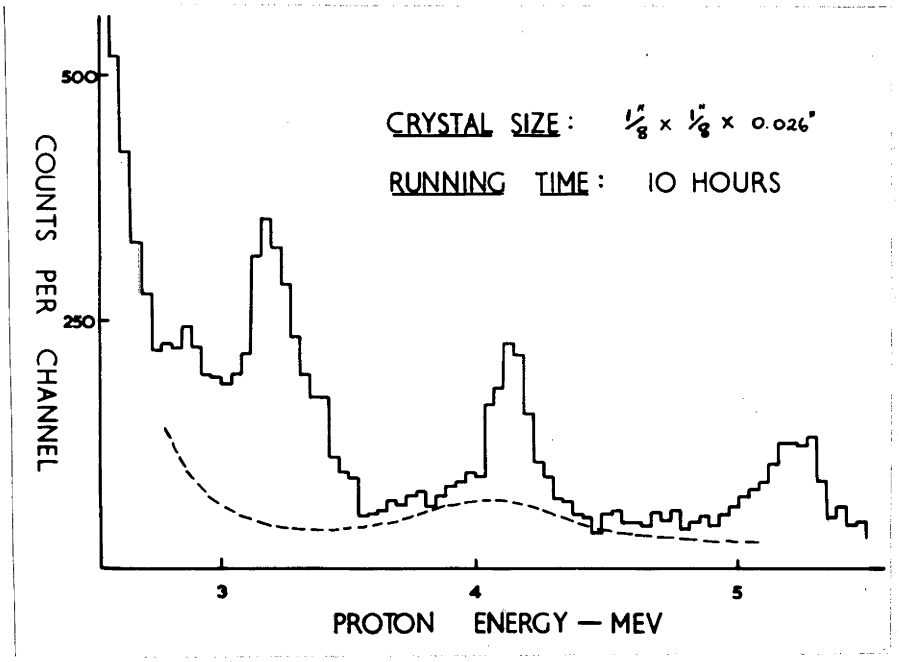

Fig. 3.5. Spectrum showing detail between 2.5 and 5.5 Mev. Crystal size 1/8" x 1/8" x 0.026", and running time 10 hours.

The observed spectra contain photoprotons from both the sharp 17.6 Mev line and the broad 14.8 Mev line of the $Li^7(p,\gamma)$ spectrum. To assist in the identification of photoproton groups due to the 17.6 Mev component, a spectrum produced with non-resonance radiation at a proton bombarding energy of 850 Kev with a thin (~100 Kev) lithium target* was obtained along with a spectrum recorded under identical conditions with resonance radiation (see Chapter II, Section 3). The two spectra are shown in Fig.3.6.

Comparison of the spectra of Fig.3.6 enables assignments to be made as follows:- The 8.4, 7.2 and 5.2 Mev groups are due to 17.6 Mev gamma rays. Between 3 and 5 Mev the position is not so clear. The spectrum of Fig.3.3 shows peaks at 4.1_5, 3.8, 3.2_5 and 3.0 Mev, with a further probable peak at 2.5 Mev, whereas the spectra of Fig.3.6 show no direct evidence for the 3.8 Mev peak or for the doublet structure at approximately 3 Mev (see also Fig.3.1(c)). This difference could be due to the poor statistics of the spectrum of Fig.3.3 or to the slightly inferior resolution of the spectrum of Fig.3.6 and the fact that it occupies fewer channels. The effect of the latter can be appreciated from the inset of Fig.3.3 where the spectrum is replotted with the adjacent channels added together.

Fig.3.5, in which the energy region 2.6 - 5.5 Mev covers the full 80 channels, shows that there is no peak at 3.8 Mev and that there

*The target thickness was initially measured by determining the width of the 441 Kev resonance. The target was heated to 60°C with hot water and a liquid air trap inserted in the beam tube to minimise carbon deposition. Check measurements of the resonance width and the yield variation with time were made during the runs to ensure that the carbon deposit did not become excessively thick.

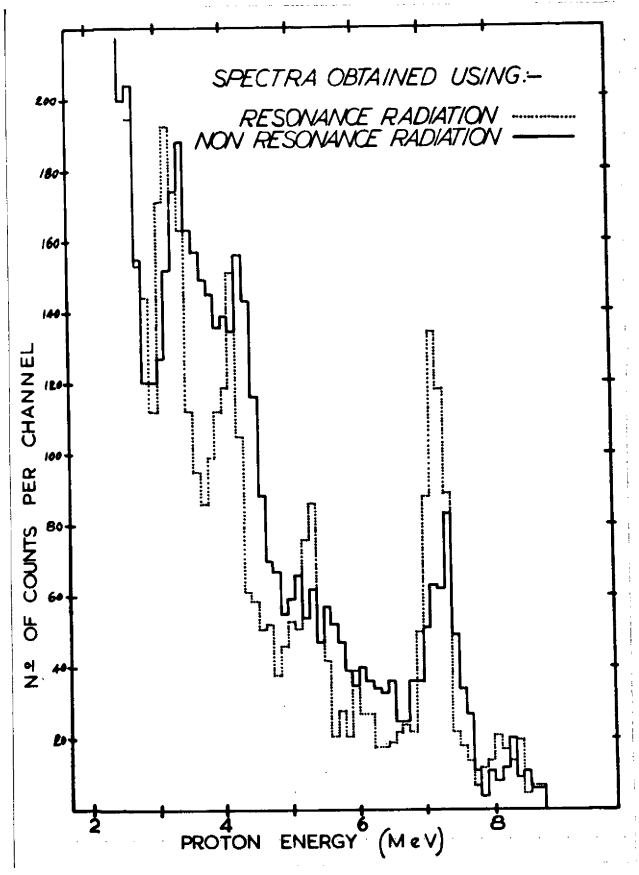

Fig. 3.6. Spectrum obtained using resonance and non-resonance radiation. The gamma-ray flux was approximately the same for both. Crystal size 1/4" x 1/4" x 0.018", and non-resonance running time was 11 hours.

are separate peaks at 3.2 and 2.9 Mev. In comparing the two spectra of Fig.3.6, it appears that the number of counts in the groups at 4.2 and 3 Mev has been reduced and that the peaks have been lifted by an increase in an underlying group at about 4 Mev. The protons in the peaks at 4.1_5, 3.2 and 2.9 Mev are therefore attributed to 17.6 Mev radiation. The upward energy displacement of the peaks relative to the resonance spectrum is further evidence for this identification since the energy of the peaks produced by the 17.6 Mev radiation will be increased by an amount corresponding to the increase in the gamma-ray energy at the higher proton bombarding energy. On the other hand, the energies of the resulting proton groups would be unaltered by an energy displacement of the 14.8 Mev line because this broad component can only produce sharp peaks by selective absorption into narrow levels of Na^{23}.

The above data are summarised in Table 3.1, which also lists the corresponding excitation energies of the residual Ne^{22} nucleus for these transitions.

3.2. Spectrum due to the 14.8 Mev component. Using the ratio of the number of counts in the 7.2 Mev group of the spectra of Fig.3.6 as a measure of the relative intensities of the two gamma-ray components at the 441 Kev resonance and at 700 Kev (assumed as the effective proton energy to compensate for the thickness of the lithium target and the carbon deposit on the target), the spectra of Fig.3.6 were differenced to yield the spectrum of photoprotons due to the 14.8 Mev component. The resulting spectrum is shown in Fig.3.7 and a broad group at approximately

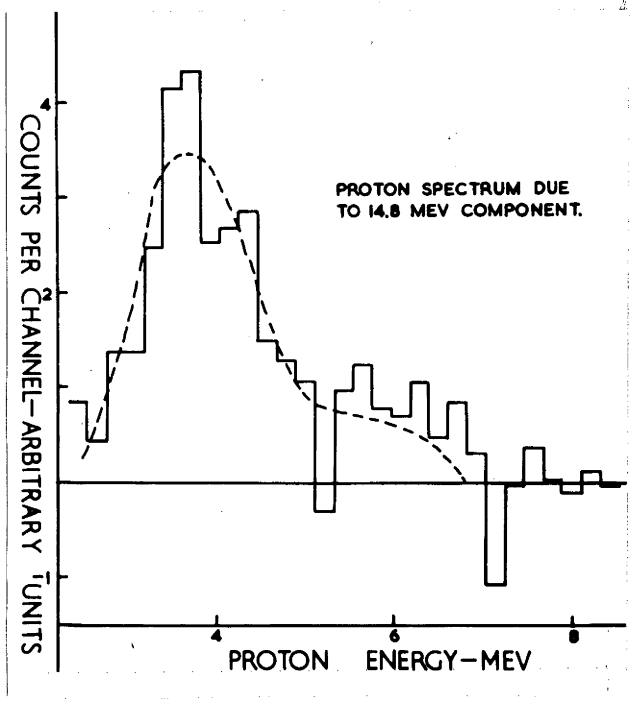

Fig. 3.7. Proton spectrum due to the 14.8 Mev component (see text).

TABLE 3.1.

Proton energy (Mev)	8.4	7.2	5.2_5	4.1_5	3.2	2.9
Excitation energy of Ne^{22} (Mev)	0	1.3	3.3	4.4	5.4	5.7
Cross-section (mb)	0.31	2.5	0.6	0.9	approx.2*	

* Our best estimate of the ratio of the cross-sections for the 3.2 and 2.9 Mev peaks is 3:2.

TABLE 3.2.

Run	Crystal dimensions	No. of protons	$\Omega/4\pi$	f*	Cross-section
16/3/57	0.510" x 0.521" x 0.045"	1816	0.025	0.82	2.49
19/3/57	0.508" x 0.506" x 0.037"	3465	0.031	0.79	2.46
20/3/57	0.503" x 0.505" x 0.021"	2226	0.026	0.64	2.57
21/3/57	0.507" x 0.503" x 0.028"	2228	0.027	0.73	2.68

*f is the fraction of protons stopped in the crystal.

4 Mev, which could correspond to the transition through the 1.28 Mev level of Ne^{22} for 14.8 Mev radiation, is evident. The apparent structure of the group is not real since the valleys occur at the energies at which the comparatively large 17.6 Mev peaks have been subtracted. However, in the course of non-resonance measurements made at a later date with KI (Chapter V), it was found that contamination of the crystal with (ThC + ThC') from the source could occur. Since this background, which only becomes important for long runs, would have been evident at 4 Mev in the $Na^{23}(\gamma,p)$ spectrum, no definite identification of the group can be made.

For subsequent measurements, contamination of crystals was prevented by placing a thin aluminium foil between the polythene slide and the alpha source.

3.3. Cross-section measurements. The cross-section of the 7.2 Mev group was established by four independent measurements with well-defined geometries using crystals of approximately $\frac{1}{2}$" x $\frac{1}{2}$" and of thickness 0.043", 0.037", 0.028" and 0.021". Cross-sections for the other groups were estimated from all of the appropriate spectra available.

A major source of error in such an estimation is the uncertainty of the background. Electron pulses and photoprotons from iodine and aluminium (Chapter IV) contribute in part to the background, and between 3 and 6 Mev a portion of it will comprise photoprotons from the $Na^{23}(\gamma,p)$ reaction induced by 14.8 Mev gamma rays.* Since the contributions of all

*Other, but smaller, contributions to the background will result from (i) knock-on protons produced in the polythene by neutrons associated with the operation of the H.T. set (d-d reaction) and neutrons produced in materials around the crystal by the gamma rays; (ii) alpha particles from the $C^{12}(\gamma,3\alpha)$ reaction in the polythene. This effect will be small since the cross-section for this reaction is an order of magnitude smaller than the $Na(\gamma,p)$ cross-section.
Activities induced in the crystals such as the decay of Na^{22}, I^{126} and I^{127} will not contribute since the maximum energy that can be expended in the crystal from any of these decay schemes does not exceed 2.5 Mev.

three are unknown, a smooth background passing through the valleys was assumed (see Figs. 3.5 and 3.9), and, as a result, the estimated cross-sections may be considerably in error. Loss corrections were made assuming isotropic angular distributions and the range-energy curve for protons in sodium iodide given in Fig.2.7. The accuracy of the cross-section of the 7.2 Mev group can be judged from the internal consistency of the four measurements which gave values of 2.49, 2.46, 2.68 and 2.57 mb. Details of the four runs are summarised in Table 3.2.

3.4. High-energy protons. The proton groups beyond 8.5 Mev cannot be attributed to the $Na^{23}(\gamma,p)$ reaction. A discussion of these high-energy protons is given in Chapter IV.

3.5. Spectra obtained with very thin crystals. Some preliminary spectra were obtained with very thin (approximately 0.005") crystals in an attempt to identify proton groups of energy less than 2.5 Mev. One such spectrum, in which a possible group at 1.9 Mev appears as a shoulder on the rising edge of the electron background, is shown in Fig.3.8. Some evidence for a group at approximately 1.5 Mev was also obtained but, because of the long runs necessary to establish good statistics and the difficulty in assigning accurate energy calibrations with the large escape losses from the higher energy groups, no further investigations were made.

3.6. Energy calibration. The calibration sequence (Chapter II, Section 5) consisted of two $B^{10}(d,p)$ runs, which preceded and followed a $Na^{23}(\gamma,p)$ run. The gain of the system was checked with the (ThC + ThC') alpha source before and after each individual run for both the $B^{10}(d,p)$ and the $Na^{23}(\gamma,p)$

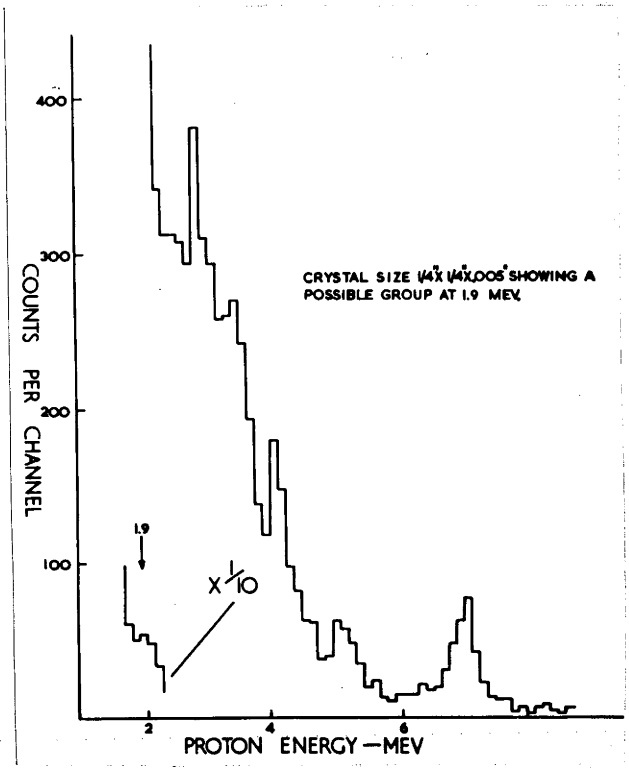

Fig. 3.8. Spectrum obtained with crystal of dimensions 1/4" x 1/4" x 0.005" showing a possible group at 1.9 Mev.

TABLE 3.3.

Normalized results of calibration runs.

Run	Photoproton peak energies (Mev)			
16/12/56	8.3	7.2	5.2_0	4.1_6
13/12/56	8.4	7.2	5.2_5	4.2_6
12/12/56	8.4	7.2	5.2_4	4.1_2
27/11/56	8.5	7.2	5.2_1	4.1_2
25/11/56	8.3	7.2	5.2_8	

measurements. An alpha source on the back of the lithium target served to check changes in photomultiplier response due to the large number of small pulses present when the crystal was irradiated with gamma rays. The alpha particle pulse height was generally increased very slightly when the beam was on but the change was never more than 0.5%. A correction was made for this shift.

The two $B^{10}(d,p)$ runs were always in excellent agreement, the displacement between corresponding points being generally less than a few tenths of 1%.

The calibration line and photoproton spectrum of a typical set of measurements are shown in Fig.3.9. Because of the increase in the background of electron pulses consequent on the increase in crystal thickness, the lower energy peaks do not appear in the $Na^{23}(\gamma,p)$ spectrum but all peaks above 4 Mev are resolved. Altogether five sets of measurements were made, but the agreement between the five sets of values for the energies of the photoproton peaks is not as good as would be expected from the above consistency between the two calibrations in an individual set of measurements. Thus the results for the energy of the '7.2' Mev peak are 7.4_4, 7.1_0, 7.0_8, 7.2_5 and 7.6_1 Mev. The cause of this scatter is not known but is thought to be due to an unlocated source of gain variation. If the results are normalised by adjusting all the above energies to the one value, then the results for the other peaks are in good agreement. The most natural assumption is that the '7.2' Mev proton group represents the transition to the first excited state in Ne^{22} at 1.28 Mev.

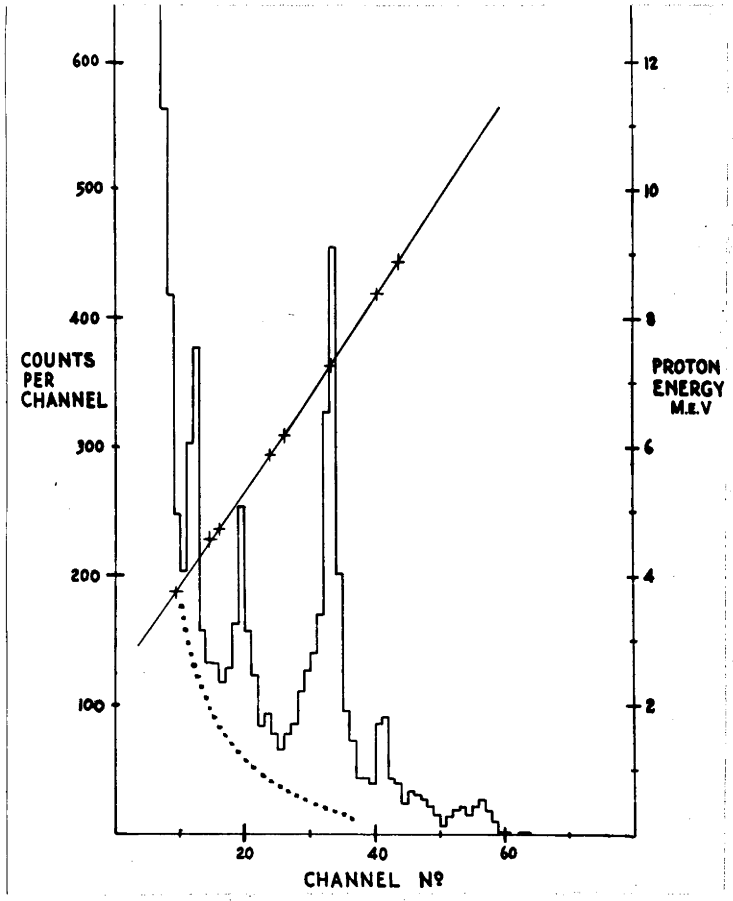

Fig. 3.9. $Na^{23}(\gamma,p)$ spectrum and proton calibration curve obtained for the spectrum.

Therefore the energies have been normalised to 7.2 Mev - the photoproton energy for this transition. Corresponding results are listed in Table 3 4.3 from which we assign energies of 8.4, 7.2, 5.2_5 and 4.1_5 Mev to the four $Na^{23}(\gamma,p)$ peaks. The calibration of the spectra in Fig.3.1 and Figs. 3.3-3.9 was made by assuming a linear relationship between energy and channel number and using these four points to fix the straight line. From the fit obtained, the experimental error in the calibration is estimated as less than $\pm$ 0.1 Mev between 4 and 8.5 Mev.

4. Discussion.

4.1. Review of the energy levels of Ne^{22}. Although a number of workers have investigated the Ne^{22} level scheme in some detail, inferior techniques, coupled with experimental difficulties associated with reactions leading to the Ne^{22} nucleus, have resulted in conflicting reports. Two reactions, viz. $F^{19}(\alpha,p)$ and $Ne^{21}(d,p)$, are suitable for study and the decay of Na^{22} provides information concerning the first excited state. The $Ne^{21}(d,p)$ reaction is difficult to observe since good targets (Ne^{21} absorbed in silver) cannot be prepared, so that almost all previous data have resulted from measurements made with the $F^{19}(\alpha,p)$ reaction. Evidence for each reported level is discussed individually.

0.6 Mev. Although early measurements of the proton spectrum from the $F^{19}(\alpha,p)$ reaction by Chadwick and Constable (Ch 32); Jolley and Champion (Jo 51) and Hjalmar and Slatis (Hj 52) indicated the existence of a level in the region of 0.6 Mev, proton spectra, of superior statistics and resolution, obtained by May and Vaidyanathan (Ma 36),

Foster, Stanford and Lee (Fo 54) and Fader (Fa 54) show no evidence for a level at this excitation.

The gamma-ray spectrum following proton emission has been obtained by Sherr, Li and Christy (Sh 54), Heydenberg and Temmer (He 54) and Breen and Hertz (Br 55) but no transitions involving a level in the vicinity of 0.6 Mev were identified.

The existence of this level must therefore be discounted.

1.28 Mev. This level was established as being at 1.277 Mev by Alburger (Al 49) following a measurement of the β^+-spectrum of Na^{22} with a magnetic spectrometer. A level has been reported at 1.51 (Speh - Sp 36), 1.5 (Ma 36), 1.41 (Jo 51), 1.38 (Hj 52) from measurements of the proton spectrum from the $F^{19}(\alpha,p)$ reaction and at 1.37 (Zucker and Watson - Zu 50) and 1.39 Mev (Ambrosen and Bisgaard - Am 50) from measurements of the proton spectrum from the $Ne^{21}(d,p)$ reaction. There is no doubt, however, that in each experiment the level observed was in fact the 1.28 Mev level.

Gamma-ray spectra from the $F^{19}(\alpha,p)$ reaction (Heydenberg and Temmer; Foster et al., Sherr et al. and Breen and Hertz) and from the $Ne^{22}(p,p')$ scattering experiments (Cox et al. - Co 54) confirm the existence of this level.

3.35 Mev. May and Vaidyanathan reported a proton group from the $F^{19}(\alpha,p)$ reaction corresponding to a Ne^{22} excitation of 3.5 Mev. Foster et al. and Fader have determined the excitation energy as 3.35 Mev with more accurate measurement of the energy of the proton group and Foster et

al. identified a 3.35 Mev gamma-ray transition in coincidence with the proton group. Both the ground-state transition (3.35 Mev) and a cascade gamma ray through the first excited state (2.1 Mev) were observed. It is likely that the 1.5 Mev gamma ray reported by Breen and Hertz and erroneously attributed to a 1.5 Mev level (on the basis of the level reported by Speh) is the escape peak of the 2.1 Mev cascade gamma ray.

Above 3.35 Mev. Both May and Vaidyanathan and Foster et al. report a higher level. May and Vaidyanathan found a level at 4.6 Mev while Foster et al., from a gamma-ray spectrum measured in coincidence with protons of energy less than those which proceed through the 3.35 Mev level, claim a level at 4.9 Mev. Both results are discussed in relation to the present experiment in the next section.

4.2. Comparison of previous data with the present level scheme. Of the levels listed in Table 3.1, the energies of the lowest two agree well with the established levels at 1.28 Mev and 3.35 Mev.

The level scheme of May and Vaidyanathan, viz. 1.5, 3.5 and 4.6 Mev, agrees with the established states and the present result (4.4) if a systematic energy error of 0.2 Mev is assumed. Their results have been re-analysed using more accurate range-energy tables but no substantial difference from the original result was found. However, the accuracy of energy determination is stated as $\pm$ 0.2 Mev so that a systematic error may be explicable in terms of this limitation.

Foster et al. measured the spectrum of protons from the $F^{19}(\alpha,p)$ reaction and found that it contained low-energy protons corresponding to a state in Ne^{22} above 3.35 Mev but of indeterminate energy. They then used a sodium iodide spectrometer to examine the gamma rays in coincidence with these low-energy protons and from this latter spectrum (Fig.3.10) assigned a value of 4.9 Mev to the excitation energy of the level. However, Foster et al. point out that the high-energy peaks of the gamma-ray spectrum do not fit exactly with those expected for a 4.9 Mev gamma ray and in any case, since the spectrum falls off rapidly from 50 counts/channel in the region above 3.2 Mev, identification of the peaks in this region is doubtful. Also, the peaks at 3.1 and 2.6 Mev, which Foster et al. identify as the first and second escape peaks corresponding to the cascade transition from 4.9 Mev to 1.28 Mev, may equally well be the 'photo-peak' and the first escape peak of the same transition from a 4.4 Mev level. In view of this and the fact that the present experiment gives no evidence of a level at 4.9 Mev, it is likely that the level observed by Foster et al. was in fact the 4.4 Mev level identified in this experiment.

The levels observed at 5.4 and 5.7 Mev are in a region which has not been investigated previously.

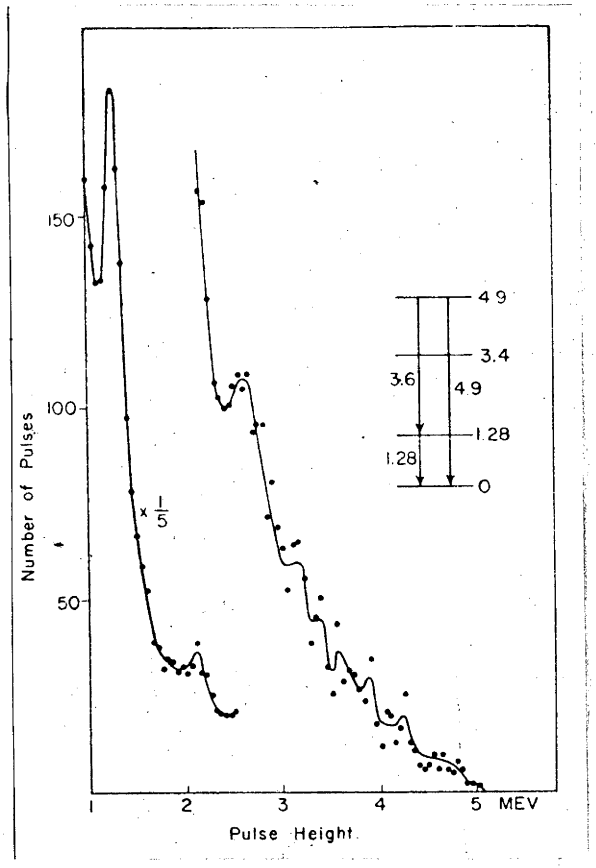

Fig. 3.10. Gamma-ray spectrum from the $F^{19}(\alpha,p)$ reaction in coincidence with low-energy protons (Foster et. al.).

CHAPTER IV

THE PHOTODISINTEGRATION OF IODINE.

1. Introduction. In Chapter III it was pointed out that photoproton spectra obtained by irradiating NaI crystals contained, in addition to a spectrum of protons from the $Na^{23}(\gamma,p)$ reaction, protons of energy in excess of 8.5 Mev, the energy of the ground-state transition of the $Na^{23}(\gamma,p)$ reaction. The $Al^{27}(\gamma,p)$ reaction, with a threshold of 8.26 Mev (En 54), would yield protons of a maximum energy of 9.1 Mev, and from the $I^{126}(\gamma,n)$ threshold (Sh 51) and the energy release in the decay of I^{126} to Te^{126} (Ko 55; Pe 54), the expected energy of the ground-state protons from the $I^{127}(\gamma,p)Te^{126}$ reaction for 17.6 Mev gamma rays is 11.4 ± 0.2 Mev, corresponding to a Q-value of -6.1 ± 0.2 Mev. Thus the observed protons were most likely to have originated from these reactions; in fact, any other possible reactions would be inadmissible on the basis of the observed cross-section.

Data obtained from proton spectra of the $Na^{23}(\gamma,p)$ reaction are considered, and further spectra which were designed to allow some discrimination between the above two reactions are discussed.

2. Identification of groups. Fig.3.4 shows that there are groups in the region beyond 8.5 Mev at 10.9, 10.3 and 9.6 Mev and in the vicinity of 9 Mev. The three highest-energy groups must clearly be attributed to the $I^{127}(\gamma,p)$ reaction since no other reaction in the crystal or its immediate environment will produce such energetic protons. However, in this energy scale, 7.2 Mev actually means 7.2 Mev proton energy plus an energy contribution from the recoil of the Ne^{22} nucleus in the crystal. In determining the energies (and the corresponding excitation energies)

of groups attributed to the $Na^{23}(\gamma,p)$ reaction, this energy scale, which arises from the normalisation of the calibration (Chapter III, Section 3.6), is satisfactory since the contribution from the recoil nucleus associated with each group is very nearly proportional to the group energy. The response of NaI(Tl) to particles of $\frac{Z}{A}$ greater than 1 is not linear, but in the energy region considered here, viz. 0-500 Kev, the departure from linearity is small (Chapter II, Section 2.1(c)). The data of Allison and Casson (Al 53) for the response of NaI(Tl) to doubly-charged Ne^{22} ions relative to the proton response were used to calculate the true energies of the groups. The values so obtained* were 11.3, 10.7 and 10.0 Mev, with an estimated error of at least $\pm$ 0.2 Mev for each group energy since other spectra similar to Fig.3.4 indicated that the nominal energy was as large as 11.1 Mev. It was supposed that saturation was responsible for this difference because the primary purpose of these spectra was to obtain the $Na^{23}(\gamma,p)$ spectrum and, as a result, the pulse height corresponding to energies in excess of 10 Mev considerably exceeded the rated maximum of the amplifier used (50 volts). Further spectra were obtained in order to establish the group energies as accurately as possible and, at the same time, an attempt was made to find the extent to which the $Al^{27}(\gamma,p)$ reaction contributed protons of energies beyond 8.5 Mev.

3. Contribution from the $Al^{27}(\gamma,p)$ reaction. The spectra obtained in Chapter III and discussed here contain photoprotons from the $Al^{27}(\gamma,p)$ reaction by reason of the thin aluminium foil over the crystal which

*It was assumed that the energy contribution of the recoil nucleus Te^{126} is negligible.

serves as a moisture-proof seal. The energy of the ground-state group from this reaction is 9.1 Mev and the group should appear at very nearly 9 Mev on the normalised energy scale. There is a group of this energy in the spectrum of Fig.3.4 but it is possible that this group could arise from the $I^{127}(\gamma,p)$ reaction as a transition through a hitherto unreported level of Te^{126}. To distinguish between the two possible origins of the group, a spectrum obtained with a total of 9 mgm/cm^2 of aluminium foil over the crystal* was compared with a spectrum recorded under identical conditions with the normal 1.5 mgm/cm^2 of aluminium.

The two spectra (Fig.4.1) were of equally good statistics and were normalised (only a small correction was necessary to compensate for a difference in the total gamma-ray flux for the two runs) by means of the number of counts (over 5,000 counts in each spectrum) in the 7.2 Mev group of the $Na^{23}(\gamma,p)$ spectrum. The energy calibration of the spectra was made using the normalised energies of the groups of the $Na^{23}(\gamma,p)$ reaction. Comparison of the spectra indicates no significant difference above the nominal energy of 9.3 Mev and an increase in the number of counts betwen 8.8 Mev and 9.0 Mev. This increase, for a six-fold increase in the amount of aluminium present, is sufficiently small to warrant the conclusion that the 1.5 mgm/cm^2 foil contributes few 9-Mev protons. In addition, the spectra of Fig.4.1 cast doubt on the existence of a group at 9.0 Mev.

4. Discussion of the group energies and the level scheme of Te^{126}. The nominal and corrected energies of the groups as obtained from the two

*Crystal dimensions 1/4" x 1/4" x 0.052".

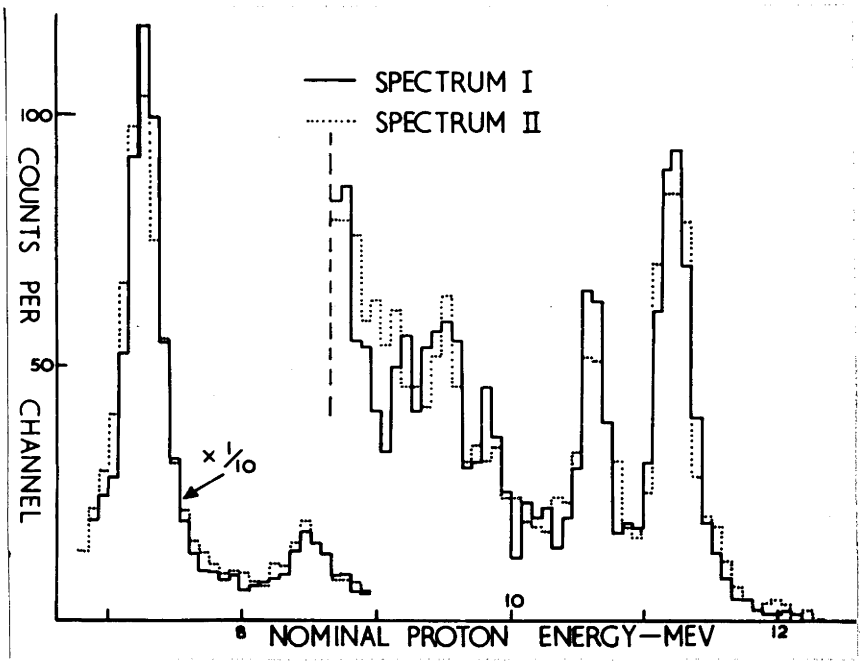

Fig.4.1. $I^{127}(\gamma,p)$ spectra. Spectrum I was recorded with 1.5 mgm/cm^2 aluminium foil and spectrum II with 9.0 mgm/cm^2.

spectra of Fig.4.1 are listed in Table 4.1 along with the corresponding excitation energies of Te^{126}. Levels at 0, 0.65 and 1.4 Mev, reported by Koerts et al. (Ko 55) and Perlman and Welker (Pe 54) from a study of the beta decay of I^{126}, are in good agreement with the present scheme. Levels above 1.4 Mev are not excited in the decay of I^{126} and, largely because of this reason, have not been investigated previously. Thus the level found at an excitation energy of 1.77 Mev is new.

5. Cross-section estimations. The cross-sections of the four groups attributed to the $I^{127}(\gamma,p)$ reaction were estimated by a comparison with the 7.2 Mev group of the $Na^{23}(\gamma,p)$ reaction using the previous data for proton ranges in sodium iodide and assuming isotropic distributions. The cross-sections of the groups are tabulated in Table 4.2. Measurements more closely approximating the total $I^{127}(\gamma,p)$ cross-section have been made by Wright (Wr 58) using CsI. The thresholds of the $Cs^{133}(\gamma,p)$ and $I^{127}(\gamma,p)$ reactions are very nearly the same, as also are the level schemes (up to 1.5 Mev) in the residual nuclei Xe^{132} and Te^{126}. The spectrum obtained showed group structure beyond a proton energy of 7 Mev and a broad distribution between 3 and 7 Mev in which no groups were well-defined. The $Cs^{133}(\gamma,p)$ and $I^{127}(\gamma,p)$ cross-sections above 8.5 Mev can be identified by means of a comparison of the photoproton spectra recorded with sodium iodide and cesium iodide and preliminary measurements have been made. The cross-section for all of the protons observed beyond an energy of 3 Mev was 4 mb. or 3 mb. if averaged over both the 14.8 and 17.6 Mev gamma-ray components. It can therefore be inferred that the total $I^{127}(\gamma,p)$ cross-section is of the order of 2 mb.

TABLE 4.1.

Nominal group energies		Corrected group energies		Mean energy	Excitation of Te^{126}
I	II	I	II		
11.2_2	11.2_0	11.6_6	11.6_3	11.6_4	0
10.6_1	10.6_0	11.0_2	11.0_1	11.0_1	0.6_3
9.84	9.83	10.2_2	10.2_1	10.2_1	1.4_3
9.4_8	9.5_2	9.8_5	9.9_0	9.8_7	1.7_7

TABLE 4.2.

Group energy (Mev)	11.6	11.0	10.2	9.9
Cross-section (mb)	0.3	0.2	0.1	0.2

CHAPTER V

PHOTODISINTEGRATION OF POTASSIUM.

1. Experimental method. The apparatus and experimental procedure were essentially the same as those described in Chapter III and, as such, require no further description. Likewise, the preparation and properties of potassium iodide, the scintillator used to investigate the $K^{39}(\gamma,p)$ reaction, are given in Chapter II, Section 2.2.

The calibration chamber was modified slightly to obviate a gain monitoring difficulty which was encountered with the calibration of the $Na^{23}(\gamma,p)$ spectra. During this previous work, it was not possible to make gain checks of the alpha pulse height simultaneously with the bombardment of the lithium target unless an alpha particle source was also deposited on the backing of the lithium target. Apart from the inconvenience associated with the deposition of this source, the inevitable contamination of the calibration chamber was undesirable.

The problem was overcome by mounting an alpha source on the polythene shutter (Fig.5.1), thus introducing a third shutter position for gain checks; the previous two positions being retained to surround the crystal with polythene for the (γ,p) runs and allow entry of the $B^{10}(d,p)$ protons.

Aluminium absorber thicknesses of 5.5, 20.0, 48.4 and 91.3 mgm/cm^2 were used for the calibration.

2. Results.

2.1. Identification of transitions. The spectra (each representing a summation of a number of individual runs of approximately 30 minutes'

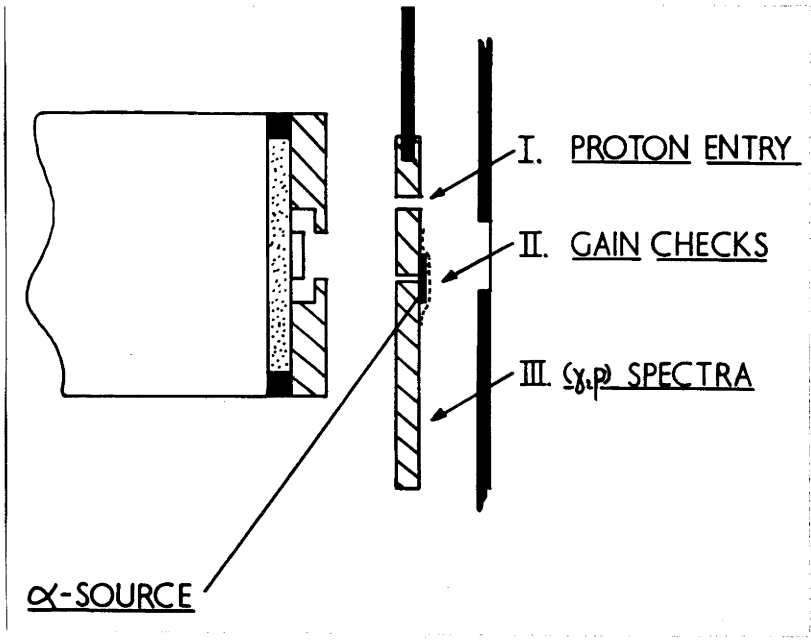

Fig. 5.1. Schematic diagram of modified polythene shutter arrangement of the calibration chamber.

duration) listed in Table 5.1 were recorded with resonance radiation.

The energy calibration of the spectra in Figs. 5.2 - 5.7 was obtained from two calibration runs, one of which is shown in Fig.5.5. The energies of the groups as determined from the two calibrations are listed in Table 5.2, the experimental error being estimated as less than $\pm$ 0.1 Mev between 3 and 8.8 Mev. Since the two calibration runs were in good agreement, normalisation of the group energies was not necessary (see Chapter III, Section 3.6). The calibration of the spectra shown in Figs.5.2 - 5.7 was made by assuming a linear relationship between energy and channel number and using the measured energies of the appropriate groups to fix the straight line.

All of the groups listed in Table 5.2 are clearly identifiable with the exception of the group at 6.06 Mev (Figs.5.3 and 5.5), but the expanded spectrum of Fig.5.4 supports the existence of a group at this energy.

The spectra listed in Table 5.1 will contain photoprotons from both the narrow 17.6 Mev line and the broad 14.8 Mev Line. Thus the observed sharp groups can be attributed to either absorption of the 17.6 Mev line or selective absorption of the 1.48 Mev component into narrow levels of K^{39}. Two spectra (Figs.5.6 and 5.7) were recorded using non-resonance radiation in order to distinguish between the possible origins of the groups (Chapter II, Section 3.1 and Chapter III, Section 3). Fig.5.6 was obtained at a proton bombarding energy of 850 Kev with a

TABLE 5.1.

Figure No.	Crystal dimensions	Energy region examined
5.2	1/4" x 1/4" x 0.060"	6.0 - 12 Mev
Inset 5.2	1/4" x 1/4" x 0.060"	8.5 - 12 Mev
5.3	1/4" x 1/4" x 0.030"	3.5 - 12 Mev
5.4	1/4" x 1/4" x 0.030"	5.0 - 8.5 Mev
5.5	1/4" x 1/4" x 0.030"	2.5 - 12 Mev

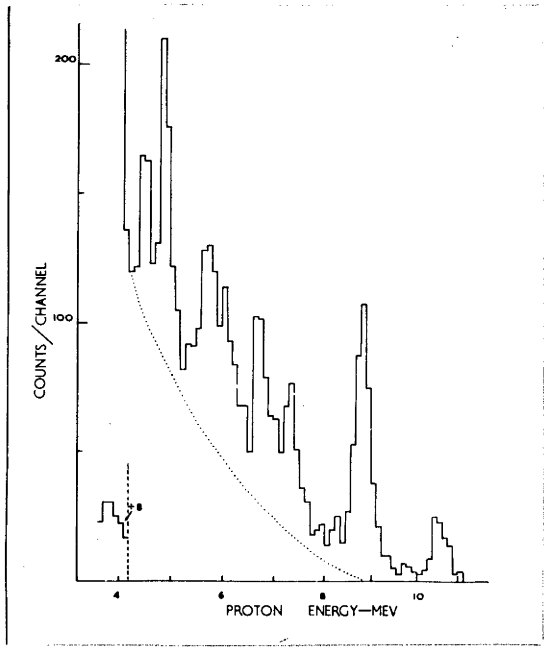

Fig. 5.2. $K^{39}(\gamma,p)$ spectrum for crystal 1/4" x 1/4" x 0.060". Inset shows detail between 8.5 and 12 Mev.

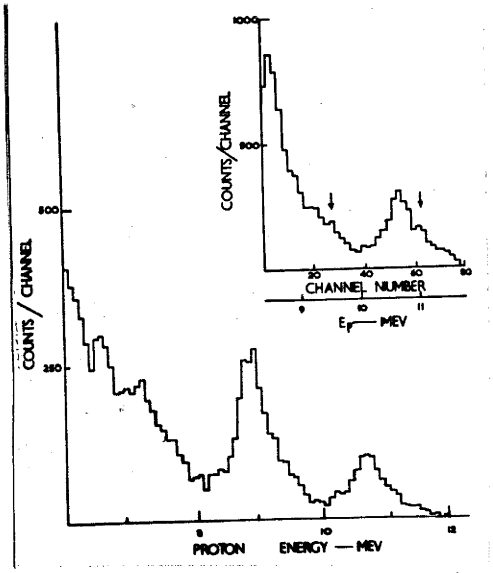

Fig. 5.3. Spectrum for crystal 1/4" x 1/4" x 0.030".

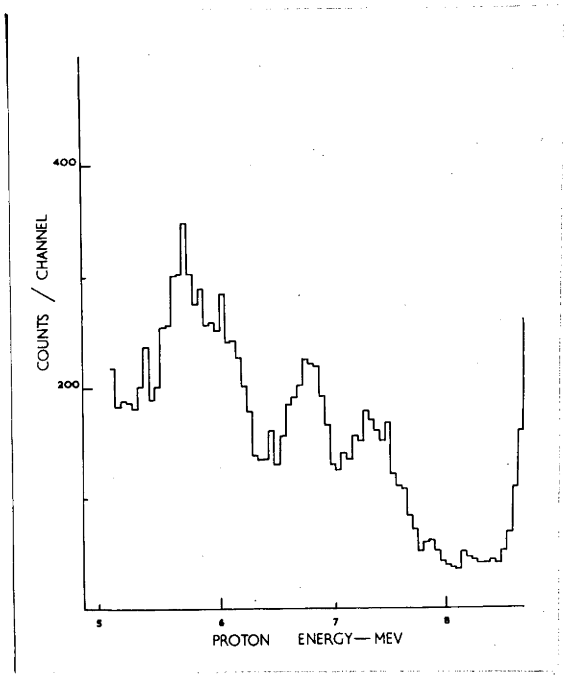

Fig. 5.4. Spectrum showing detail between 5 and 8 Mev.

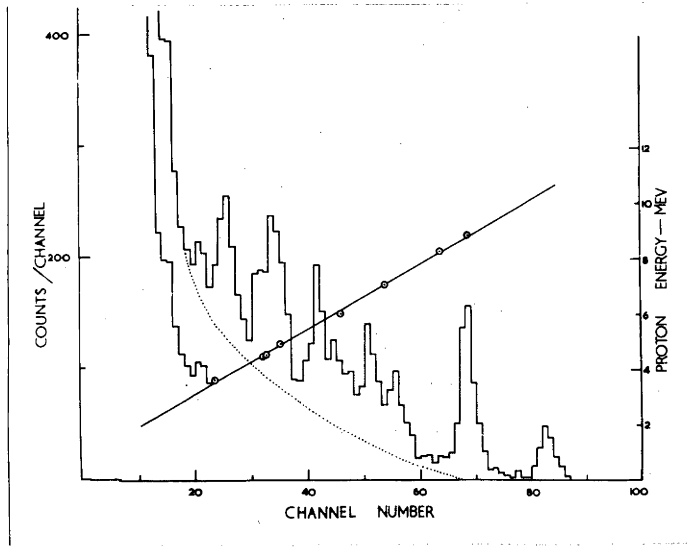

Fig. 5.5. $K^{39}(\gamma,p)$ spectrum and proton calibration curve obtained for the spectrum.

target approximately 100 Kev thick, and the latter spectrum at 760 Kev with a 150 Kev thick target. The corresponding resonance spectrum for each is also given; in Fig.5.7 the two spectra were produced by the same total gamma-ray flux, but in the case of Fig.5.6, a monitoring failure prevented a similar comparison. Both non-resonance spectra, in particular that of Fig.5.6 which was expanded more (i.e. a greater pulse height/energy interval), display an upward energy displacement of all the proton groups relative to the relevant resonance spectrum. In Fig.5.7, there is an overall decrease in the number of counts in the non-resonance spectrum as compared to the resonance spectrum. Consequently, all groups are attributed to transitions induced by 17.6 Mev radiation. The corresponding excitation energies of the residual A^{38} nucleus for these transitions are listed in Table 5.2 (see Section 3).

For a given gamma-ray flux, the intensity ratio of the 17.6 Mev gamma rays at the two proton bombarding energies is approximately 1.3 (Chapter II, Section 3.1). The ratios of the numbers of protons in groups attributed to 17.6 Mev gamma rays by means of non-resonance/resonance comparisons of the $Na^{23}(\gamma,p)$ and $Cs^{133}(\gamma,p)$ reactions (Chapter III and Wr 58) were in fair agreement with the above figure, whereas the ratio of the number of protons detected in the 8.8 Mev group of the two spectra of Fig.5.7 is 2.6. It is possible that the cross-section falls rapidly between 17.6 and 17.8 Mev but the present data, although self-consistent,* is not regarded as sufficient evidence for such an interpretation.

*The electron edge is the same for both spectra of Fig.5.7 and, furthermore, the two geiger counters, which independently monitored the gamma-ray flux, were in good agreement.

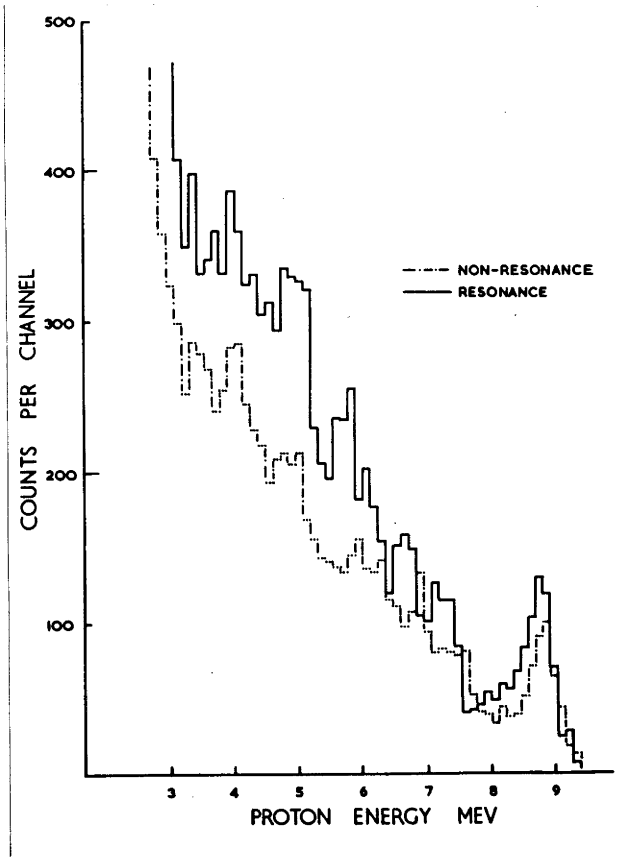

Fig. 5.6. Spectrum obtained using non-resonance and resonance radiation. Relative magnitudes of the spectra are arbitrary. Crystal dimensions 1/4" x 1/4" x 0.030" and non-resonance running time was 13 hours.

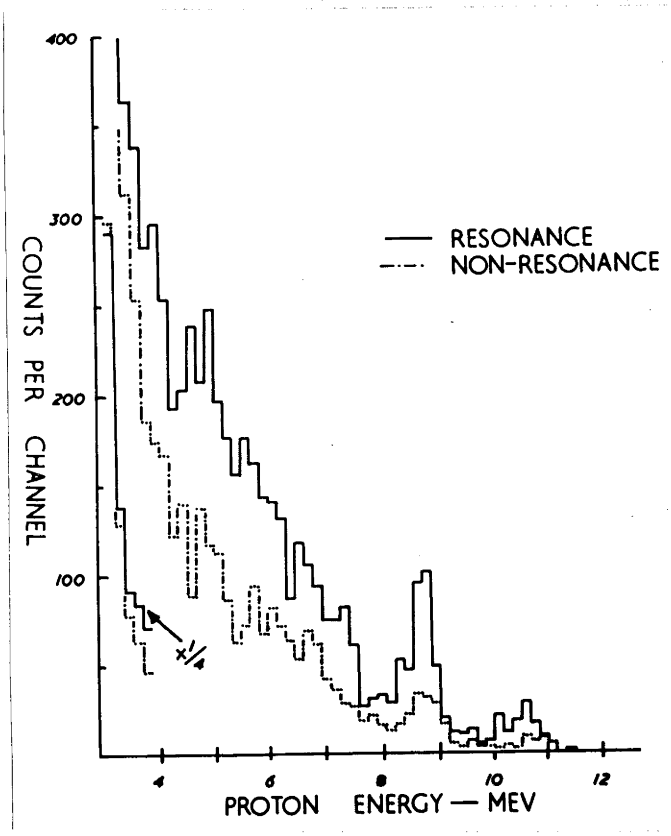

Fig. 5.7. Spectrum obtained using resonance and non-resonance radiation. The gamma-ray flux was the same for both. Crystal size 1/4" x 1/4" x 0.030", and non-resonance running time was 9.5 hours.

2.2. Cross-section measurements. The cross-section of the 8.8 Mev group was established with a well-defined geometry using a crystal of dimensions 0.516" x 0.531" x 0.048". Cross-sections for the other groups were estimated using all the appropriate spectra available and the results are tabulated in Table 5.2. As before (Chapter III, Section 3.3), a major source of error in the determination is the uncertainty of the nature of the background and the discussion given in Chapter III applies equally well in the present instance.

Loss corrections were made assuming isotropic angular distributions and the range-energy relation for protons in potassium iodide given in Chapter II, Section 2.2(d). A correction was also made for the isotopic composition of natural potassium (Wh 56). The error in determining the cross-section of the 8.8 Mev group is estimated at 20%, giving a result of 2.4 ± 0.5 mb.

2.3. Other reactions in the crystal. Small, but statistically significant, groups are evident at approximately 11.3 Mev (Inset Fig.5.2), 8.3 and 8.0 Mev (Figs.5.3 and 5.5) and a shoulder on the higher energy side of the 8.8 Mev group indicates a possible peak at approximately 9.6 Mev (Inset Fig.5.2 and Fig.5.5).

The group at 11.3 Mev is attributed to the $I^{127}(\gamma,p)$ reaction (Chapter IV) while the doubtful group at 9.6 Mev and the 8.3 Mev group could correspond to transitions to the ground state and first excited state from the $K^{41}(\gamma,p)$ reaction (En 57). The relative abundance of K^{41} is 6.5%.

TABLE 5.2[1]

Group energy	10.5	8.81	7.33	6.75	6.06	5.7	4.78
Excitation of A^{38}	0	2.16	3.74	4.3	5.0	5.4	6.3
Cross-section (mb.)	0.9	2.4	1.0	1.4	2.4		1.2

Group energy	4.55	3.8	3.3
Excitation of A^{38}	6.6	7.3	7.8_5
Cross-section (mb.)	0.5	1.3	0.3

[1]The group at 2.5 Mev (see text) corresponding to a level at 8.6 Mev is not included in Table 5.2.

CHAPTER VI

DISCUSSION.

2.4. Spectra obtained with very thin crystals. Some spectra (not shown) were recorded with crystals of dimensions 1/16" x 1/16" x 0.010" and 1/8" x 1/8" x 0.010", and though interpretation of these spectra is doubtful because of the statistical errors and the large escape losses from the higher energy groups (which serve as energy calibration points), they tend to confirm the possible group at 2.5 Mev which appears as a shoulder on the electron edge in Fig.5.5 and indicate further proton groups of energies down to and even below 2 Mev.

3. Discussion.

3.1. Comparison of present data with the previous level scheme. Endt and Braams (En 57) give a Q-value of -6.389 Mev for the $K^{39}(\gamma,p)$ reaction on the basis of the observed $K^{39}(\gamma,n)$ threshold and the energy release in $K^{38}(\beta^+)A^{38}$. Excited states have been established at 2.16 and 3.75 Mev (En 57). Therefore, proton groups would be anticipated at 10.95, 8.85 and 7.3 Mev and these correspond to the observed groups at 10.5, 8.81 and 7.33 Mev. The energies of the lowest groups are in good agreement; the discrepancy in the ground-state transition energy probably arises from the extrapolation of the proton calibration line almost 2 Mev beyond the highest calibration point. The excitation levels in A^{38} which correspond to the lower groups are given in Table 5.2.

Levels at approximately 5 Mev and 6.7 Mev have been reported by Towle et al. (To 57). They obtained the gamma-ray spectra of the $Cl^{37}(p,\gamma)$ reaction at the 1070, 1135, 1533 and 1725 Kev resonances and identified gamma-ray transitions corresponding to levels at 5.0 and 6.7 Mev. These two levels are presumably the levels at 5.0 and 6.6 Mev established by the present experiment.

1. Introduction. Before discussing the present results, a brief summary is given of the statistical model of nuclear reactions as applied to photodisintegration and of the direct processes which have been proposed to supplement or replace the statistical model.

This is done in order to assess the value of our measurements in so far as they have been made and, where possible, as a means of indicating complementary measurements which should ultimately allow an examination of the emission process in some detail.

2. The statistical model. The statistical model supposes that an excited compound nucleus is produced by the absorption of incident radiation and nucleons are "boiled off" from this nucleus. Following the statistical theory of nuclear reactions proposed by Weisskopf and Ewing (We 40), the energy distribution of the emitted particles will depend on the level distribution in the residual nucleus. Low-energy emission would be most probable since the level density increases rapidly with energy and, in consequence, the coulomb barrier will inhibit proton evaporation (except for the light nuclei). Thus for reactions in the middle-weight nuclei ($A \sim 100$), the ratio of proton to neutron emission is estimated to be between 10^{-3} and 10^{-5} (Co 51). Normally, the angular distribution of evaporated nucleons would be isotropic.

These predictions are not always confirmed experimentally.

2.1. Measurements of photoproton spectra and angular distributions. In

the main, photoproton spectra have been measured by irradiating foils with bremsstrahlung of E_{max} about 23 Mev (Chapter I). The photoproton spectra from reactions in light nuclei such as $Mg^{25}(\gamma,p)$ - To 51; $Al^{27}(\gamma,p)$ - Di 50; $A^{40}(\gamma,p)$ - Sp 55; $Co^{59}(\gamma,p)$ - To 54 and $Cu^{63,65}(\gamma,p)$ - By 51; were in fair agreement with distributions predicted from the statistical theory (with a suitable choice of level density and coulomb barrier and normalisation), and the angular distributions of the protons were very nearly isotropic. However, for the heavier of these nuclei (A^{40}, Cu), there were more high-energy protons (10%) than the statistical model predicts and these high-energy protons were produced preferentially at 90°.

Subsequently measurements of the photoproton spectra from (γ,p) reactions in heavier nuclei, e.g. $Mo^{92,100}(\gamma,p)$ - Bu 53; $Rh^{103}(\gamma,p)$ - Cu 50; $In^{115}(\gamma,p)$ - To 53; $Ce^{140,142}(\gamma,p)$ - To 53; $Ta^{181}(\gamma,p)$ - Ho 53; $Pb^{208}(\gamma,p)$ - To 55 and $Bi^{209}(\gamma,p)$ - To 53, found increasing numbers of photoprotons with energies exceeding the calculated evaporation spectra and, in each instance, the angular distribution was anisotropic and peaked at 90° (with the exception of Ce (γ,p)).

2.2. Measurements of $(\gamma,p)/(\gamma,n)$ ratios. Hirzel and Waffler (Hi 47) found that the $(\gamma,p)/(\gamma,n)$ ratios in nuclei with A in the region of 100 were as much as 1,000 times greater than predicted by statistical theory, and later measurements have shown similar discrepancies (To 53; Bu 53). Hirzel and Waffler actually obtained the (γ,p) and (γ,n) cross-sections in different nuclei and compared the data as though the cross-sections

applied to the same nucleus. Although this feature of the method has been criticised, the fact remains that (γ,p) cross-sections for heavy nuclei are considerably in excess of the cross-sections predicted by the statistical theory.

3. Direct photodisintegration processes.

In view of the discrepancies from statistical theory, Courant (Co 51) and later Wilkinson (Wi 56), have proposed "direct" models whereby individual nucleons absorb quanta and escape from the nucleus without the intermediate formation of a compound nucleus. The cross-section for such a process need only be small relative to compound nucleus formation to explain the (γ,p) cross-sections in heavy nuclei since, in light nuclei, where the coulomb barrier is smaller, the evaporation of protons could predominate. Calculations by Courant for (γ,p) reactions in the middle-weight nuclei are, though still too small, in much closer agreement with the observed cross-sections than are similar estimations on the basis of the statistical model, and the angular distributions of direct nucleons would be of the form $A + B\sin^2\theta$ where B/A is determined by the orbital momentum of the nucleon within the nucleus. Thus Courant was able to explain, in general terms at least, the features of photoproton emission from the heavier nuclei.

Wilkinson proposes a "resonance direct effect" based on the shell model. In this theory, gamma-ray absorption takes place by means of transitions from closed shells of the nuclear core. The strengths of

the possible transitions were calculated as a function of gamma-ray energy and Wilkinson was able to show that the most probable transitions were grouped about a resonance energy which presumably corresponds to the giant resonance although there is a discrepancy between the theoretical and experimental values for which the resonance occurs. The (γ,p) cross-sections calculated by this method are in fair agreement with experiment.

4. The present measurements.

All of the experimental evidence for one or other of the processes has been obtained with bremsstrahlung measurements. The comparisons with statistical theory and, to a lesser extent, with direct effects rely upon the bremsstrahlung spectrum to smear the effects of low-level densities, and the value of such measurements as a means of discriminating between the various proposed mechanisms is uncertain. Though the present data are much more detailed and are free from the complications which entailed in the use of a complex gamma-ray spectrum, current theory is not sufficiently adequate to enable a calculation of the consequences of particular models so far as energy distributions involving individual levels are concerned.

Even so, it is of value to consider the energy spectra which have been obtained in relation to the models discussed in Sections 2 and 3.

4.1. $Na^{23}(\gamma,p)$ reaction. The energy spectra given in Chapter III indicate that, at the excitation energies attained with 17.6 Mev radiation, the level density in Ne^{22} is too low to be able to attach any significance

to the relative magnitudes of the groups. The cross-section is distributed fairly uniformly over the available levels down to a proton energy of 2.9 Mev and the fluctuations from level to level are no more than one would expect for transitions in a nucleus of so few levels. Thus the result would appear to be consistent with the statistical model.

4.2. $K^{39}(\gamma,p)$ reaction. As in the case of the $Na^{23}(\gamma,p)$ reaction, the cross-section is distributed uniformly over the available levels for proton energies ranging from 11 Mev to at least 2.5 Mev. There is no indication of high-energy proton emission being more favoured.

At 17.6 Mev, the (γ,p) cross-section is in excess of 11 mb., while the (γ,n) cross-section is approximately 9 mb. (Wa 48, Mc 50, Bo 55). This difference is probably the result of the proton threshold being .7 Mev lower than the neutron threshold.

The low-level density of A^{38} casts doubt on the interpretation made by Wilkinson and Carver (Wi 53) of the photproton spectrum of the $A^{40}(\gamma,p)$ reaction which they obtained using monochromatic gamma rays (17.6 Mev). They identified* transitions to the ground state and the first excited state of Cl^{39} and interpreted a large group at 2.5 Mev as a statistical peak. In view of the level density of A^{38}, it would be more reasonable to suppose that this group is only one or perhaps two transitions through levels of Cl^{39} rather than the aggregate of a much larger number of transitions.

---

*There is some uncertainty of this identification since the mass value for Cl^{39} derived from this experiment differs considerably from other, and apparently reliable, mass data.

4.3. $I^{127}(\gamma,p)$ reaction. The $I^{127}(\gamma,p)$ spectrum has not been established below a proton energy of 8.5 Mev, but it is significant that a large part of the estimated 2 mb.* total cross-section is in the higher energy transitions. The preliminary results for the $Cs^{133}(\gamma,p)$ reaction indicate a similar predominance of the higher energy transitions. It can be inferred that these protons arise from a direct effect.

Measurements for the (γ,n) cross-section at 17.6 Mev range from 180 mb. to nearly 400 mb. (Mc 50; Mo 53 and Na 54a). Thus, the $(\gamma,p)/(\gamma,n)$ ratio of between 0.5 and 1% is in better agreement with the Wilkinson model than statistical theory.

5. Complementary data to the photoproton energy spectra.

The discussion of each reaction in Section 4 is extremely limited in scope but, in the absence of a theoretical treatment, a comprehensive discussion must await complementary experimental data. The purpose of this section is to suggest the nature of such data and consider the means by which it could be obtained.

5.1. Angular distributions. Unlike the energy spectra of photoprotons, angular distributions are amenable to theoretical prediction and, for this reason, measurement of the angular distributions of each of the transitions, which have been identified in the various (γ,p) reactions, would be desirable. Now that the energy distributions for a number of reactions have been established, the Canberra group proposes to attempt these measurements.

---

*As indicated in Chapter IV, this is a preliminary value.

The number of protons which escape from a crystal depends on the crystal thickness, the proton range and the angular distribution of the proton emission (Chapter II, Section 6). Thus, for an 11.5 Mev photoproton produced in a crystal 0.050" thick, the fraction of protons wholly stopped within the crystal is 66% for an isotropic distribution and 76% for a pure $\sin^2\theta$ distribution. By a careful comparison of proton spectra obtained with crystals of various thicknesses, it should be possible to decide between an isotropic and an anisotropic distribution. In the absence of any preliminary measurements, the accuracy to which the anisotropy can be determined is uncertain.

5.2. Proton spectra from the break-up of nuclei excited by alternative modes of formation. Particle reactions (apart from stripping reactions), like photonuclear reactions, might be expected to proceed either by a direct process or via a C.N., and evidence has been found to support this view. It would be of considerable interest to compare the proton spectra from a series of reactions which lead to proton transitions in the same residual nucleus, especially in the instance where the maximum energy available to the protons is the same. A quantitative comparison of the reaction mechanisms would require a knowledge of the energy spectra, preferably at a number of incident particle energies, and angular distributions of each transition.

For instance, the $Na^{23}(\gamma,p)$ spectrum could be compared with $F^{19}(\alpha,p)$ and $Ne^{21}(d,p)$ spectra and the $K^{39}(\gamma,p)$ spectrum with the proton spectrum of the $Cl^{35}(\alpha,p)$ reaction. A few measurements of the proton

spectra of the above particle reactions are to be found in the literature, but these studies have neither been comprehensive enough nor have the bombarding energies used corresponded to the excitation provided by absorption of 17.6 Mev gamma rays by Na^{23} or K^{39}. Figs.6.1 and 6.2 show the results obtained by Foster et al.* (Fo 54) and Kranz and Watson (Kr 53) for the $F^{19}(\alpha,p)$ and $Cl^{35}(\alpha,p)$ reactions. Clearly, the ratios of the ground-state and first excited state transitions are similar in each case to those obtained for the corresponding photoproton spectra but, for each spectrum, the magnitude of the lower energy transitions is markedly different. The alpha bombarding energies used were 7.6 and 7.45 Mev respectively, whereas energies of 8.8 and 11.5 Mev are needed to give the required excitations.

No reliable proton spectra of the $Ne^{21}(d,p)$ reaction have been made to the present time (Chapter III). Preliminary observations of this reaction have been attempted in this laboratory at a deuteron bombarding energy of 700 Kev. Contaminant reactions ($N^{14}(d,p)$; $C^{12}(d,p)$; $Ne^{20}(d,p)$ and $H^{2}(d,p)$) were troublesome, and the proton yield was too low to make any measurements since the target thickness was less than 1 $\mu gm/cm^2$. This work will be continued if thicker (10 $\mu gm/cm^2$) targets become available.

5.3. Excitation functions. A complete discussion of the processes involved in any (γ,p) reaction will require some knowledge of the excitation function; in particular the position and the width of the giant resonance.

* There is reason to believe that the Yale cyclotron group will reinvestigate the $F^{19}(\alpha,p)$ reaction in more detail up to an alpha bombarding energy of 8.1 Mev (Br 58).

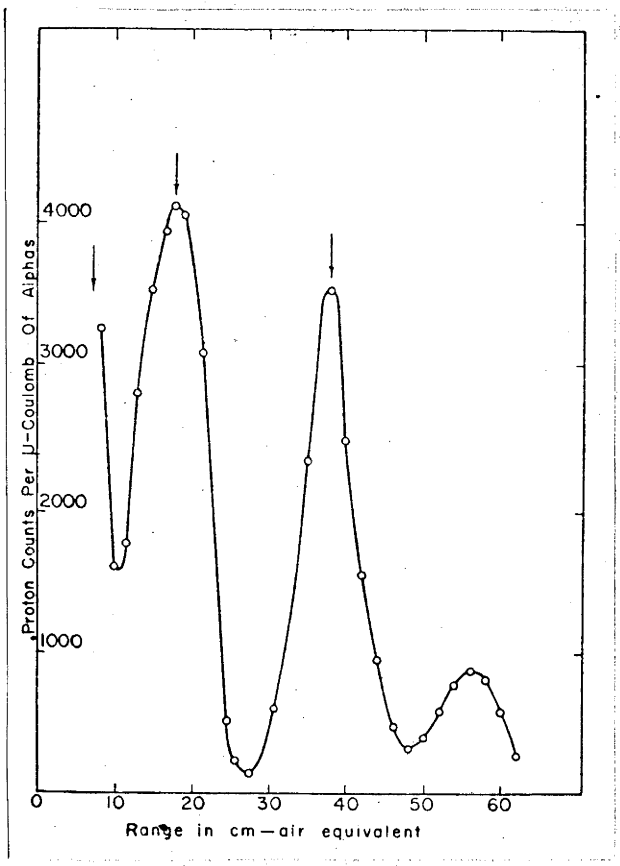

Fig. 6.1. Proton spectrum of the $F^{19}(\alpha,p)$ reaction obtained by Foster et al.

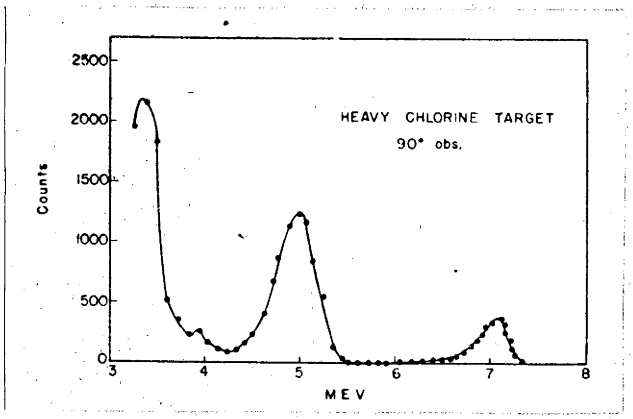

Fig. 6.2. Proton spectrum of the $Cl^{35}(\alpha,p)$ reaction obtained by Kranz and Watson.

Excitation functions of the (γ,p) reactions under study have not been measured since the end nuclei are stable. However, it should be possible to obtain a yield curve of the number of protons produced with a crystal by bremsstrahlung of increasing end energies and so obtain the excitation function. The eventuality of pulse pile-up would have to be avoided.

5.4. $(\gamma,p)/(\gamma,n)$ ratios. Direct comparisons of the cross-sections of the (γ,p) and (γ,n) reactions in the same nucleus have been made for only a few nuclei (Ca 58) and, in general, such determinations are only possible when the residual nuclei from both reactions are unstable. A scintillator can be used to detect protons from the (γ,p) reaction and the residual activity produced within it at the same time by the (γ,n) reaction - i.e., it is only necessary that the residual nucleus from the (γ,n) reaction is unstable and that the half-life and the decay scheme are suitable for measurement by a small crystal. Such is the case for both the $Na^{23}(\gamma,n)$ and $K^{39}(\gamma,n)$ reactions. No measurements have been attempted as yet, but a sodium iodide crystal of dimensions 1/4" x 1/4" x 0.040" showed considerable activity after 3 hours' bombardment with $Li^{7}(p,\gamma)$ radiation. A spectrum, recorded immediately after the irradiation ceased (Fig.6.3) showed gamma-ray lines at 500 and 700 Kev; the 700 Kev line had a half-life of much less than 10 minutes and was not identified, while the 500 Kev line, arising presumably from positron capture, had a half-life of approximately 14 minutes and is attributed to the decay of residual nuclei produced by (γ,n) reactions in materials around the counter. A much longer-lived activity, probably Na^{22}, was present. A spectrum was not recorded since

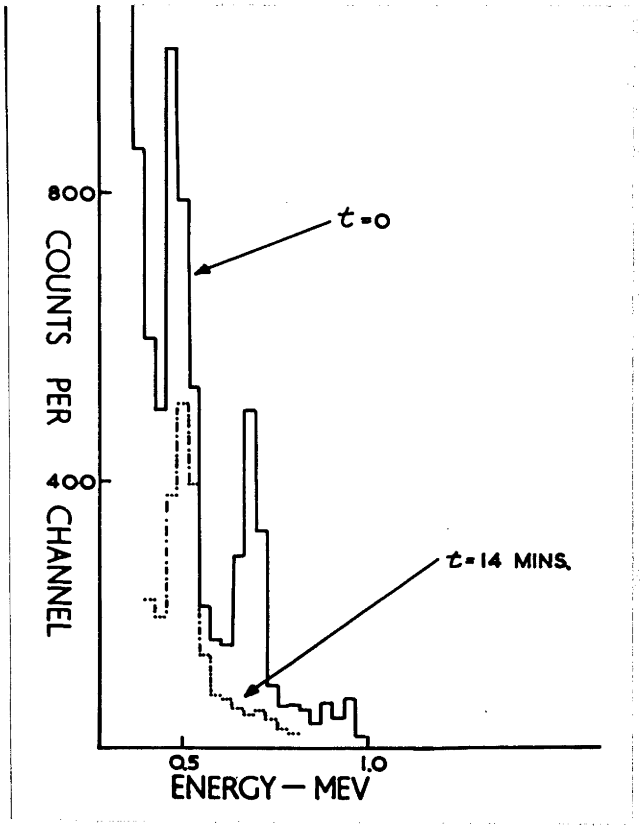

Fig. ~~8.2~~ 63. Spectra of the residual activity in NaI (and surroundings) recorded immediately irradiation ceased and 14 minutes later.

the counting rate was extremely low.

This method, in common with double activation methods, eliminates absolute flux determinations but suffers in that the total (γ,p) cross-section cannot be obtained (Chapter III, Section 3.3). Nevertheless, it could extend present data considerably.

CHAPTER VII

A PRELIMINARY SURVEY OF PHOTONUCLEAR REACTIONS IN LiI AND Li^6I.

1. Introduction.

Reactions in such light nuclei as Li^6 and Li^7 could not be expected to yield much information on the systematics of photoproton emission. However, previous measurements of the $Li^7(\gamma,p)$ excitation function have shown little agreement and the $Li^6(\gamma,p)$ reaction has not been observed in any detail.

Excitation functions of the $Li^7(\gamma,p)$ reaction have been obtained by Katz et al. (Ka 53); Titterton and Brinkley (Ti 53); Rubin and Walter (Ru 54) and Tucker and Gregg (Tu 54). With the exception of Titterton and Brinkley, who used lithium-loaded emulsions, the excitation functions were determined by examining the He^6 activity as a function of maximum bremsstrahlung energy. Tucker and Gregg obtained a slowly increasing variation of cross-section in the region between 10 and 20 Mev, while each of the others found a broad resonance centred about 15 Mev although there was no general agreement for the value of the cross-section or for the width of the resonance. The difference in the widths of the resonance as found by Katz et al. and Titterton and Brinkley was considered by Titterton and Brinkley (Ti 54) to be evidence that an excited state of He^6, which de-excited by gamma-ray emission, was involved in the reaction. Further evidence for such a level was reported by Titterton and Brinkley, who obtained the proton spectrum of the reaction at gamma-ray energies of 14.8 and 17.6 Mev with radiation from the $Li^7(p,\gamma)$ reaction and identified a proton group corresponding to a level in He^6 at approximately 1.6 Mev. This latter result may also be interpreted as a resonance in the excitation

function at a gamma-ray energy of 16 Mev, and subsequent measurements by Titterton and Brinkley (Ti 58), which demonstrated a similar resonance at 16 Mev in the spectrum of the $Li^7(\gamma,t)$ reaction obtained with $Li^7(p,\gamma)$ radiation, support this latter interpretation. Thus the discrepancy between the two results with regard to the width remains.

The $Li^6(\gamma,p)$ reaction was observed by Titterton and Brinkley (Ti 54a) in lithium-loaded emulsions which had been exposed to $Li^7(p,\gamma)$ radiation. The high proton energy resulted in large escape losses from the emulsion and insufficient statistics were obtained for a detailed discussion of the reaction.

Thus, a study of these reactions in LiI and Li^6I might indicate which of the excitation functions is the most correct and also allow an examination of the states of He^5. Other reactions such as $Li^7(\gamma,t)$, $Li^7(\gamma,n)Li^{6*} \rightarrow \alpha + d$ and $Li^6(\gamma,n)Li^5 \rightarrow \alpha + n$ could be observed.

1.1. Difficulties introduced by the use of scintillators.

Natural lithium iodide* contains 92.5% Li^7 and 7.5% Li^6, and a spectrum obtained by irradiating LiI will contain contributions from a number of photonuclear reactions involving each nucleus. In view of the small amount of Li^6, it would be supposed that reactions involving Li^6 will be responsible for only a small portion of the total spectrum so that misinterpretation of groups should not occur. On the other hand, the $Li^6(n,t)$ reaction is troublesome. Neutrons will be produced from (γ,n) reactions in materials around the crystal and in the target which acts as the gamma-ray

*Natural lithium iodide will be referred to as LiI in the text.

source from the $Li^7(p,\alpha)$ and $Li^7(\alpha,n)$ reactions. The largest contribution from the $Li^6(n,t)$ reaction will be at thermal energies where the energy of the (triton plus alpha) group is 3.25 Mev (Chapter II, Section 2.3), but the cross-section of the reaction is still considerable at higher neutron energies and a continuous background due to the reaction can be expected to extend to higher energies. Nevertheless, this higher energy background should be small and can be estimated from measurements made with Li^6I.

More important in an investigation of the above reactions are the relative responses of the scintillators to the various reaction products. Whereas for the reactions previously studied (Chapters III, IV, V) only a small contribution arose from the recoil of the heavy residual nucleus after proton emission, reactions in both Li^6 and Li^7 give rise to tritons, alpha particles, deuterons and He^6 ions, in addition to either neutrons or protons, and a considerable portion of the energy liberated in any particular event is carried by these heavier particles. Some measurements of the proton, triton and alpha responses of both LiI and Li^6I have been made (Chapter II, Section 2.3) and it is to be inferred that the proton and deuteron responses are very nearly equivalent (Ta 51). No data for the response of He^6 ions in any material are known although the response will presumably be not greatly different from that of alpha particles.

The problem introduced by the different responses of the various particles is not entirely the question of group identification; also, the responses become important for those reactions in which the residual nucleus in turn disintegrates, e.g. $Li^{6*} \rightarrow \alpha + d$, $He^5 \rightarrow \alpha + n$ and $Li^5 \rightarrow \alpha + p$. For

such reactions, the energy of each of the disintegration products depends on the direction of the break-up relative to the recoil of the unstable nucleus. The dynamics of break-up present no problems to measurements made using photographic emulsions or gas counters because, in the first case, the track lengths and their relative orientation in the emulsion can be obtained and, in the second, because the amount of ionisation in a gas depends (with second order departures only) on the total energy of the products (except for neutron emission). However, the scintillator will record a different pulse height for each particular energy distribution of the two particles and the widths of the groups are increased accordingly. The only reactions which will not be affected in this way* are the $Li^7(\gamma,p)$; $Li^7(\gamma,t)$ and $Li^7(\gamma,n)$ (in which case the reaction will not be observed).

The $I^{127}(\gamma,p)$ reaction will contribute protons to spectra obtained with LiI but the cross-section for protons of energies between 3 and 8.5 Mev is small (Chapter IV).

2. Experimental method.

The apparatus and experimental procedure were identical with those described in Chapters III and V.

Both LiI and Li^6I (95% Li^6) were used and details of the preparation and mounting of these scintillators have been given in Chapter II. Detailed measurements were not attempted with Li^6I. The emphasis was placed on reactions in Li^7, and Li^6I was only used for comparison runs to ensure that none of the groups observed in the spectra obtained with LiI

*Ignoring the gamma-ray momentum.

were due to neutrons.

Energy calibration of the LiI spectra was obtained as previously, using protons from the $B^{10}(d,p)$ reaction. Cross-sections were estimated in two ways. The groups attributed to reactions in Li^7 were compared to the proton groups from the $I^{127}(\gamma,p)$ reaction using the data given in Chapter IV for the cross-sections of these groups and, also, the cross-sections were deduced from a comparison measurement of the photproton spectra obtained under identical conditions with NaI and LiI crystals of identical dimensions. Corrections were made for the number of atoms per c.c. in each of the crystals and for the loss corrections appropriate to each scintillating material.

3. Results.

3.1. Identification of transitions. The following spectra (each representing a summation of a number of individual runs of approximately 30 minutes' duration) were recorded with LiI using resonance radiation:-

(a) crystal dimensions 1/4" x 1/4" x 0.050" (Fig. 7.1)

(b) crystal dimensions 1/4" x 1/4" x 0.030" (Fig. 7.2)

(c) crystal dimensions 1/4" x 1/4" x 0.014" (Fig. 7.3)

(d) crystal dimensions 1/4" x 1/4" x 0.040" (calibration spectrum) (Fig. 7.4).

Definite identification can be made of groups at 7.2_5, 10.2, 11.0, 11.6 and 12.2 Mev (Figs. 7.1, 7.2 and 7.4), and there are possible groups at 5.5 (Figs. 7.2, 7.3 and 7.4), 8.6 (Figs. 7.2 and 7.4) and

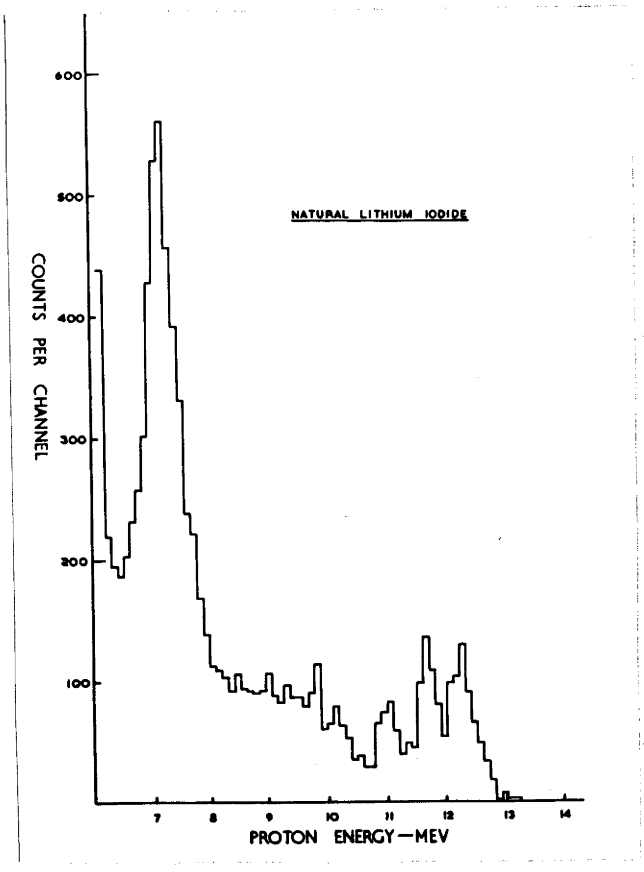

Fig. 7.1. Spectrum obtained with a LiI crystal of dimensions 1/4" x 1/4" x 0.050".

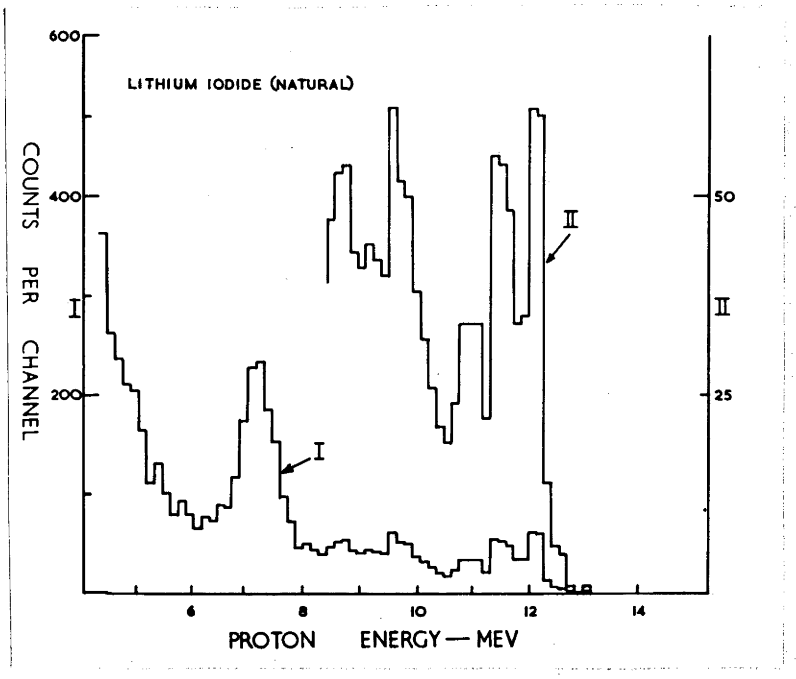

Fig. 7.2. Spectrum obtained with a LiI crystal of dimensions 1/4" x 1/4" x 0.030".

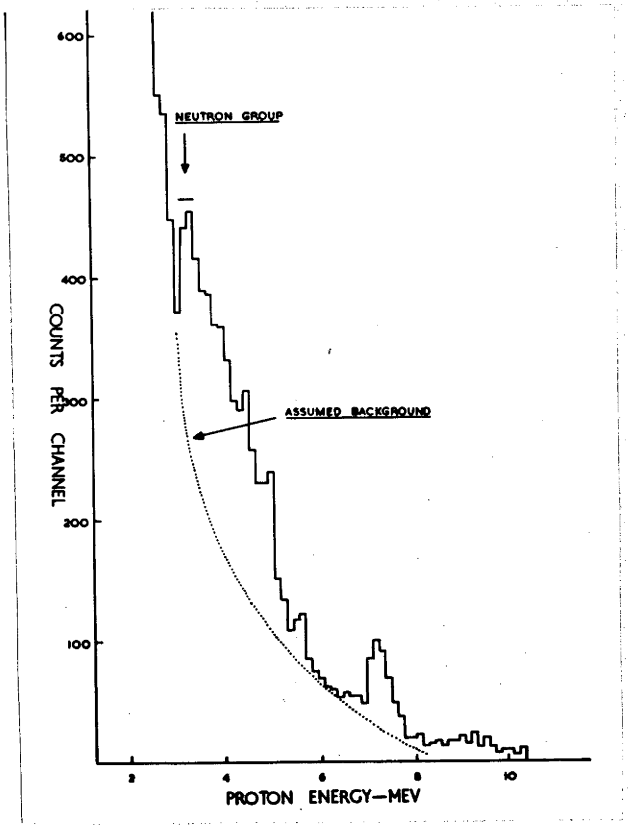

Fig. 7.3. Spectrum recorded with a LiI crystal of dimensions 1/4" x 1/4" x 0.014" in an attempt to identify the 14.8 Mev transition of the $Li^7(\gamma,p)$ reaction. Running time 7 hours.

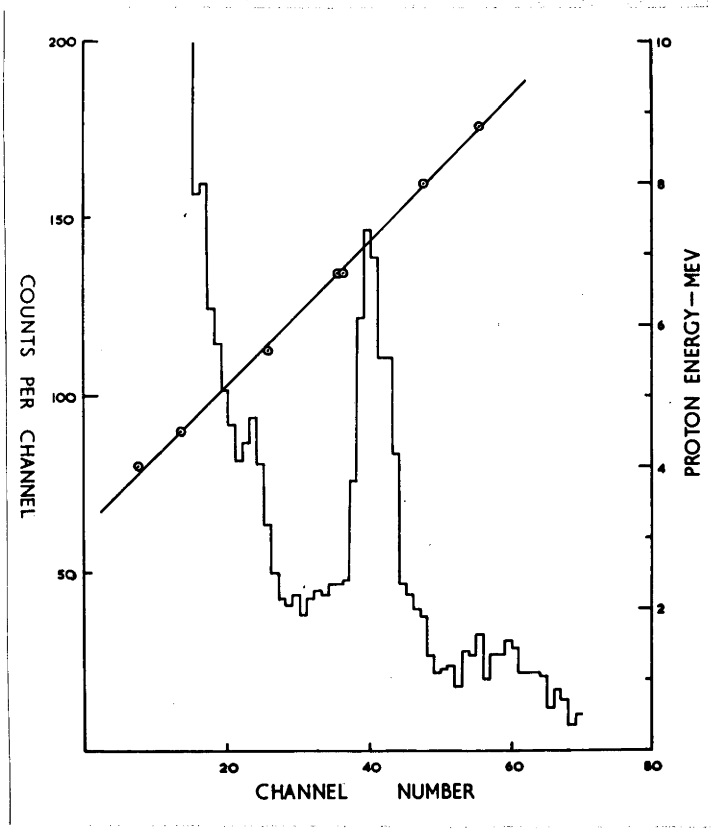

Fig. 7.4. Spectra obtained with a 1/4" x 1/4" x 0.040" crystal and the corresponding calibration line.

9.7 Mev (Fig. 7.2). The energies of the groups which would be expected from the $Li^7(\gamma,p)$ and $Li^7(\gamma,t)$ reactions are listed in Table 7.1. The equivalent proton energies have been calculated using the relative proton-alpha response given in Chapter II, Section 2.3, assuming that the triton response is identical to the proton response and that the He^6 response is the same as the alpha response. If the groups at 9.7, 10.2, 11.0 and 11.6 Mev are attributed to the $I^{127}(\gamma,p)$ reaction (Chapter IV), then the prominent groups at 7.25 and 12.2 Mev remain unexplained by the reactions set out in Table 7.1. Furthermore, the comparison measurement of LiI and Li^6I (Fig.7.5) demonstrates quite clearly that neither of the groups is due to the $Li^6(n,t)$ reaction.

(a). <u>The 12.2 Mev group</u>. The most natural assumption is that the group at 12.2 Mev is due to the $Li^7(\gamma,t)$ reaction (for 17.6 Mev gamma rays). Such an assumption would require the response of an 8.7 Mev triton to be equivalent to that of a 9.7 Mev proton. This result is not inconsistent with the earlier measurement of the response of a 2.6 Mev triton since the difference between the responses at 2.6 Mev would be only 0.2 Mev (assuming a linear relationship). If the assumption is valid, then the energy of the 14.8 Mev transition would be 9.4 Mev rather than 8.6 Mev. As an experimental check, spectra were obtained with non-resonance radiation (Chapter III, Section 3) and the results are shown in Fig.7.6. Spectrum I was recorded with a 200 Kev thick target at 850 Kev and spectrum II with a 100 Kev thick target at 800 Kev. Each non-resonance spectrum contains more counts in the

TABLE 7.1.

a. $Li^7(\gamma,p)$

E_γ	E_p	E_{He^6}	Equivalent proton energy released in the crystal.
17.6	6.14	1.1	6.4 + 0.3 = 6.7 Mev
16.0	5.14	0.86	5.14 + 0.2 = 5.34 Mev
14.8	4.0	0.65	4.0 + 0.1 = 4.1 Mev

b. $Li^7(\gamma,t)$

E_γ	E_t	E_α	Equivalent proton energy released in the crystal.
17.6	8.67	6.5	8.67 + 2.5 = 11.2 Mev
14.8	7.01	5.26	7.01 + 1.6 = 8.6 Mev

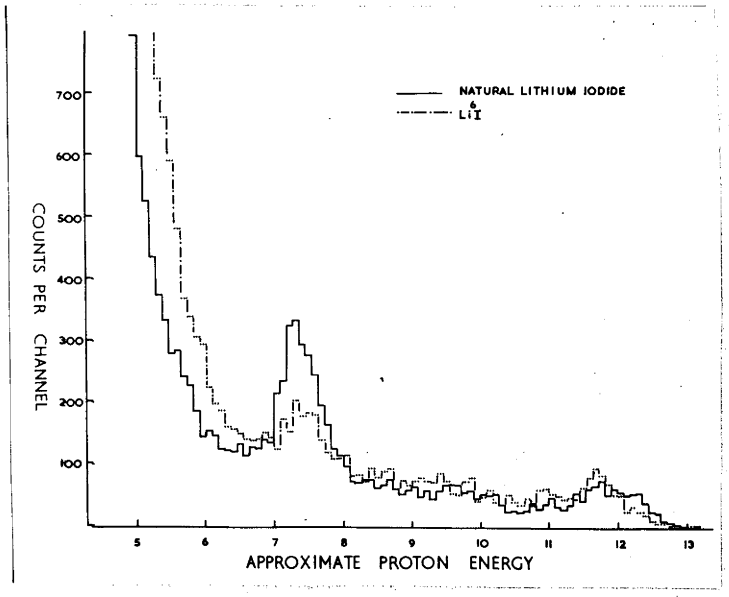

Fig. 7.5. LiI - Li^6I comparison measurement. The spectra have been normalised to the same gamma-ray flux.

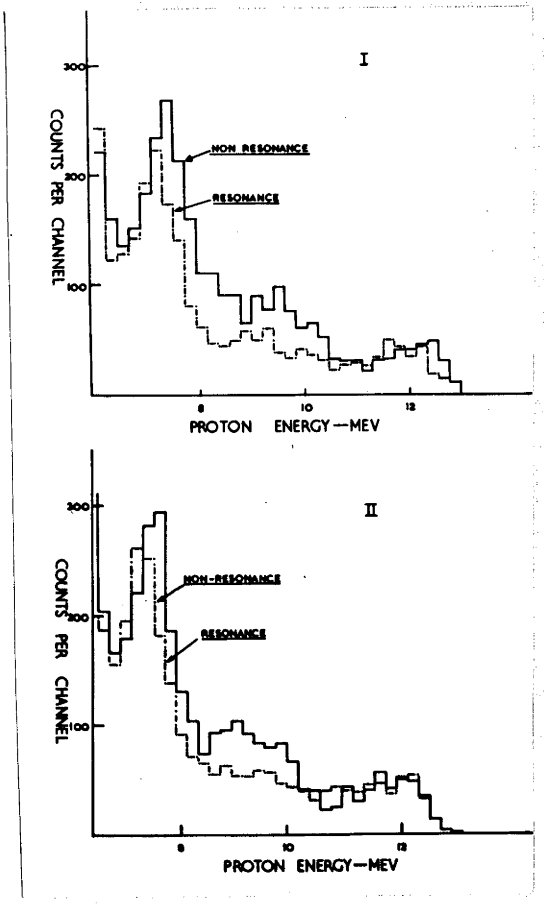

Fig. 7.6. Non-resonance and resonance spectra measurements made with LiI. Crystal dimensions 1/4" x 1/4" x 0.040", and non-resonance running time was 4 hours (Spectrum I) and 7 hours (Spectrum II).

region from approximately 8 to 10.3 Mev than does the corresponding resonance spectrum. The $I^{127}(\gamma,p)$ ground-state transition for 14.8 Mev gamma rays would have an energy of 8.5 Mev so that the increase of counts would appear to be due to the $I^{127}(\gamma,p)$ reaction in the region 8-9 Mev and to the $Li^{7}(\gamma,t)$ reaction beyond this energy.

(b). The 7.25 Mev group. The reactions remaining to which the 7.25 Mev group can be attributed are $Li^{7}(\gamma,p)$; $Li^{7}(\gamma,n)Li^{6*} \rightarrow \alpha + d$ and $Li^{7}(\gamma,d)He^{5} \rightarrow \alpha + n$. The latter reactions were examined but they could not account for the energy of the group nor, more importantly, for the width which, in both cases, would be considerably broader than the observed width.

On this basis, the group is assigned to the $Li^{7}(\gamma,p)$ reaction. The group energy is higher than anticipated, which could be explained by an anomalous response of He^{6} although there is no obvious reason why this should be so. Supposing that the group at 7.25 Mev is the ground-state transition, the energies of the groups produced by the 16.0 and 14.8 Mev gamma rays should also be higher than the predicted energies of 5.3 and 4.1 Mev. The group at 5.5 Mev could therefore be the 16.0 Mev resonance group, but the position is not so clear with the 14.8 Mev transition. A spectrum recorded with a thin crystal (Fig. 7.3) showed an excess of counts in the energy region 3-5 Mev above a background of the type normally assumed. However, the presence of a broad group centred at between 4 and 5 Mev could not be established because of a background of pulses from the $Li^{6}(n,t)$ reaction. The group at 3.25 Mev is due to thermal neutrons and there

appears to be a considerable contribution from higher energy neutrons.

Evidence which would tend to support the assignment of the 7.25 Mev group to the $Li^7(\gamma,p)$ reaction can be obtained from the non-resonance/resonance comparisons which show that the group is probably* due to 17.6 Mev gamma rays, and not resonance absorption, because there is an upward energy displacement of the group for the increase of gamma-ray energy.

3.2. Cross-section measurements.

(a). The 7.25 Mev group. The comparison with the $I^{127}(\gamma,p)$ groups gave a value of 1.57 mb., and the comparison with the $Na^{23}(\gamma,p)$ spectrum (Fig.7.7) a value of 1.73 mb. The cross-sections were calculated on the basis of loss corrections for a 6.4 Mev proton.

(b). The 12.2 Mev group. The comparison with the $I^{127}(\gamma,p)$ groups gave a value of 0.31 mb. for the cross-section of 12.2 Mev group. Loss corrections were calculated using the range-energy relation for tritons in LiI given in Chapter II, Section 2.

3.3. Energy calibration. Two calibrations were recorded with LiI and the results for one of the measurements are shown in Fig.7.4. The two runs were in excellent agreement and the calibration error is considered to be less than 0.1 Mev.

---

*The apparent increase in the magnitude of the group is difficult to explain on this basis.

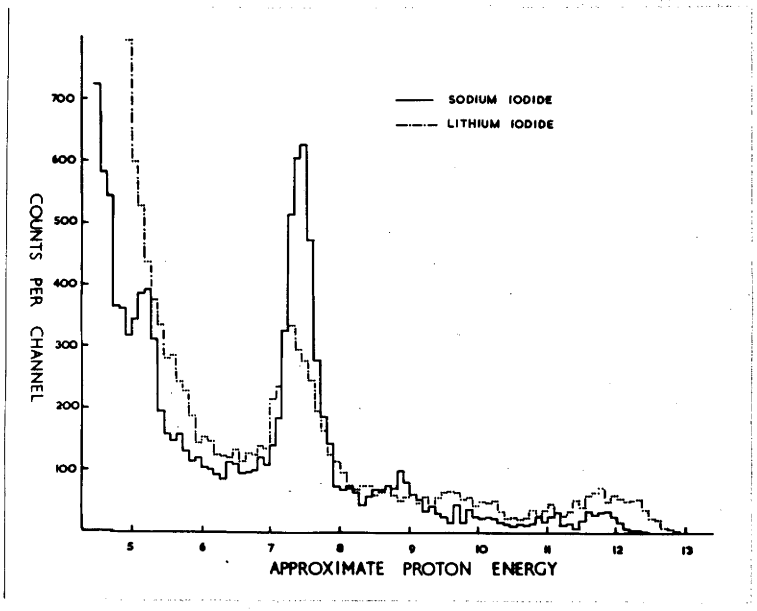

Fig. 7.7. NaI - LiI comparison measurement. The spectra have been normalised to the same gamma-ray flux and corrected for the number of atoms/cc.

4. Discussion.

The results which have been obtained cannot be regarded as conclusive, but at least they serve to show that some measurements of the reactions in Li^6 and Li^7 can be made using this method.

Identification of the $Li^7(\gamma,t)$ reaction at 17.6 Mev would appear satisfactory, although the same cannot be said for the $Li^7(\gamma,p)$ reaction. The identification of the ground-state transition of the latter reaction is based on an anomalous response of He^6 ions and a measurement of the He^6 response, in order to confirm the assignment, is difficult to envisage. A more satisfactory check would be to actually observe the 14.8 Mev transition. The present measurements indicate that, to do this, the neutron background would have to be eliminated - i.e., the measurement made with separated Li^7I (which is not available at the present time).

The cross-sections given by Titterton (Ti 58) for the (γ,t) and (γ,p) reactions at 17.6 Mev are:-

$$\sigma(\gamma,t) = 0.57 \text{ mb.}$$
$$\sigma(\gamma,p) = 0.86 \text{ mb.}$$

The present value for the (γ,t) cross-section is in reasonable agreement with the above data. The (γ,p) cross-section differs considerably, but it may be necessary to apply a further correction to the value of 1.65 mb. The spectrum obtained with Li^6I showed a small group at approximately 7.3 Mev, as did spectra obtained with CsI (Wr 58). If this group, which has a cross-section of 0.4 mb. (this value was obtained from the CsI data; the

Li^6I group is slightly larger), is attributed to the $I^{127}(\gamma,p)$ reaction, then the cross-section for the 7.25 Mev group must be reduced accordingly.

The ground-state group of the $Li^6(\gamma,p)$ reaction would have an equivalent proton energy of approximately 11.2 Mev. Only one spectrum was obtained with Li^6I and the resolution achieved beyond 10 Mev was not sufficiently good for any distinction to be made between the $Li^6(\gamma,p)$ and $I^{127}(\gamma,p)$ reactions. Measurements of the $Li^6(\gamma,p)$ reaction could be made with Li^6I, but lithium fluoride would be a more suitable scintillator to use because the maximum photoproton energy from the $F^{19}(\gamma,p)$ reaction is 9.25 Mev. Similarly, measurements with LiF would enable identification of the 14.8 Mev transition of the $Li^7(\gamma,t)$ reaction.

CHAPTER VIII

FUTURE MEASUREMENTS WITH SCINTILLATORS.

1. Introduction.

In preceding chapters photonuclear reactions in four scintillators, NaI, KI, LiI and CsI, have been discussed. Other scintillators, containing a variety of nuclei, lend themselves to similar experiments and, moreover, the general technique can be extended to study other aspects of nuclear reactions. Some of these, which concern photodisintegration, have been mentioned in Chapter VI. Further discussion of possible applications to photonuclear reactions is given here, along with a brief consideration of the means whereby scintillators might be employed in neutron studies.

2. Other scintillators.

Of the large number of substances known to be scintillators, the most suitable ones with regard to decay time, light output and particle response (excluding the above group) would appear to be RbI, $CaWO_4$, CsBr and CaF_2. Separated isotope scintillators such as $K^{41}I$ and Li^7I, and the alkali chlorides and fluorides, are also worthy of consideration. Little information on the properties of the above phosphors has been reported in the literature but a preliminary investigation of some of them (CaF_2 and NaCl(Ag)) has been made in this laboratory.

A small chip of CaF_2, cleaved from a piece of mineral fluorspar and polished, resolved the two (ThC + ThC') alpha-particle groups with resolution better than 15% (Fig.8.1) even though there were a number of internal flaws in the chip.

Silver-activated sodium chloride was less promising. The

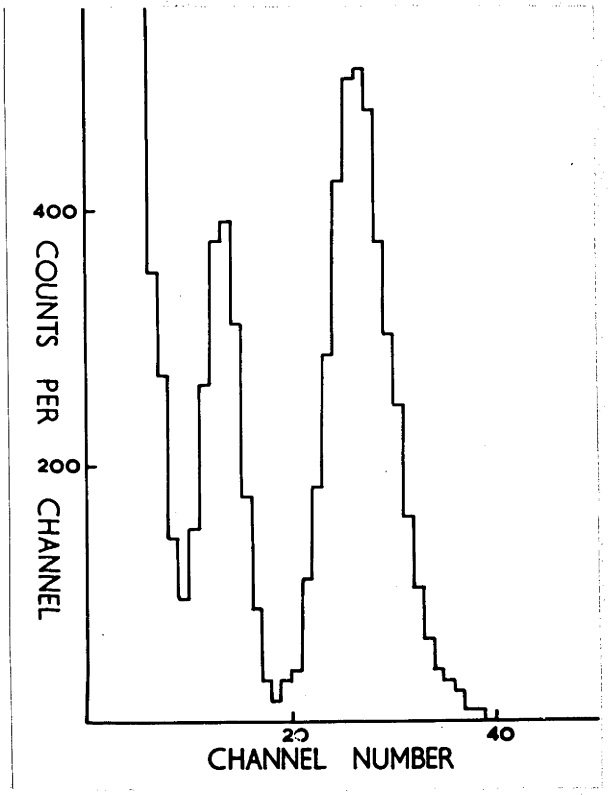

Fig. 8.1. (ThC + ThC') alpha particle spectrum obtained with a chip of mineral CaF_2. The resolution is less than 15%.

light output was barely greater than phototube noise and the best resolution obtained for the (ThC + ThC') alpha groups at room temperature was 20%. It may be possible to make a worthwhile study of the $Cl(\gamma,p)$ reactions by cooling the phototube with liquid air.

Organic scintillators would, in principle, allow a re-examination of the $C^{12}(\gamma,3\alpha)$, $N^{14}(\gamma,p)$ and $N^{14}(\gamma,\alpha)$ reactions, but the unfavourable proton and alpha responses relative to the electron response for organic scintillators (Ta 51) lead to prohibitively small phosphor dimensions which would be required to reduce the electron background sufficiently.

Another avenue of investigation could lie in the use of gaseous scintillators (No 56) which could be used to study photonuclear reactions in the rare gases. However, a number of these reactions have already been observed in gas proportional counters (Chapter I, Section 2) and the use of proportional counters must be regarded as a superior technique at the present time (even though the decay times of the gases are of the order of 10^{-8} sec.) in view of the contamination difficulties associated with gas scintillometry.

3. Alternative gamma-ray sources.

Although the $Li^7(p,\gamma)$ reaction is the most intense source of high-energy monochromatic gamma rays available, two other proton capture reactions, viz. $H^3(p,\gamma)$ and $B^{11}(p,\gamma)$, could be employed to obtain photoproton spectra at gamma-ray energies other than 17.6 Mev and so supplement the data obtained at that energy.

The former reaction has a very low yield* of pure 20 Mev gamma rays and has not previously been used for photodisintegration studies. The $B^{11}(p,\gamma)$ reaction gives rise to two gamma rays with energies of 12.3 and 16.7 Mev, the intensity ratio of the gamma rays depending on the proton bombarding energy. Preliminary measurements have shown that the radiation from a thick boron metal target at 1 Mev is comparable in intensity with non-resonance radiation from a 100 Kev lithium target at 800 Kev (Chapter II, Section 3). Barnes et al. (Ba 52) obtained the proton spectrum of the $H^2(\gamma,p)$ reaction produced by radiation from the $B^{11}(p,\gamma)$ reaction, and there is no reason why the spectra of the $Na^{23}(\gamma,p)$, $K^{39}(\gamma,p)$ and $I^{127}(\gamma,p)$ reactions should not be obtained likewise.

The use of bremsstrahlung has been discussed in Chapter VI.

4. Detection of externally produced photonuclear particles.

Methods have been discussed in Chapter I whereby photoprotons, produced in target foils by bremsstrahlung, can be detected with nuclear emulsions or scintillation counters. Even with the high intensity bremsstrahlung, the necessary shielding of the detector and the use of thin foils for good energy resolution result in marginal counting rates. Using low intensity $Li^7(p,\gamma)$ radiation, any attempt to detect externally produced protons can ill afford to shield the detector so that a background spectrum of the detector must be considered; if a scintillator is used, the background will be the proton spectrum of the (γ,p) reactions within the crystal. The obvious choice of scintillator is cesium iodide since

*The $H^3(p,\gamma)$ radiation has a $\sin^2\theta$ distribution and measurements at 0° will be extremely difficult.

the (γ,p) cross-sections for each of the constituent nuclei is small.

Preliminary spectra of protons from 0.010" thick aluminium and nickel foils have been measured with a cesium iodide crystal. The crystal was covered with a 1.5 mgm/cm^2 aluminium foil throughout to maintain constant light collection and allow direct comparison of the spectra obtained with the foils and of the background of the crystal. Protons from the foils, particularly nickel, were evident, but no energy resolution was possible since the foils were placed directly on top of the crystal. However, counting rates comparable to synchrotron experiments could be obtained even with a foil-detector geometry that would allow good energy resolution (10%). The basic features of the apparatus envisaged for use in this fashion are shown in Fig.8.2.

5. Neutron studies.

The study of neutron-induced reactions has suffered the same limitations as photonuclear investigations in that residual activation methods have provided the major portion of the present data concerning these reactions. Measurement of the spectra of the emitted particles is difficult and few measurements have been attempted.

As with photonuclear reactions, scintillators could be used to measure the spectra of particles (particularly protons) produced within them by a flux of fast neutrons. However, the use of fast neutrons introduces a difficulty that is not encountered with gamma rays, viz. the momentum of the neutron will produce a considerable energy spread of the observed

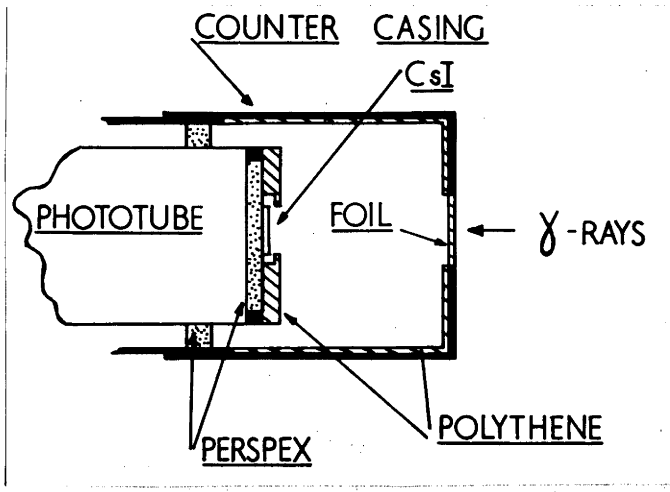

Fig. 8.2. Proposed apparatus to detect photoprotons produced in foils with a scintillation spectrometer.

proton groups since the crystal does not detect anywhere near the full energy of the recoil nucleus. If very thin crystals (0.005" or less) were to be used, sharp groups could be obtained since only protons (or other particles) emitted at 90° to the direction of the neutrons would be detected. In view of the high neutron fluxes available from such reactions as the $H^3(d,n)$ reaction, the use of thin crystals would not entail prohibitively long running times.

Preliminary measurements* with a thick cesium iodide crystal (covered with platinum to exclude protons produced externally) have indicated a broad spectrum of pulses which are attributed to protons from reactions in cesium and iodine. Measurements have not yet been made with thin crystals to confirm that the broad distribution can be resolved into individual transitions.

*These measurements were made by K. H. Purser.

REFERENCES.

Aj 52 Ajzenberg, Rev. Sci. Inst., 23, 649.

Aj 55 Ajzenberg and Lauritsen, Rev. Mod. Phys., 27, 77.

Al 49 Alburger, Phys. Rev., 76, 435.

Al 53 Allison and Casson, Phys. Rev., 90, 880.

Am 50 Ambrosen and Bisgaard, Nature, 165, 888.

Ar 51 Aron, Hoffman and Williams, U.S.A.E.C. Report No. AECU 663.

Ba 52 Barnes, Carver, Stafford and Wilkinson, Phys. Rev., 86, 359.

Be 50 Belcher, Nature, 166, 743.

Be 52 Bernstein and Shardt, Phys. Rev., 85, 919.

Be 55 Bell, Davis and Bernstein, Rev. Sci. Inst., 26, 726.

Be 56 Bernstein, Nucleonics, 14, 43, (April).

Bo 55 Borello, Goldemberg and Santos, Dos Anais da Academia Brasileira de Ciencias, 27, 417.

Br 55 Breen and Hertz, Phys. Rev., 98, 599.

Br 57 Brink, Nucl. Phys., 4, 215.

Bu 53 Butler and Almy, Phys. Rev., 91, 58.

By 53 Byerly and Stephens, Phys. Rev., 83, 54.

Ca 54 Caldwell and Turner, Nucleonics, 12, 47.

Ca 55 Carver, Hay and Titterton, Phil. Mag., 46, 841.

Ca 56 Campbell, Aust. J. Phys., 9, 156.

Ca 56a Carver, private communication.

Ca 57 Carver, Edge and Lokan, Proc. Phys. Soc., 70A, 415.

Ca 58 Carver and Turchinetz, private communication.

Ch 32 Chadwick and Constable, Proc. Roy. Soc., 135A, 48.

Co 51 Courant, Phys. Rev., 82, 703.

Co 54 Cox, Van Loeff and Lind, Phys. Rev., 93, 925.

Cu 50 Curtis, Hornbostel, Lee and Salant, Phys. Rev., 77, 290.

De 49 Devons and Hine, Proc. Roy. Soc., 199A, 56.

Di 50 Diven and Almy, Phys. Rev., 80, 407.

Eb 54 Eby and Jentschke, Phys. Rev., 96, 911.

En 54 Endt and Kluyver, Rev. Mod. Phys., 26, 95.

En 57 Endt and Braams, Rev. Mod. Phys., 29, 683.

Ev 54 Evans and Parkinson, Proc. Phys. Soc., 67A, 684.

Fa 54 Fader, M.I.T. Progress Report, May, 1954.

Fo 54 Foster, Standford and Lee, Phys. Rev., 93, 1069.

Fr 50 Franzen, Pelle and Sher, Phys. Rev., 79, 742.

Fr 50b Freeman, Phil. Mag., 41, 1225.

Fr 52 Franzen and Likely, Phys. Rev., 87, 667.

Ga 51 Gaerttner and Yeater, Phys. Rev., 83, 146.

Go 48 Goldhaber and Teller, Phys. Rev., 74, 1046.

Go 53 Goward and Wilkins, Proc. Roy. Soc., 217A, 357.

Gr 48 Green and Livesy, Phil. Trans. Roy. Soc., 241, 323.

Ha 51 Halpern and Mann, Phys. Rev., 82, 733.

Ha 52 Harshaw, Kremers, Steward, Warburton and Hay, A.E.C. Report NYO-1577 (unpublished).

Ha 56 Hay, private communication.

Ha 56a Hay and Warren, private communication.

He 54 Heydenberg and Temmer, Phys. Rev., 94, 1252.

Hi 47 Hirzel and Waffler, Helv. Phys. Acta, 20, 373.

Hj 52 Hjalmar and Slatis, Arkiv Fysik, 4, 323.

Ho 51 Hofstadter, McIntyre, Roderick and West, Phys. Rev., 82, 749.

Ho 53 Hoffman and Cameron, Phys. Rev., 92, 1184.

In 53 Inall and Boyle, Phil. Mag., 44, 1081.

Jo 51 Jolley and Champion, Proc. Roy. Soc., 64A, 88.

Ka 53 Katz, Johns, Baker, Haslam and Douglas, prive communication to E. W. Titterton.

Ko 55 Koerts et al., Phys. Rev., 98, 1230.

Kr 53 Kranz and Watson, Phys. Rev., 91, 1472.

Lo 51 Lovenberg, Phys. Rev., 84, 852.

Lo 58 Lokan, private communication.

Ma 36 May and Vaidyanathan, Proc. Roy. Soc., 155A, 519.

Mc 50 McDaniel, Walker and Stearns, Phys. Rev., 80, 807.

Mo 53 Montalbetti, Katz and Goldemberg, Phys. Rev., 91, 659.

Mo 56 Morrison, Preston and Wright, Physica, 22, 1145A.

Na 54 Nabholtz, Stoll and Waffler, Helv. Phys. Acta, 25, 153.

Na 54a Nathans and Halpern, Phys. Rev., 93, 437.

Ni 55 Nicholson and Snelling, Brit. J. App. Phys., 6, 104.

Pe 54 Perlman and Welker, Phys. Rev., 95, 133.

Ph 50 Philips, Lawson and Kruger, Phys. Rev., 80, 326.

Ru 54 Rubin and Walter, Helv. Phys. Acta, 27, 163.

Sc 52 Schenk and Heath, Phys. Rev., 85, 923.

Sc 54 Schenk and Neiler, Nucleonics, 12, 28 (March).

Sh 51 Sher, Halpern and Mann, Phys. Rev., 84, 387.

Sh 54 Sherr, Li and Christy, Phys. Rev., 96, 1258.

Sp 36 Speh, Phys. Rev., 50, 689.

Sp 55 Spicer, Phys. Rev., 100, 791.

St 51 Stearns and McDaniel, Phys. Rev., 82, 450.

St 53 Strauch, Ann. Rev. Nucl. Sci., 2, 105.

Ta 51 Taylor, Jentschke, Remley, Eby and Kruger, Phys. Rev., 84, 1034.

Ti 53 Titterton and Brinkley, Proc. Phys. Soc., 66A, 194.

Ti 54 Titterton and Brinkley, Proc. Phys. Soc., 67A, 469.

Ti 54a Titterton and Brinkley (unpublished).

Ti 55 Titterton, Prog. Nucl. Phys., 4, 1.

Ti 58 Titterton, private communication.

To 51 Toms and Stephens, Phys. Rev., 82, 709.

To 53 Toms and Stephens, Phys. Rev., 92, 363.

To 54 Toms, Geraldo and Stephens, private communication to E. W. Titterton.

To 55 Toms and Stephens, Phys. Rev., 98, 626.

To 57 Towle, Berenbaum and Mathews, Proc. Phys. Soc., 78, 84.

Tu 54 Tucker and Gregg, Phys. Rev., 91, 1579.

Wa 48 Waffler and Hirzel, Helv. Phys. Acta, 21, 200.

We 40 Weisskopf and Ewing, Phys. Rev., 57, 472.

We 55 Webb, USNRDL-TR-48.

Wh 56 White, Collins and Rourke, Phys. Rev., 101, 1786.

Wi 53 Wilkinson and Carver, Phys. Rev., 83, 466.

Wi 56 Wilkinson, Physica, 22, 1039.

Wr 56 Wright, Morrison, Reid and Atkinson, Proc. Phys. Soc., 69A, 77.

Wr 58 Wright, private communication.

Zu 50 Zucker and Watson, Phys. Rev., 78, 14.